

DOCTORAL THESIS

**Synthesis of Phase Controlled Nickel Sulfide Nanostructures and
their Catalytic Applications**

R. Karthikeyan

**Graduate School of
Science and Technology, Educational Division**

**Department of Optoelectronics and Nanostructure Materials
Shizuoka University**

July 2015

ACKNOWLEDGEMENTS

First and foremost, I would like to express my sincere gratitude to my advisor **Prof. Yasuhiro Hayakawa** , Research Institute of Electronics, Shizuoka University, for the continuous support of my research, for his patience, motivation, enthusiasm, and immense knowledge. His guidance helped me in all the time of research and writing of this thesis.

My profound gratitude to **Prof. R. Kita**, **Prof. K. Hara** and **Assoc. Prof. Y. Inoue**, Shizuoka University for the evaluation of the thesis and valuable comments to improve the research in future.

I wish to express my thank **Mr. T. Koyama** and **Mr. W. Tomoda** for their assistance in instrumentation handling and characterizations of the samples.

I am also very grateful to my laboratory members for all their supports on me during the research period.

I would like to thank **MEXT – Japan** for the financial assistance to complete the research work.

Finally, I thank my parents and family members for their patience, assistance and constant source of support throughout my research work.

Contents

	page
Abstract	vii
Chapter 1 Introduction	
1.1 Background	1
1.2 Water purification	2
1.3 Catalytic activity	3
1.3.1 Para-nitrophenol (4-nitrophenol)	5
1.4 Nanomaterials	9
1. 5 Inorganic nanomaterials	10
1.5.1 Transitional metal sulfides	12
1.5.2 Nickel sulfide	13
1.5.3 Review of literature	14
1.5.3.1 Nickel sulfide	14
1.5.3.2 Catalytic activity	15
1.6 Problem statement	16
1.6.1 Catalytic activity	16
1.6.2 Importance of nickel sulfide synthesis	17
1.7 Purpose of the research	17
References	18
Chapter 2 Synthesis of hierarchical nickel sulfide by hydrothermal method and its catalytic activity	
2.1 Background	26
2.2 Synthesis procedure of hierarchical structure	28

2.2.1 Characterization techniques	29
2.3 Results and discussion	34
2.3.1 Effects of EDTA	34
2.3.2 Effects of precursor concentrations	37
2.3.3 Effect of sulfur source concentrations	42
2.3.4 Effect of nickel source concentrations	44
2.3.5 Catalytic activity of nickel sulfide catalysts for the reduction of 4-nitrophenol	47
2.3.6 Mechanism of hierarchical structures evolution	49
2.4 Conclusion	52
References	53
Chapter 3 Single-step synthesis and catalytic activity of structure-controlled nickel sulfide nanoparticles	
3.1 Background	57
3.2 Synthesis procedure of phase controlled nickel sulfide	59
3.2.1 Materials	59
3.2.2 Experimental procedure	59
3.2.3 Catalytic study	62
3.2.4 Characterizations	62
3.3 Results and discussion	63
3.3.1 NiS phase	63
3.3.2 NiS ₂ phase	64
3.3.3 Ni ₃ S ₄ phase	65
3.3.4 Ni ₇ S ₆ phase	67
3.3.5 FTIR analysis	68

3.3.6 XPS analysis	70
3.4 Catalytic activities of nickel sulfide catalysts	72
3.5 Conclusion	76
References	77
Chapter 4 Synthesis of reduced graphene oxide functionalized nickel sulfide nanoparticles and its catalytic activity	
4.1 Background	82
4.2 Experimental procedures	84
4.2.1 Materials	84
4.2.2 Synthesis of graphene oxide by improved Hummer's method	86
4.2.3 Synthesis of reduced graphene oxide/nickel sulfide by hot injection method	86
4.2.3.1 Single solvent	86
4.2.3.2 Multi-solvent	87
4.2.4 Catalytic study	87
4.2.5 Characterization techniques	88
4.3 Results and discussion	88
4.3.1 Concentration ratio of 1:1	91
4.3.2 Concentration ratio of 1:2	95
4.3.3 Concentration ratio of 3:4	98
4.3.4 Concentration ratio of 3:2	101
4.3.5 Growth process	104
4.4 Catalytic activities for the reduction of 4-nitrophenol	105
4.5 Conclusion	110
References	111

Chapter 5 Summary and future work	
5.1 Summary	115
5.2 Future works	118
List of publications and conferences	120

ABSTRACT

Wastewater pollution has always been a major problem throughout the world. The availability of suitable water used for drinking, agriculture, farming etc. has been decreased through the years. 4-nitrophenol is one of the artificially created pollutants through industries such as, leather, pharmaceutical, paint colorings. It is one of the hazardous and toxic pollutants, which is known to cause adverse health effects in living organisms. The decay time for these chemicals in air and water takes long time and it is easily soluble in water. Out of many methods, catalytic reduction is one of the easy way to reduce the 4-nitrophenol to environmental friendly 4-aminophenol.

In the growing trends of advanced nanostructured materials, nickel sulfide is one of the important materials in the metal sulfide family because of the variety in its phases and diversity in applications. It is an abundant and cheap material, therefore nickel sulfide is a good candidate for catalytic reduction application. There are several reports exist on synthesis of nickel sulfide nanostructures by controlling the concentration, pH, growth period, temperature and surfactants. However synthesis of well-defined growth processes and the parameters affecting its phase and morphology has never been investigated for the synthesis of nickel sulfide nanomaterials. Specifically, structural and morphological changes and its effects on catalytic applications has not been studied yet.

The objective of the thesis is to investigate (1) the role of source concentration on the

formation of hierarchical nickel sulfide nanostructures by hydrothermal method, (2) the effect of organic ligand for the phase control by hydrothermal and temperature assisted hot injection method, (3) synthesis of phase dependent nickel sulfide by temperature controlled injection method, (4) the effect of addition of graphene on nickel sulfide phase formation and (5) the reaction rate and catalytic activity of 4-nitrophenol reduction with the synthesized nickel sulfide nanomaterials.

Monodispersed hierarchical architectures of nickel sulfide nanomaterials were synthesized by hydrothermal method using ethylenediaminetetraacetic acid (EDTA) as a capping agent. The molar concentration of the source material such as nickel nitrate and thiourea was varied as 0.5, 0.75 and 1.0 M. The role of EDTA was investigated by varying its concentrations for the phase and morphological behavior. The number of phases was restricted for the interaction of EDTA with nickel source. Concentration of 1:2 nickel to sulfur ratio yielded a highly monodispersed hierarchical structures of Ni_3S_4 and $\text{Ni}_{17}\text{S}_{18}$ phases. To study the phase formation of hierarchical structures, whole precursor concentrations were varied by keeping the constant growth temperature and period. Catalytic reduction of 4-nitrophenol was carried out with the fabricated nickel sulfide nanostructures and good catalytic activity was achieved by the sheet composed and ball-like architecture of $\text{Ni}_{17}\text{S}_{18}$ and Ni_3S_4 phases.

Highly structure controlled nickel sulfide nanoparticles with an average size of less than 20 nm were prepared using oleylamine as a solvent by temperature assisted hot injection method.

The complexity on the formation of single phase nickel sulfide was overcome by forming the sulfur-amine mixture for the controlled reaction. The effect of concentration ratio such as 1:1, 1:2, 3:4 and 3:2 was studied for the formation of highly uniform nanoparticles of NiS, NiS₂, Ni₃S₄ and Ni₇S₆ phases. The NiS phase exhibited high reaction rate as $8.949 \times 10^{-3} \text{ s}^{-1}$ for the reduction of 4-nitrophenol to 4-aminophenol. The stability of the NiS phase was investigated and there was no phase change observed even after its catalytic reduction and the repeated reaction rate was well matched with the initial experiments.

Reduced graphene oxide (rGO) functionalized nickel sulfide nanoparticles with uniform phase control were prepared using mixed solvent such as, oleylamine, octadecine, oleic acid by hot injection method. The reduction of graphene oxide was confirmed in the presence of oleylamine by XRD and TEM analysis. Single solvent as oleylamine experiments for rGO/nickel sulfide hybrid structures had less control on nickel sulfide phases. The excess of sulfur source concentration was required to achieve a single phase nickel sulfide nanoparticles on rGO supports. The multi solvents experiments resulted the better phase control of nickel sulfide on rGO sheets over the single solvent method. The particle dispersion on rGO nanosheets was uniform with the sizes less than 20 nm for all the nickel sulfide phases. The higher surface of rGO/nickel sulfide hybrid was utilized for the catalytic reaction because of its higher adsorption sites, which increases the contact between the 4-nitrophenol and nickel sulfide. The catalytic activity was enhanced for the rGO/NiS phase with the best reaction rate of $16.332 \times 10^{-3} \text{ s}^{-1}$.

The above results clearly confirmed that source concentration and capping agent played an important role on the formation of phase controlled nickel sulfide nanostructures. NiS and rGO/NiS had enhanced catalytic activity. The phase dependent catalytic activity of nickel sulfide was investigated for the first time.

Chapter 1

Introduction

1.1 Background

Modern era of science and technology often coins a term “nano” in every field of new invention. When it comes to the history of nano, it exists in nature with different forms of matter around us. One of the earliest nano-sized objects known to us was made of gold. In ancient Egypt over 5,000 years ago, nano gold was used for medicinal purposes. Several thousand years later by modern chemical methods, Faraday first prepared colloidal gold in 1952 and he called it as “divided state of gold”. In 1890 German bacteriologist Robert Koch found that compounds made with gold inhibited the growth of bacteria. He won the Noble prize for medicine in 1905. The use of gold in medicinal properties is not new. In the Indian medical system called Ayurveda, gold is used in several preparations. One popular preparation is called ‘Saraswatharishtam’ prescribed for memory enhancement.

The first use of the concepts in nano-technology was in “There’s a plenty of room at the bottom”, a talk given by physicist Richard Feynman at an American physical society meeting at Caltech in the year 1959. Feynman described a process by which the ability to which manipulates individual atoms and molecules might be developed. Later the term “nanotechnology” was defined by Norio Taniguchi of Tokyo Science University Professor in a 1974 paper as follows, “‘Nano-technology’ mainly consists of the processing, separation,

consolidation and deformation of materials by one atom or by one molecule”. In the 1980s the basic idea of this definition was explored in much more depth by different group of researchers all around the world. The birth of cluster science and the invention of scanning tunneling microscope (STM) boosted the technology to the next level. The initial discovery of Fullerenes and carbon nanotubes led many number of researches to work in the development of synthesis and properties of semiconductor nanocrystals. Researchers of the increase in the metal oxide, metal sulfide and quantum dots were followed and nanotechnology becomes a most popular and important technology.

A twenty first century, technology requires miniaturization of devices into nanometer sizes while the ultimate performance is drastically enhanced. This raises many issues regarding to new materials for achieving specific functionality and selectivity.

1.2 Water purification

Clean water is essential for living a healthy life as everyone should have access for it. Drinking water conditions have great impacts on people’s everyday life, especially in the developing countries where access to safe drinking water is very crucial. Surface water is the only source, thus water contaminations are very difficult to avoid it due to rigorous and reckless use of surface water. Water is susceptible to contaminant exposure at almost every stage of its transport. During and prior to collection, surface water or water to found in rivers and lakes, is vulnerable by interaction with acid rain, storm water runoff, pesticide runoff and

industrial waste. Human contact many contaminants such as perchlorates and phenols. The other hazardous materials (Ex: Arsenic, Radium and etc.) may result in number of acute and chronic illness.

1.3 Catalytic activity

Catalysis as a scientific discipline originated in the early part of the 20th century. Catalytic substance is that when added in small quantities to the reaction it affects reaction rate and selectivity. Thermodynamics would define the proper conditions at which catalysts should be utilized for catalytic reactions. Based on the reaction system and the phase of catalysts it can be distinguished as homogeneous catalysts and heterogeneous catalysts. Homogeneous catalysts function in the same phase as reactants (Ex: catalysts and the reactant both are liquid medium). There are many advantages of homogeneous catalysts. For instance, they are all exposed to the reactant, promotion of diffusion and heat transfer; possess well defined active sites. The reaction mechanisms are well understood by scientists. However, separation and recycling of homogeneous catalysts are extremely difficult, especially when expensive and toxic heavy metal complexes are employed. On the other hand, heterogeneous catalysts act in the different phases of reactants. They are generally solids with metallic nature and exhibit catalytic activity in a liquid or gas reaction system so that the filtration and removal processes are easier than homogeneous catalysts. But the reaction occurs only on the surface of heterogeneous catalysts.

There are various factors which affect the performance of the catalysts. The most important factors are size, shape, support materials and bimetallic synthetic effects. The catalysts are generally selected by considering reaction rate, adsorption energy and cost.

Fig. 1.1 shows relationship of cost and activity measure of the catalysts¹.

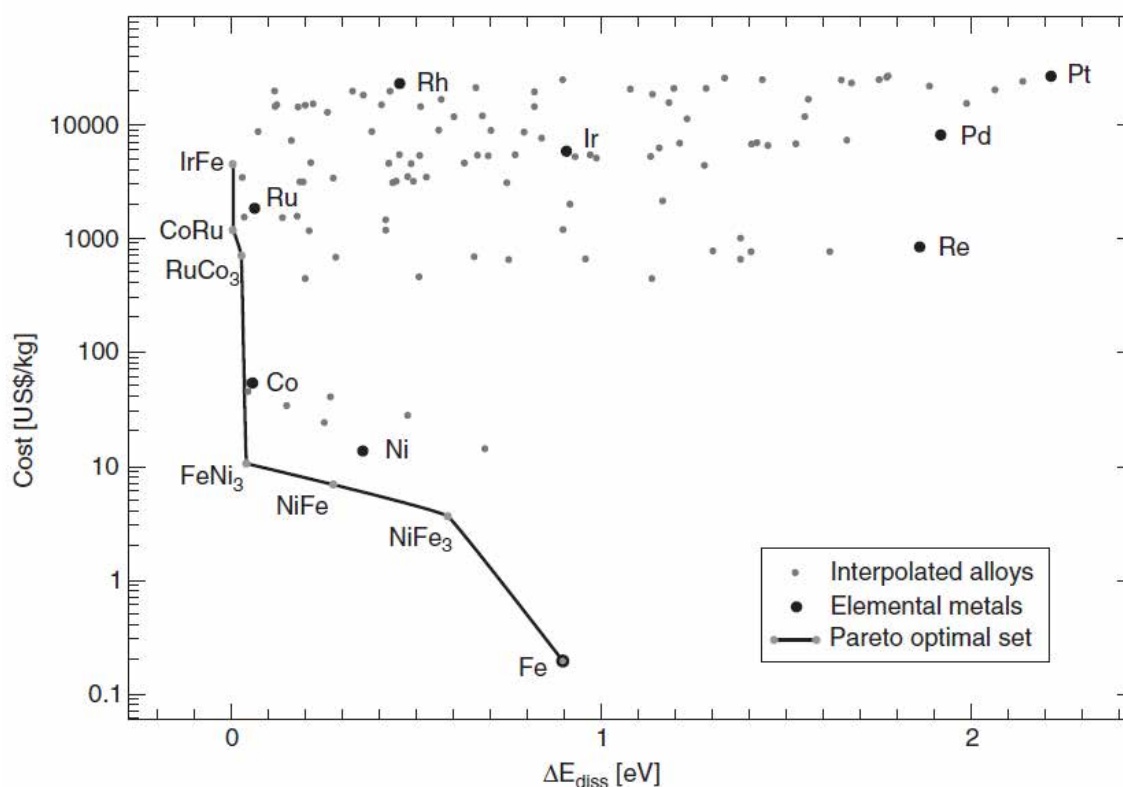


Fig. 1.1 Pareto plot of activity measure and the cost of elemental metal.

Here the most active catalysts fall in the expensive category such as platinum, palladium and rhenium. A large number of research papers were published on the catalytic activity of these materials for different applications such as solid oxide fuel cells, batteries, solar cells and etc.

1.3.1 Para-nitrophenol (4-nitrophenol)

Nitrophenols are a family of nitrated phenols with the formula of $\text{HOC}_6\text{H}_4\text{NO}_2$. These isomeric nitrophenols exist in three different forms; Ortho-nitrophenol (1-hydroxy-2-nitrobenzene), Meta—nitrophenol (1-hydroxy-3-nitrobenzene), Para-nitrophenol (1-hydroxy-4-nitrobenzene).

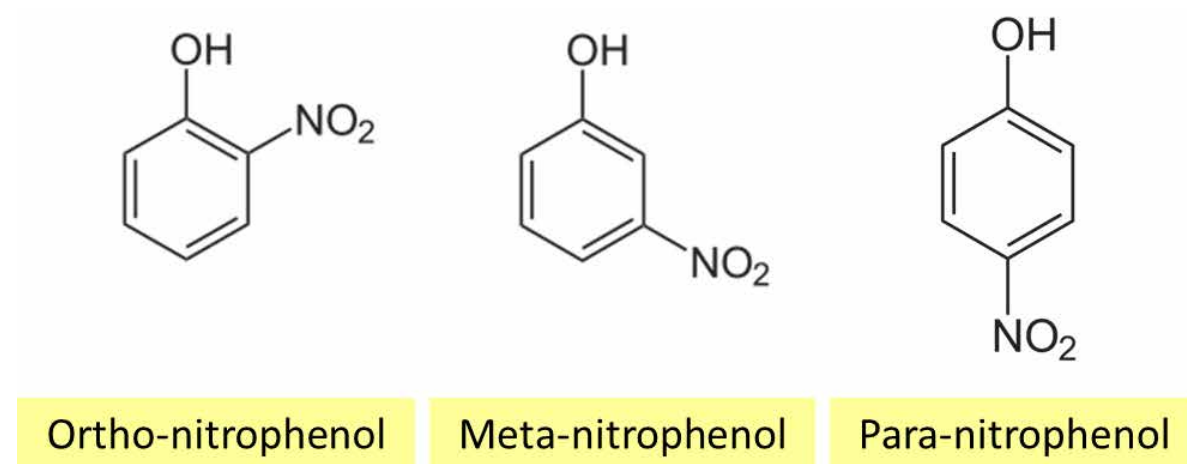


Fig. 1.2 Structures of Nitrophenols family

Out of these three structures, para-nitrophenol (4-nitrophenol) is one of the hazardous and toxic pollutants, which is known to cause adverse health effects in living organisms. In 1992 U.S public health service has mentioned these nitrophenols in “Toxic substances and Disease registry²”. Human exposure to nitrophenols by three pathways, inhalation, ingestion (eating and drinking) and dermal contact. These are the man-made chemicals with no evidence of their formation from any natural source. The main sources of the chemicals are industrial manufacturing and processing. 2-nitrophenols (Ortho-nitrophenols) is used mainly to produce dyes, paint coloring, rubber chemicals, and

substances that kill molds (fungicides). 4-nitrophenol is used mainly for manufacture drugs, fungicides, dyes and darkens leather. It is an intermediate material in the synthesis of most common medicine of paracetamol. The decay time needed for these chemicals to disappear chemically in air is not known. These nitrophenols are highly soluble in and stable in water bodies such as fresh water, marine environments and in industrial wastewaters. The breakdown takes long at shallow soil depths and groundwater. Therefore, they are expected to stay longer in the deep soil of dump sites compared to surface soil.

Due to its solubility, traditional water purification methods to remove 4-nitrophenol from contaminated waste water are not effective. Scientists have therefore developed many techniques for 4-nitrophenol removal such as absorption³, microwave assisted catalytic oxidation, microbial degradation, and etc. The reduction of 4-nitrophenol is the most often used reaction to study the catalytic activity of metal nanoparticles in aqueous solution. Many researchers work on free or immobilized nanoparticles to study the catalytic activity through reduction method. The advantage of the catalytic activity measurements using 4-nitrophenol is that it can be monitored easily by ultraviolet (UV) - visible spectroscopy measurements with respect to time. The decrease in the strong absorption of 4-nitrophenolate ions at 400 nm can be readily monitored and thus determination of rate constant k_{app} from the slope of linear correlation of $\ln (A/A_0)$ with time t is straightforward⁴. After the time t_0 in which no reaction takes place, the reaction starts and reaction rate can be described by first-order state law. The

apparent rate constant k_{app} is proportional to the total surface area S of metal nanoparticles.

Hence, two kinetic constants k_{app} and k_1 can be defined by,

$$-\frac{dC_t}{dt} = k_{app}C_t = k_1SC_t$$

Where, C_1 is the concentration of 4-nitrophenol at time t , k_1 is the rate constant normalized to S , the total surface area of metal nanoparticles normalized to the unit volume of the solution.

Fig. 1.3 (a) and (b) shows the typical 4-nitrophenol reduction to 4-aminophenol by gold nanoparticle. Fig. 1.3 (a) indicates to the absorption spectra as a function of time. The time between the consecutive curves is 2 min. Full conversion takes place in 20 min. Fig. 1.3 (b) is the typical time trace of the absorption of 4-nitrphenolate ions at 400 nm during their reaction⁴.

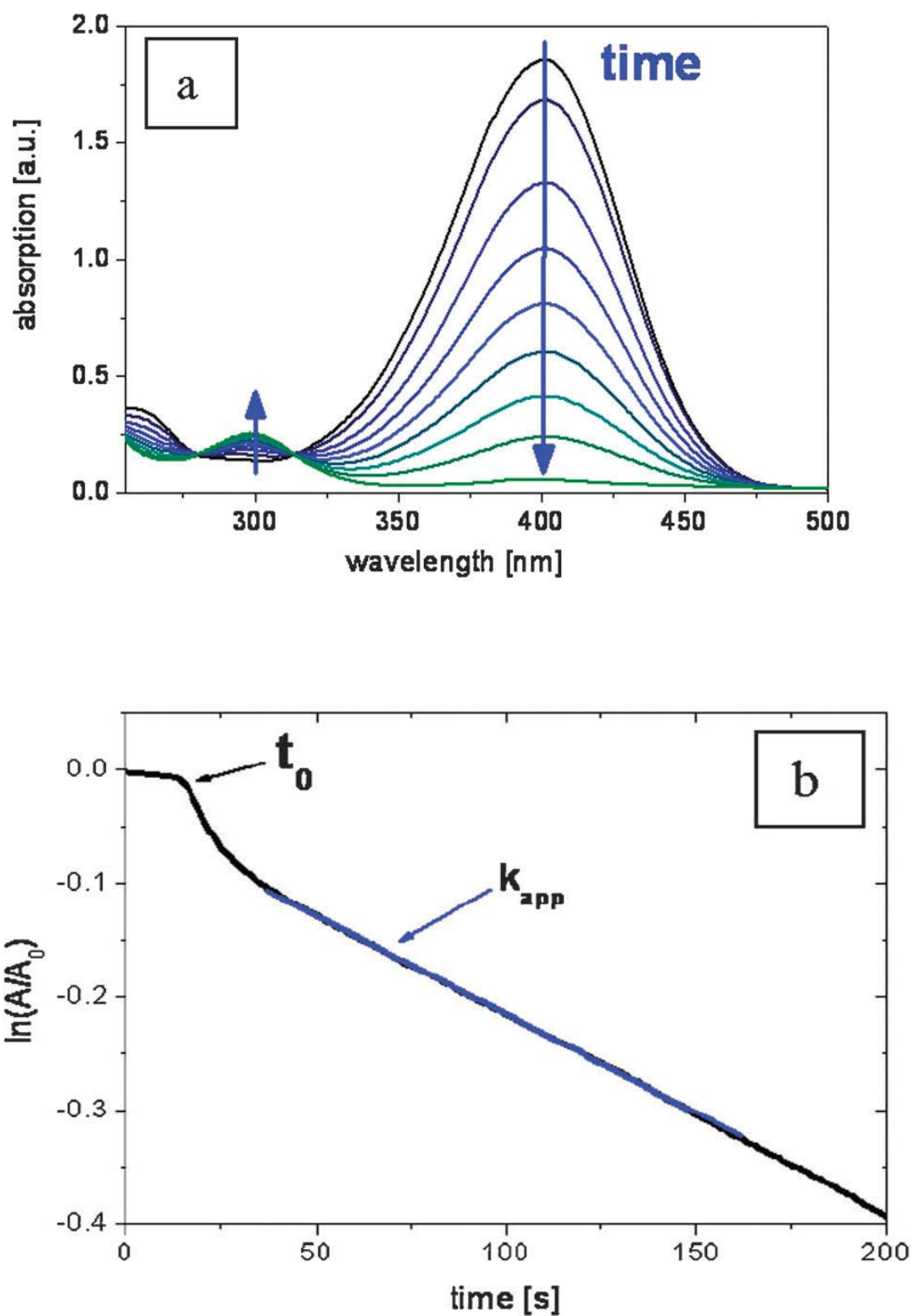


Fig. 1.3 (a) Reduction of 4-nitrophenol to 4-aminophenol (b) Time trace of absorption of 4-nitrophenolate ions⁴.

1.4 Nanomaterials

Nanomaterials are materials processing grain sizes on the order of a billionth of a meter. These materials often called as nanocrystalline materials. The extremely fascinating and useful properties of these materials exploited for a variety of structural and non-structural applications. Nanophase or nanostructured materials, a new branch of materials research, are attracting a great deal of attention because of their potential applications in areas such as electronics⁵, optics⁶, catalysis⁷, magnetic⁸, nanocomposites⁹ and biology¹⁰. The unique properties and the improved performances of nanomaterials are determined by their sizes, surface structures and inter-particle interactions. The nanometer size covers a wide range between several nanometer (nm) and several hundred nanometer. To distinguish nanomaterials from bulk, it is vitally important to demonstrate the unique properties of nanomaterials and their perspective impacts in nanotechnology.

Diversity of nanomaterials can be found depending on its chemical nature and its synthesis procedures. Nucleation and growth are two important processes in synthesizing particles. Nucleation is a process in which an aggregation of atoms is formed, and is the first step of phase transformation. The growth of nuclei results in the formation of large crystalline particles. Therefore, the study of size-dependent structures and properties of a nanoparticle is a key in understanding the nucleation and growth of crystals.

In general, synthesis methods of nanocrystalline materials classified into two groups,

top-down approach and bottom-up approach. The miniaturization of components for the construction of useful devices and machines has been pursued by top-down approach. An alternative and most-promising strategy to exploit science and technology at the nanometer scale is offered by the bottom-up approach, which starts from nano or sub-nano scale objects (atoms or molecules) to build up nanostructures. Imperfection of the surface structure and defects can be minimized by bottom-up approach. The main driving force behind the bottom-up approach is reduction of Gibb's free energy. Therefore, the materials produced are closer to their equilibrium state with more homogeneous chemical composition, better short and long range ordering.

1.5 Inorganic nanomaterials

The field of nanomaterials is loosely organized into organic nanomaterials such as fullerenes, carbon nanotubes and etc., and inorganic nanomaterials based on their elements, such as silicon, transitional metals and etc. Group II-VI members are vital materials for high-performance optoelectronics devices such as light-emitting diodes (LEDs) and laser diodes (LDs) operating in the blue or ultraviolet spectral range. II-VI category includes, transitional metal oxides (such as ZnO, TiO₂ and etc.), transitional metal sulfides (such as NiS, CuS, PbS and etc.), metal selenides (such as ZnSe, CdSe and etc.), metal telluride's (such as ZnTe, SnTe and etc.) and various other materials. This group of materials includes metallic, semiconducting and insulating nature, which attracts more attention towards

application.

A synthesis method lays an important role in the practical uses of inorganic nanomaterials for commercial applications. While inorganic nanomaterials have been generated by physical methods such as laser ablation^{11,12}, arc discharge^{13–15} and evaporation¹⁶, Chemical methods have been proved to be more effective as they provide better control of sizes, shapes and functionalization. Chemical synthesis of inorganic nanomaterials has been reviewed by several groups^{17,18} innumerable improvements have been reported continually in the last few years.

Several chemical methods such as wet chemical, chemical bath deposition, sonochemical growth¹⁹, microwave-induced deposition²⁰, hydrothermal method²¹, temperature controlled injection method and etc., have been used to synthesize the nanocrystals. Most of the methods produce irregular shape, size and structure. Out of all the above methods, hydrothermal and temperature controlled injection method have unique advantages controlling the size and shape. It is possible to grow semiconducting as well as metallic quantum dots. Temperature controlled injection method offers a greater control over the physical and chemical properties. It is possible to finely control the growth and thus obtain quantum dots with small and narrow size distribution and desired stoichiometry. The growth can be size selective by varying parameters as temperature, precursor's type and concentration, surfactant type and concentration, and the reaction time. Hydrothermal and

temperature injection methods have several other advantages such as low cost facilities, possibilities of production of large amount of material, small size, high crystallinity and formation of surface modifiable nanoparticles.

1.5.1 Transitional metal sulfides

Nanostructured metal sulfides have been extensively studied due to their importance in interpreting quantum size effects and applications in emerging devices, such as solar cells^{22–24}, sensors, light-emitting diodes (LED's), fuel cells, nonvolatile memory devices, thermoelectric devices²⁵ and lithium-ion batteries^{26–28}. These are the major group of minerals that provide the crystal chemist a rich field for investigation due to their diverse structural types. They are abundant and cheap since they exist as minerals such as heazlewoodite (Ni_3S_2), pyrite (FeS_2), Chalcocite (Cu_2S) and so on.

Zinc sulfide (ZnS) nanostructures have versatile potential applications as optoelectronic devices due to their excellent properties of luminescent and photochemistry. ZnS has a very wide bandgap of ~ 3.7 eV energy and considered to be one of the well-studied important semiconducting materials^{29,30}. Copper sulfide (Cu_2S) is an another important II-VI metal sulfide which has an ideal bandgap of 1.2 eV for the use in solar cells as an extremely thin absorber³¹. A p-type Cu_2S semiconductor has great potential applications as cathode materials for lithium-ion batteries, nonlinear optical materials and solar radiation absorbers³². Cobalt sulfide (Co_9S_8) is found to have the highest catalytic activity for dioxygen reduction in

acidic solution among a variety of transitional metal sulfides. Because of this property it is promising for the anode material for solid oxide fuel cells (SOFC)^{33,34}, dye sensitized solar cells^{35–37}, rechargeable lithium-ion batteries³⁸ and super-capacitors³⁵. Magnetic susceptibility results suggest that it is of Pauli paramagnetism used for magnetic devices. Colloidal Lead sulfide (PbS) nanocrystals has been utilized for optical switching and photonic applications³⁹. PbS is one of the earliest synthesized and well-studied quantum dots^{39,40}. It is also utilized for IR detector applications.

Nickel sulfide is of another metal sulfide. Because of its complications in its phases, it has not studied in detail toward structural control. In this work, I report the detailed study on nickel sulfide.

1.5.2 Nickel sulfide

Nickel sulfide is of importance in the metal sulfide family^{41–44} because of the variety in its phases and diversity in applications such as in lithium ion batteries⁴⁵, supercapacitors⁴⁶, and dye-sensitized solar cells⁴⁷. The relatively complex nickel sulfide system was first investigated by Kullard and Yard in 1962⁴⁸. Fig.1.4 showed the binary nickel sulfide phase diagram. The nickel sulfide system contains a number of phases including NiS₂, Ni₃S₄, Ni₇S₆, Ni₉S₈, α - Ni_{3+x}S₂, Ni₃S₂, NiS, Ni₁₇S₁₈ and NiS₂⁴⁹. Most of the phases are present at low temperature, which is one of the major advantages for nickel sulfide as a next generation material. According to the phase diagram of nickel sulfide, the sulfur-rich part of the system

appears to be rather simple with only a few phases compared with the complex nickel-rich phases. In recent years, many research groups have attempted to prepare different nickel sulfide phases for specific applications.

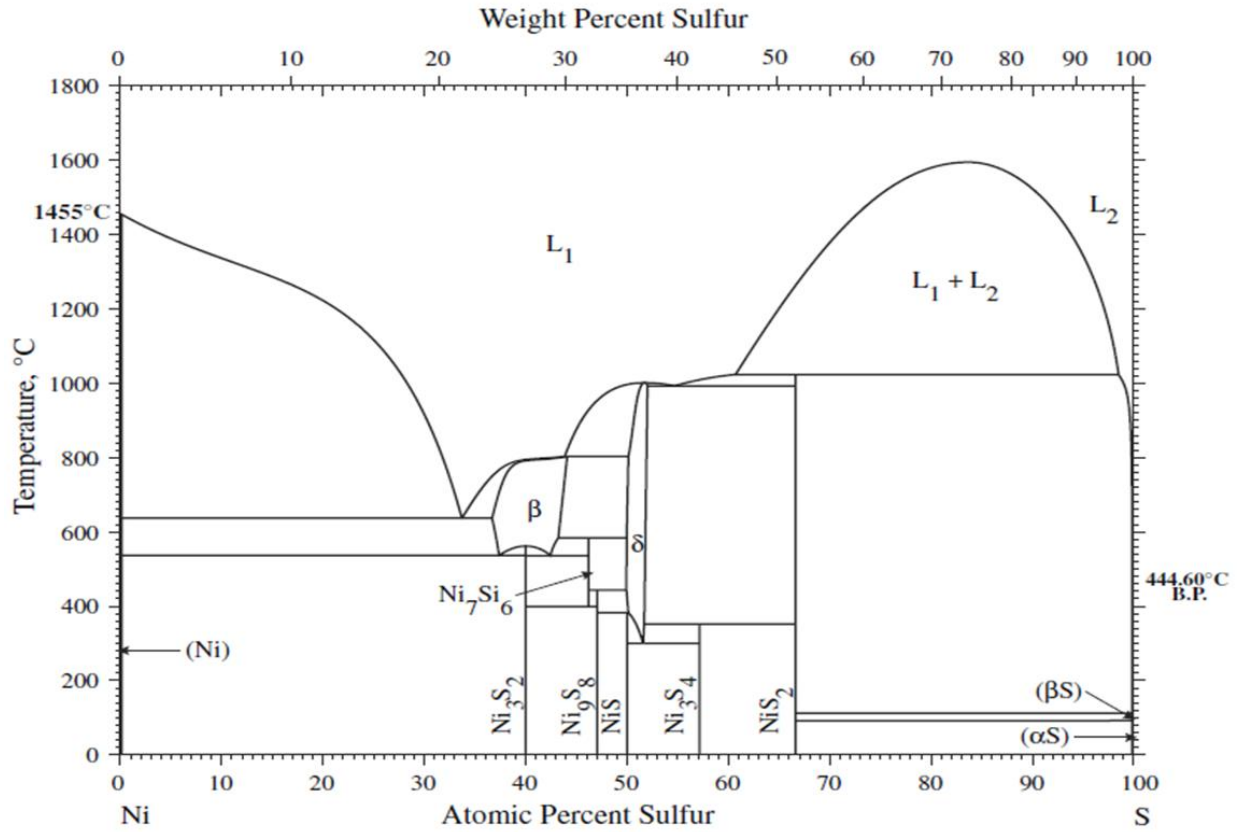


Fig.1.4 Binary phase diagram of nickel sulfide (Ni-S)

1.5.3 Review of Literature

1.5.3.1 Nickel sulfide

Many researchers have reported that the hexagonal nickel monosulfide (NiS) phase undergoes a metal-to-insulator transition at low temperature (~ 265 K)^{50–53}. When the Ni₃S₄ phase was grown on N-doped graphene, it showed a high electrolytic resistance compared with other nickel sulfide phases⁵⁴ and ferrimagnetic in nature⁵⁵. Ohtani et al. investigated the

importance of Ni deficiency on the formation of nickel sulfide which leads to a non-stoichiometric form of Ni_{1-x}S ⁵⁶. It is challenging to synthesize nickel sulfide by the low-temperature chemical route with controlled phases from complex source materials.

Several nickel sulfide nanostructure such as nanorods, nanotubes, nanowires, nanosheets, nanoprisms, layered structures⁵⁷, flower-like⁴⁹, and ball-like hollow spheres have been reported. Higher nanostructure (or microstructure) dimensions that compose the building blocks in hierarchical morphologies have shown potential use in many fields including gas sensing⁵⁸ and catalytic applications. Weiquan Cai et.al reported the structure transformation of Boehmite by mediating the sulfate under hydrothermal conditions to achieve morphologies from nanoflakes to hollow microspheres⁵⁹. The synthesis of nickel sulfide hierarchical structures has been reported previously by several research groups^{60,61}. Li et al. discussed the formation of β -NiS flower-like architectures in the presence of the citrate anion as a capping agent at various growth temperatures⁴⁹. Wang et al. explained the effect of temperature on the formation of NiS_2 spherical cuboids⁵⁶.

1.5.3.2 Catalytic activity

Pradhan et.al is the first person to identify the reaction mechanism in 2002⁶². Esumi et.al⁶³ investigated a series of size controlled nanoparticles (silver, platinum and palladium) for the reduction of p-nitrophenol to p-aminophenol. Gold in its bulk state is inactive to catalytic reactions. Composites composed of polyelectrolyte brushes with size controlled

nanoparticles of gold less than 2 nm was used to study the catalytic reduction activity by Wunder et.al⁴. Further, the size of ruthenium nanoparticles for the CO oxidation reaction was investigated by Sang Hoon Joo et.al⁶⁴. They observed 8 fold higher activities in 6 nm particles than 2nm particle. Not only the size, there have been numerous articles investigated on the shape of nanoparticles which affects its catalytic activity^{65–68}. Zhou et.al found that the high energy surfaces have an open surface structure and possess exceptional properties for high catalytic activity. Ghosh et.al, investigated the bimetallic effects of Pt-Ni and its catalytic activity. They found that the effects were superior compared to monometallic platinum⁶⁹. The kinetic prediction³³ of Co₉S₈ as a catalyst for electrochemical reduction of O₂ and battery performance⁷⁰ of CoS₂ as a catalyst were investigated in recent years.

1.6 Problem statement

1.6.1 Catalytic activity

1. The catalytic activity for the p-nitrophenol reaction was investigated by many researchers^{1,4,63,69,71–77}; however the better active material has not been investigated yet.
2. Catalysts removal is considered to be a major problem in the industry. Feasible removal of catalyst toward application is limited.
3. Most of the catalysts materials were related to platinum based composite and other expensive materials such as ruthenium, gold, silver, and etc. (see Fig. 1.1) The investigation of abundant availability of nickel based metallic catalysts was limited.

1.6.2 Importance of nickel sulfide synthesis

Several other researchers have explained the hierarchical structure formation of nickel sulfide; however structural control has not been investigated yet.

1. Size control of nanoparticle with structural control is highly unclear for the nickel sulfide synthesis.
2. Achieving phase controlled nickel sulfide towards the morphological control is necessary to understand the properties such as catalytic activity.

1.7 Purpose of the research

The aim of the research is as follows:

1. To synthesize monodispersed nickel sulfide hierarchical structures using organic ligand by hydrothermal method.
2. To investigate on the effect of source concentration for phase control by various characterization techniques.
3. To synthesize the phase dependent nickel sulfide by temperature controlled injection method.
4. To synthesize graphene incorporated phase controlled nickel sulfide by injection method.
5. To investigate the catalytic property with respect to the phase changes of nickel sulfide.

References

- (1) Van Santen, R. *Catal. from Princ. to Appl. first Ed. Ed. by M. Beller, A. Renken R. van Santen* **2012**, 3–19.
- (2) U.S. Public Health Service. *Agency Toxic Subst. Dis. Regist.* **1992**, 1–104.
- (3) Marais, E.; Nyokong, T. *J. Hazard. Mater.* **2008**, *152*, 293–301.
- (4) Wunder, S.; Lu, Y.; Albrecht, M.; Ballauff, M. *ACS Catal.* **2011**, *1*, 908–916.
- (5) Liu, Q.; Li, Z.; Liu, Y.; Zhang, H.; Ren, Y.; Sun, C.; Lu, W.; Zhou, Y.; Stanciu, L.; Stach, E. a; Xie, J. *Nat. Commun.* **2015**, *6*, 1–10.
- (6) Masters, R. C.; Pearson, A. J.; Glen, T. S.; Sasam, F.-C.; Li, L.; Dapor, M.; Donald, A. M.; Lidzey, D. G.; Rodenburg, C. *Nat. Commun.* **2015**, *6*, 6928.
- (7) George, S. M. *Chem. Rev.* **1995**, *95*, 475–476.
- (8) Frey, N. a; Peng, S.; Cheng, K.; Sun, S. *Chem. Soc. Rev.* **2009**, *38*, 2532–2542.
- (9) Miaudet, P.; Derré, A.; Maugey, M.; Zakri, C.; Piccione, P. M.; Inoubli, R.; Poulin, P. *Science* **2007**, *318*, 1294–1296.

- (10) Tzur-Balter, A.; Shatsberg, Z.; Beckerman, M.; Segal, E.; Artzi, N. *Nat. Commun.* **2015**, *6*, 6208, 1–8.
- (11) Kabashin, A. V.; Meunier, M.; Kingston, C.; Luong, J. H. T. *J. Phys. Chem. B* **2003**, *107*, 4527–4531.
- (12) Mafune, F.; Kohno, J.; Takeda, Y.; Kondow, T. *J. Phys. Chem. B* **2001**, *105*, 5114–5120.
- (13) Chhowalla, M.; Amaratunga, G. *Nature* **2000**, *407*, 164–167.
- (14) Zhou, Y.; Yu, S. H.; Cui, X. P.; Wang, C. Y.; Chen, Z. Y. *Chem. Mater.* **1999**, *11*, 545–546.
- (15) Fernández-Pacheco, R.; Arruebo, M.; Marquina, C.; Ibarra, R.; Arbiol, J.; Santamaría, J. *Nanotechnology* **2006**, *17*, 1188–1192.
- (16) Tang, H.; Ye, Z.; Zhu, L.; He, H.; Zhao, B.; Zhang, Y.; Zhi, M.; Yang, Z. *Phys. E Low-Dimensional Syst. Nanostructures* **2008**, *40*, 507–511.
- (17) Rao, C. N. R.; Vivekchand, S. R. C.; Biswas, K.; Govindaraj, a. *Dalton Trans.* **2007**, 3728–3749.

- (18) Cushing, B. L.; Kolesnichenko, V. L.; O'Connor, C. J. *Chem. Rev.* **2004**, *104*, 3893–3946.
- (19) Rajeshwar, K.; De Tacconi, N. R.; Chenthamarakshan, C. R. *Chem. Mater.* **2001**, *13*, 2765–2782.
- (20) Zhu, J. J.; Palchik, O.; Chen, S. G.; Gedanken, a. *J. Phys. Chem. B* **2000**, *104*, 7344–7347.
- (21) Yanagisawa, K.; Ovenstone, J. *J. Phys. Chem. B* **1999**, *103*, 7781–7787.
- (22) Wu, Y.; Wadia, C.; Ma, W.; Sadtler, B.; Alivisatos, a P. *Nano Lett.* **2008**, *8*, 2551–2555.
- (23) Li, T.-L.; Lee, Y.-L.; Teng, H. *J. Mater. Chem.* **2011**, *21*, 5089–5098.
- (24) Braga, A.; Giménez, S.; Concina, I.; Vomiero, A.; Mora-Seró, I. *J. Phys. Chem. Lett.* **2011**, *2*, 454–460.
- (25) Chen, B.; Uher, C. *Chem. Mater.* **1997**, *4756*, 1655–1658.
- (26) Saunders, R. C.; Park, C. *Advances* **1975**.
- (27) Xu, X.; Liu, W.; Kim, Y.; Cho, J. *Nano Today* **2014**, *9*, 604–630.

- (28) Lai, C.-H.; Lu, M.-Y.; Chen, L.-J. *J. Mater. Chem.* **2012**, *22*, 19–30.
- (29) Moore, D.; Wang, Z. L. *J. Mater. Chem.* **2006**, *16*, 3898.
- (30) Ma, B. C.; Moore, D.; Li, J.; Wang, Z. L. **2003**, 228–231.
- (31) Sakamoto, T.; Sunamura, H.; Kawaura, H.; Hasegawa, T.; Nakayama, T.; Aonob, M. *Appl. Phys. Lett.* **2003**, *82*, 3032–3034.
- (32) Lai, C.-H.; Huang, K.-W.; Cheng, J.-H.; Lee, C.-Y.; Hwang, B.-J.; Chen, L.-J. *J. Mater. Chem.* **2010**, *20*, 6638.
- (33) Sidik, R. a; Anderson, A. B. *J. Phys. Chem. B* **2006**, *110*, 936–941.
- (34) Liu, Q.; Zhang, J. *Cryst. Eng. Comm* **2013**, *15*, 5087–5092.
- (35) Rui, X.; Tan, H.; Yan, Q. *Nanoscale* **2014**, *6*, 9889–9924.
- (36) Yang, J.; Bao, C.; Zhu, K.; Yu, T.; Li, F.; Liu, J. **2014**, 1–4.
- (37) Lin, J.-Y.; Liao, J.-H.; Chou, S.-W. *Electrochim. Acta* **2011**, *56*, 8818–8826.
- (38) Shi, W.; Zhu, J.; Rui, X.; Cao, X.; Chen, C.; Zhang, H.; Hng, H. H.; Yan, Q. **2012**.
- (39) Hines, M. a.; Scholes, G. D. *Adv. Mater.* **2003**, *15*, 1844–1849.

- (40) Mourdikoudis, S.; Liz-Marzán, L. M. *Chem. Mater.* **2013**, *25*, 1465–1476.
- (41) Tilley, R. D.; Jefferson, D. a. *J. Phys. Chem. B* **2002**, *106*, 10895–10901.
- (42) Nguyen, P.; Ng, H. T.; Yamada, T.; Smith, M. K.; Li, J.; Han, J.; Meyyappan, M. **2004**.
- (43) Li, Y.-D.; Liao, H.-W.; Ding, Y.; Qian, Y.-T.; Yang, L.; Zhou, G.-E. *Chem. Mater.* **1998**, *10*, 2301–2303.
- (44) Q. Peng, K.; P. Huang, Z.; Zhu, J. *Adv. Mater.* **2004**, *16*, 73–76.
- (45) Mi, L.; Ding, Q.; Chen, W.; Zhao, L.; Hou, H.; Liu, C.; Shen, C.; Zheng, Z. *Dalton Trans.* **2013**, *42*, 5724–5730.
- (46) Zhu, T.; Wu, H. Bin; Wang, Y.; Xu, R.; Lou, X. W. D. *Adv. Energy Mater.* **2012**, *2*, 1497–1502.
- (47) Chi, W. S.; Han, J. W.; Yang, S.; Roh, D. K.; Lee, H.; Kim, J. H. *Chem. Commun. (Camb)*. **2012**, *48*, 9501–9503.
- (48) Kullerud, G.; Yund, R. a. *J. Petrol.* **1962**, *3*, 126–175.
- (49) Haibo Li, Lanlan Chai, Xiaoqing Wang, Xueying Wu, Guangcheng Xi, yankuan Liu, and Y. Q. *J. Cryst. Growth Des.* **2007**, *7*, 1918–1922.

- (50) Sparks, J. T.; Komoto, T. *J. Appl. Phys.* **1963**, *34*, 1191.
- (51) Sparks, J.; Komoto, T. *Phys. Lett.* **1967**, *25*, 5–6.
- (52) Sparks, J.; Komoto, T. *Rev. Mod. Phys.* **1968**, *40*, 752–754.
- (53) A. S. Barker, J. and J. P. R. *Phys. Rev. B* **1974**, *10*, 987–994.
- (54) Mahmood, N.; Zhang, C.; Hou, Y. *Small* **2013**, *9*, 1321–1328.
- (55) Manthiram, A.; Jeong, Y. U. **1999**, *681*, 679–681.
- (56) Ohtani, T. *J. Phys. Soc. Japan* **1974**, *37*, 701–710.
- (57) Jiang, X.; Xie, Y.; Lu, J.; Zhu, L.; He, W.; Qian, Y. *Adv. Mater.* **2001**, *13*, 1278–1281.
- (58) Lee, J.-H. *Sensors Actuators B Chem.* **2009**, *140*, 319–336.
- (59) Cai, W.; Yu, J.; Gu, S.; Jaroniec, M. *Cryst. Growth Des.* **2010**, *10*, 3977–3982.
- (60) Wang, L.; Zhu, Y.; Li, H.; Li, Q.; Qian, Y. *J. Solid State Chem.* **2010**, *183*, 223–227.
- (61) Ni, S.; Zhou, G.; Wang, X.; Sun, X.; Yang, F.; Liu, Y.; He, D. *Mater. Chem. Phys.* **2010**, *120*, 426–430.

- (62) Pradhan, N.; Pal, A.; Pal, T. *Colloids Surfaces A Physicochem. Eng. Asp.* **2002**, *196*, 247–257.
- (63) Esumi, K.; Isono, R.; Yoshimura, T. *Shikizai Kyokaishi* **2003**, *76*, 421–427.
- (64) Joo, S. H.; Park, J. Y.; Renzas, J. R.; Butcher, D. R.; Huang, W.; Somorjai, G. a. *Nano Lett.* **2010**, *10*, 2709–2713.
- (65) Zhou, K.; Li, Y. *Angew. Chemie - Int. Ed.* **2012**, *51*, 602–613.
- (66) Zhou, Z.-Y.; Tian, N.; Li, J.-T.; Broadwell, I.; Sun, S.-G. *Chem. Soc. Rev.* **2011**, *40*, 4167–4185.
- (67) Yin, A. X.; Min, X. Q.; Zhang, Y. W.; Yan, C. H. *J. Am. Chem. Soc.* **2011**, *133*, 3816–3819.
- (68) Cheong, S.; Watt, J. D.; Tilley, R. D. *Nanoscale* **2010**, *2*, 2045–2053.
- (69) Ghosh, S. K.; Mandal, M.; Kundu, S.; Nath, S.; Pal, T. *Appl. Catal. A Gen.* **2004**, *268*, 61–66.
- (70) Wang, Y.; Wu, J.; Tang, Y.; Lü, X.; Yang, C.; Qin, M.; Huang, F.; Li, X.; Zhang, X. *ACS Appl. Mater. Interfaces* **2012**, *4*, 4246–4250.

- (71) Hervés, P.; Pérez-Lorenzo, M.; Liz-Marzán, L. M.; Dzubiella, J.; Lu, Y.; Ballauff, M. *Chem. Soc. Rev.* **2012**, *41*, 5577.
- (72) Liu, P.; Zhao, M. *Appl. Surf. Sci.* **2009**, *255*, 3989–3993.
- (73) Kundu, S.; Mandal, M.; Ghosh, S. K.; Pal, T. *J. Photochem. Photobiol. A Chem.* **2004**, *162*, 625–632.
- (74) Esumi, K.; Miyamoto, K.; Yoshimura, T. *J. Colloid Interface Sci.* **2002**, *254*, 402–405.
- (75) Pozun, Z. D.; Rodenbusch, S. E.; Keller, E.; Tran, K.; Tang, W.; Stevenson, K. J.; Henkelman, G. *J. Phys. Chem. C* **2013**, *117*, 7598–7604.
- (76) Gu, X.; Qi, W.; Xu, X.; Sun, Z.; Zhang, L.; Liu, W.; Pan, X.; Su, D. *Nanoscale* **2014**, *6*, 6609–6616.
- (77) Abdel-Fattah, T. M.; Wixtrom, a. *ECS J. Solid State Sci. Technol.* **2014**, *3*, M18–M20.

Chapter 2

Synthesis of hierarchical nickel sulfide by hydrothermal method and its catalytic activity

2.1 Background

Recently, many researchers have been paying more attention to the control of morphologies of nanostructures, because the performances not only depend on their size and shape but also on their organizations¹⁻³. The formation of highly monodispersed hierarchical architectures is of great interest in advanced applications such as solar cells⁴, chemical sensors⁵, catalysis^{6,7}, lithium-ion batteries⁸ and etc. Jong-heun Lee first made a detailed review in the formation of hierarchical structures and its effective need on advanced applications such as gas sensors and etc., in 2009⁵. The bottom-up design has been widely recognized to prepare well-defined architectures, because it can easily control the micro/nano scale growth of materials. Metal chalcogenides nanostructures have wide range of potential applications such as photocatalysts⁹, gas sensors¹⁰, photovoltaic devices¹¹⁻¹³ and biological imaging¹⁴.

As an important class of metal chalcogenides, metal sulfide nanostructures have received much attention for their excellent energy storage devices for example, Bi₂S₃ combined with bismuth oxide heterostructure for lithium storage application¹⁵ and

sponge-like Ni_3S_2 as a good energy storage devices¹⁶. The study of well-defined hierarchical structures has been increased over the years by other metal sulfides such as molybdenum sulfide¹⁷, cobalt sulfide⁴, nickel cobalt sulfide composites^{18,19}, indium sulfide mixed bismuth sulfide²⁰ and etc. Up until several researchers have synthesized nickel sulfide and other metal sulfide hierarchical structures^{21–24}. However, the synthesis of well-defined growth process and the parameters affecting the formation of hierarchical architectures have less been studied. Specifically, structural changes with respect to the concentration and formation of hierarchical morphologies by the hydrothermal method have not yet been investigated. For the surfactant, ethylenediaminetetraacetic acid (EDTA) is a well-known chelating agent and crystal growth modifier. However, nickel sulfide synthesis using EDTA has not yet been discussed.

In this chapter, I report on the synthesis of nickel sulfide hierarchical structures with EDTA as a capping agent using nickel nitrate hexahydrate ($\text{Ni}(\text{NO}_3)_2 \cdot 6\text{H}_2\text{O}$) and thiourea ($\text{CH}_4\text{N}_2\text{S}$) as precursors by the hydrothermal method. EDTA was chosen as the capping agent because of its good anionic interaction with metal sulfides and control of morphology^{25–27}. The effects of precursor material concentration (i.e. $\text{Ni}(\text{NO}_3)_2 \cdot 6\text{H}_2\text{O}$, $\text{CH}_4\text{N}_2\text{S}$, and EDTA) on the formation mechanism of nickel sulfide hierarchical structures and phase control were investigated. The effect of individual concentrations such as sulfur source and nickel source was investigated for the phase and morphological control.

2.2 Synthesis procedure of hierarchical structures

All reagents (analytical-grade purity) were purchased from Wako Chemicals, Japan and were used without further purification. To synthesize the nickel sulfide hierarchical structures, 1 mol $\text{CH}_4\text{N}_2\text{S}$ was added to a 5 mol L^{-1} $\text{Ni}(\text{NO}_3)_2 \cdot 6\text{H}_2\text{O}$ solution. EDTA (0.2 mol) was added as a capping agent under vigorous stirring. Experiments were carried out with and without EDTA addition. EDTA addition resulted in a solution color change from dark green to a pale-blue with an increased solution viscosity. The precursor material concentration is abbreviated as A (0.5 mol $\text{Ni}(\text{NO}_3)_2 \cdot 6\text{H}_2\text{O}$, 1 mol $\text{CH}_4\text{N}_2\text{S}$ and 0.2 mol EDTA). A mixture of these materials was stirred continuously for 60 min, and the solution was then transferred to a 0.1 L Teflon-lined autoclave for hydrothermal reaction at 160°C for 10 h. The schematic of the experimental view is shown in Fig. 2.1. The nickel sulfide precipitate was filtered, washed with distilled water three times and dried at 60°C. To understand the formation mechanism of the hierarchical structures, low concentrations of precursor materials, such as A/10 and A/5, were prepared under identical conditions. These synthesized materials were collected and dried at the same temperature. All other conditions (100 mL distilled water, 160°C reaction temperature, and 10 h reaction time) were kept constant. To avoid the possibility of coordination of the S^{2-} anion with the nickel complex and the formation of more complex phases, the reaction temperature was fixed at 160°C.

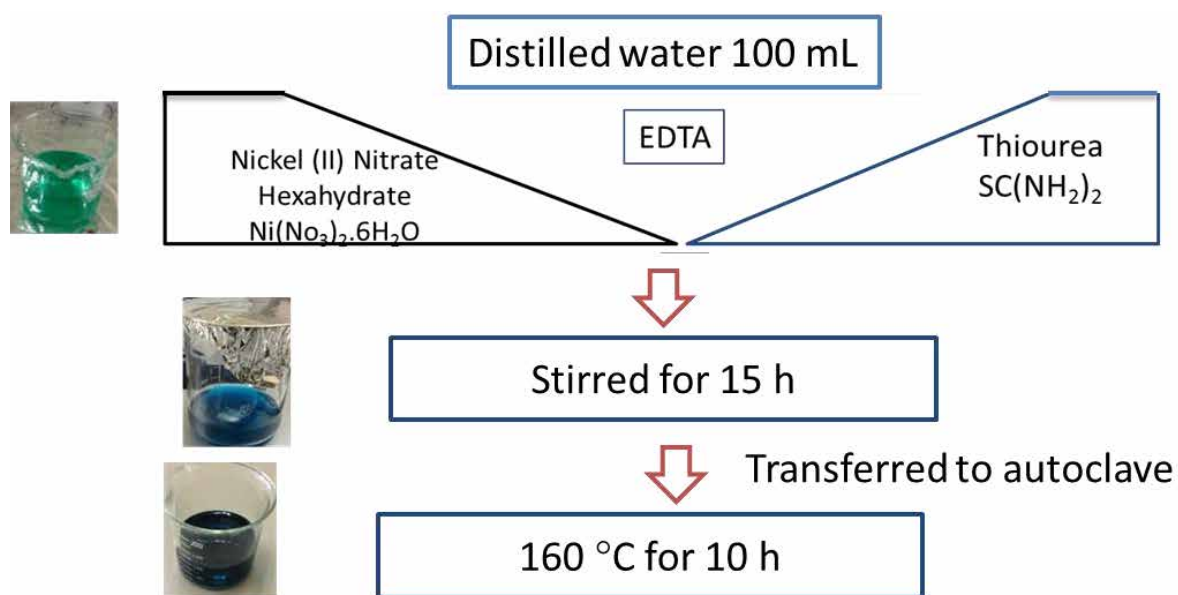


Fig. 2.1. Schematic experimental view of hydrothermal method.

2.2.1 Characterization techniques

The crystal structure was characterized by powder X-ray diffraction (XRD) with a scan rate of $0.04^\circ \text{ s}^{-1}$ in the 2θ range from 10° to 80° using a Rigaku (Japan) X-ray diffractometer (RINT-2200, $\text{CuK}\alpha$ radiation, $\lambda = 1.54178 \text{ \AA}$) as shown in Fig. 2. 2.



Fig. 2. 2. Rigaku X-ray diffractometer at Center for Nanodevice Fabrication and Analysis, Shizuoka University

Field emission scanning electron microscope (FESEM) images were taken with a JEOL JSM 7001F instrument to observe sample surface morphology as shown in Fig. 2. 3.



**Fig. 2. 3. JEOL – JSM 7001F field emission scanning electron microscope at Center
for Instrumental Analysis, Shizuoka University**

High resolution transmission electron microscope (HRTEM) images were recorded using a JEOL JEM 2100F microscope at an accelerating voltage of 200 kV as shown in Fig. 2. 4.



Fig. 2. 4. JEOL JEM 2100F transmission electron microscope at Center for Nanodevice Fabrication and Analysis, Shizuoka University.

Quantitative analysis was conducted by X-ray photoelectron spectroscopy (XPS) using a Shimadzu ESCA 3100 spectrophotometer as shown in Fig. 2. 5.



Fig. 2. 5. Shimidzu ESCA 3100 spectrophotometer X-ray photoelectron spectroscopy

UV-visible absorption analyses were performed using a Shimadzu (Japan) 3100 PC spectrophotometer with ethanol as dispersing medium as shown in Fig.2.6.

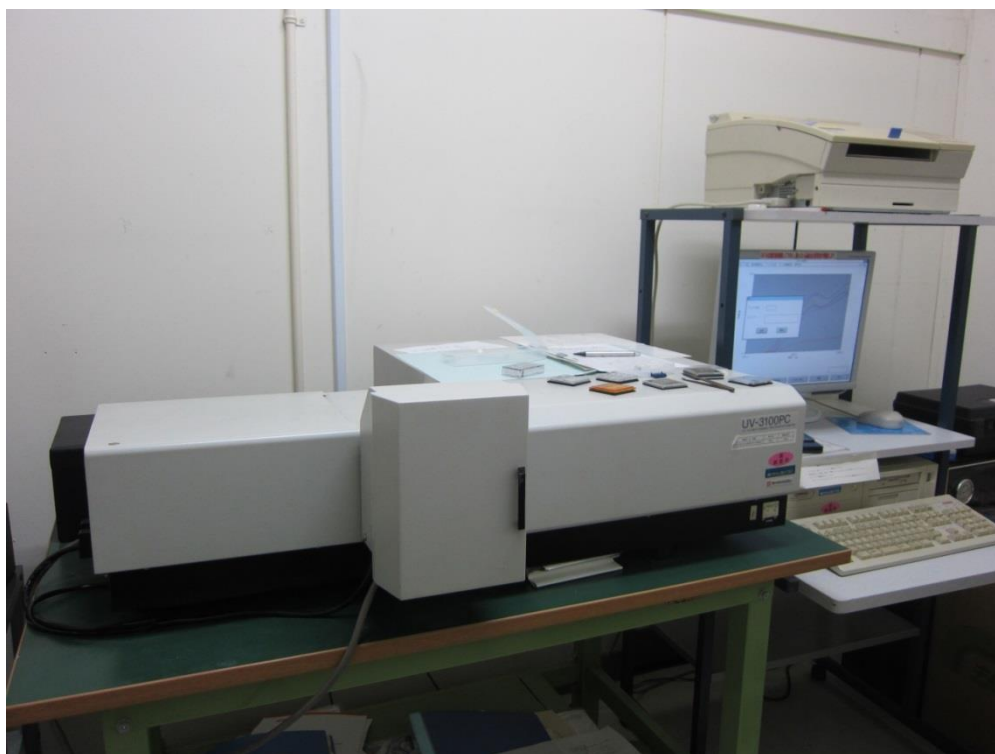


Fig.2. 6. UV 3100PC – UV visible absorptions spectrophotometer at Center for Nanodevice Fabrication and Analysis, Shizuoka University

2.3 Results and discussion

2.3.1 Effect of EDTA

When the reaction was carried out in water, the sulfur to nickel molar ratio (S: Ni) was maintained at 2:1 in all experiments. Fig. 2.7 and 2.8 show the XRD pattern and FESEM images of samples prepared with the 0.5 mol nickel source and the 1 mol sulfur source concentrations, where (a) is EDTA-uncapped and (b), (c) are EDTA-capped nickel sulfide as 0.2 mol and 0.4 mol, respectively. The EDTA-uncapped nickel sulfide particles consist of improper hierarchical morphologies hundreds of nanometers to several micrometers in size (see Fig. 2.8 (a)). The XRD pattern of uncapped material contains mixed of three phases of

nickel sulfide. From the TEM and HRTEM images of Fig. 2.9 (a,b), confirmed the presence of Sheet-composed morphology. The distance between the atomic layers of 6.1 Å was well matched with the (011) peak of $\text{Ni}_{17}\text{S}_{18}$ phase. The EDTA-capped (0.2 mol) sample contains sheets composed of ball-like structures with cube composed architectures. Fig.2.7 (b) shows two phases of nickel sulfide ($\text{Ni}_{17}\text{S}_{18}$ and Ni_3S_4). Further increase in the concentration of EDTA to 0.4 mol resulted with cube composed ball architectures and the corresponding XRD pattern shows single nickel sulfide phase.

Table 2.1 Different concentrations of capping agent experimental conditions.

Experiment	Nickel nitrate (mol)	Thiourea (mol)	EDTA (mol)	Phases observed from XRD analysis
1	0.50	1.00	0 (upcapped)	$\text{Ni}_{17}\text{S}_{18}$, NiS_2 and Ni_3S_4
2	0.50	1.00	0.20	$\text{Ni}_{17}\text{S}_{18}$ and Ni_3S_4
3	0.50	1.00	0.40	NiS_2

Addition of the EDTA anion controlled the reaction between the sulfur and nickel ions, and resulted in the formation of monodispersed hierarchical structures. The addition of EDTA to the Ni^{2+} solution produced a Ni^{2+} complex and slowed down the effect of $\text{CH}_4\text{N}_2\text{S}$ during the reaction²¹.

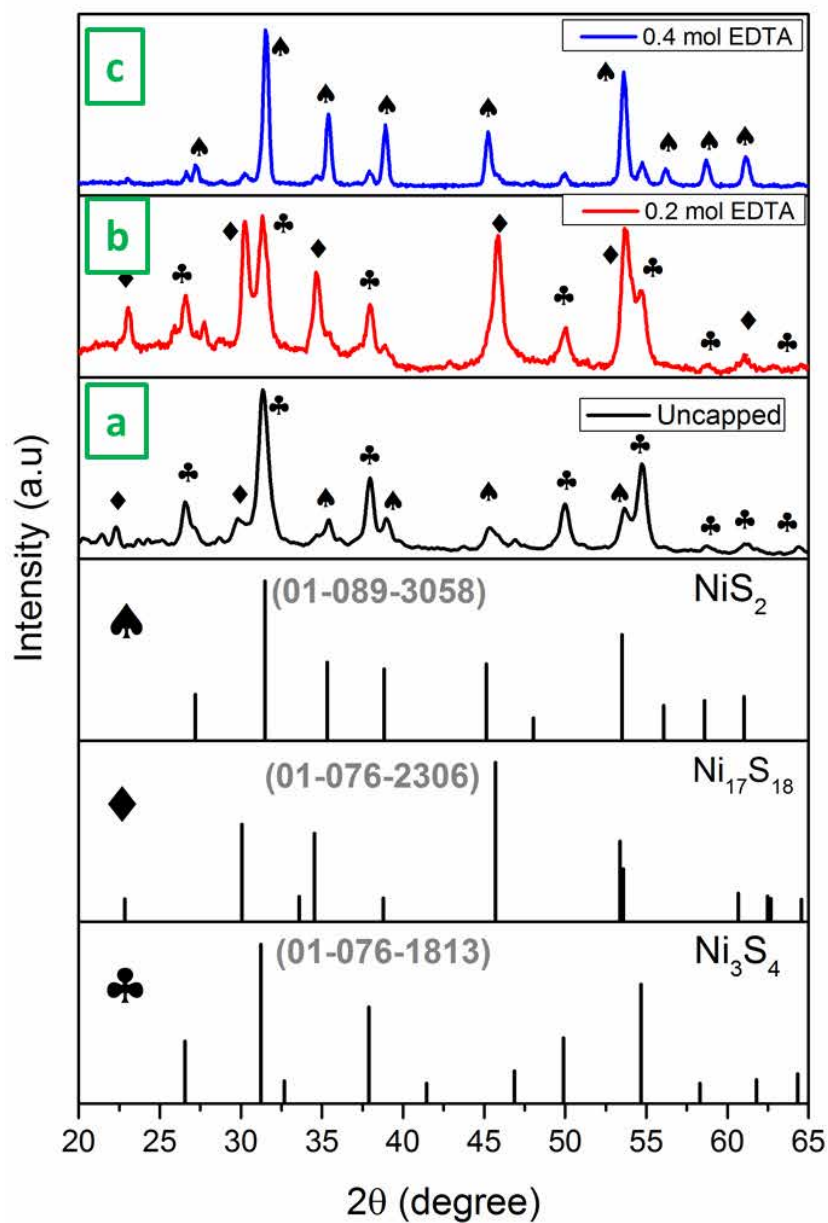


**Fig. 2.7 XRD patterns for different EDTA concentrations (a) 0 mol - uncapped
(b) 0.2 mol (c) 0.4 mol**

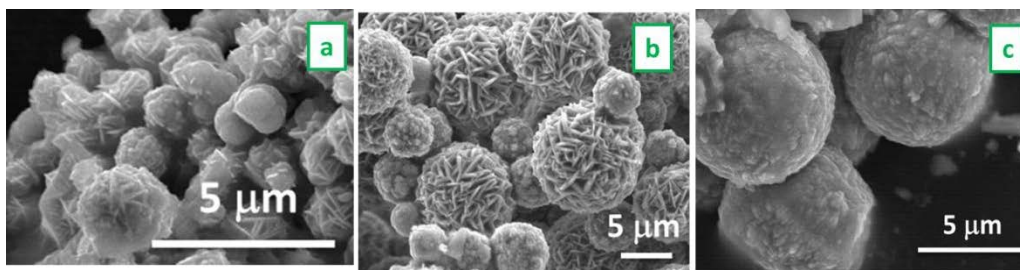


**Fig. 2.8 FESEM images of different EDTA concentrations (a) 0 mol - uncapped
(b) 0.2 mol (c) 0.4 mol**

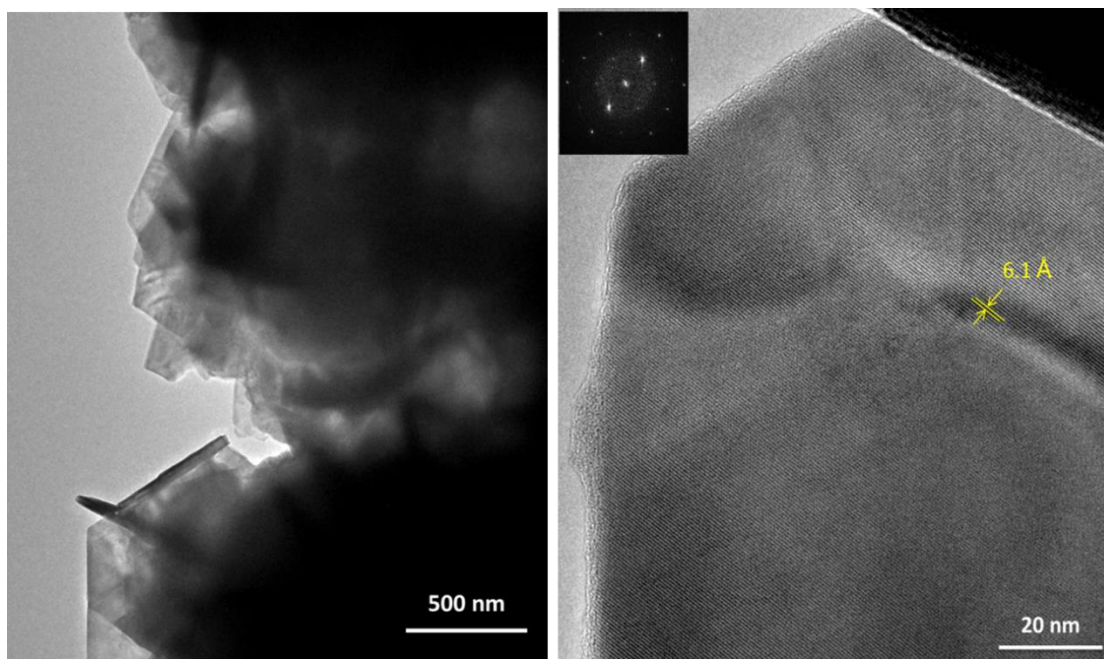


Fig. 2.9 (a) TEM and (b) HRTEM images of uncapped nickel sulfide

2.3.2 Effect of precursor concentrations

To understand the formation mechanism of hierarchical ball-like structures with respect to the phase changes, further experiments were carried out with different precursor material concentrations such as A/5 and A/10. Table 2.2 shows details of the phases present in the synthesized products with respect to concentration. At the lower A/10 concentration, the nickel source was fixed at 0.05 mol, the sulfur source at 0.1 mol and the EDTA capping agent at 0.02 mol. A typical XRD pattern of the as-prepared nickel sulfide samples is shown in Fig. 2.10. All the diffraction peaks of the A/10 sample were well matched with the Joint Committee on Powder Diffraction Standards (JCPDS) card number 01-075-0613 for the NiS_2 and 03-065-3419 for the NiS phase.

Table 2.2 Phases observed with different experimental conditions.

Different concentrations of precursor materials $\text{Ni}(\text{NO}_3)_2 \cdot 6\text{H}_2\text{O} : \text{CH}_4\text{N}_2\text{S} : \text{EDTA}$	Phases from XRD analysis
A/10 (0.05 mol : 0.1 mol : 0.02 mol)	NiS (03-065-3419) NiS ₂ (01-075-0613)
A/5 (0.1 mol : 0.2 mol : 0.04 mol)	Ni ₁₇ S ₁₈ (01-089-3058) NiS ₂ (01-075-0613)
A (0.5 mol : 1.0 mol : 0.2 mmol)	Ni ₁₇ S ₁₈ (01-089-3058) Ni ₃ S ₄ (01-076-1813)

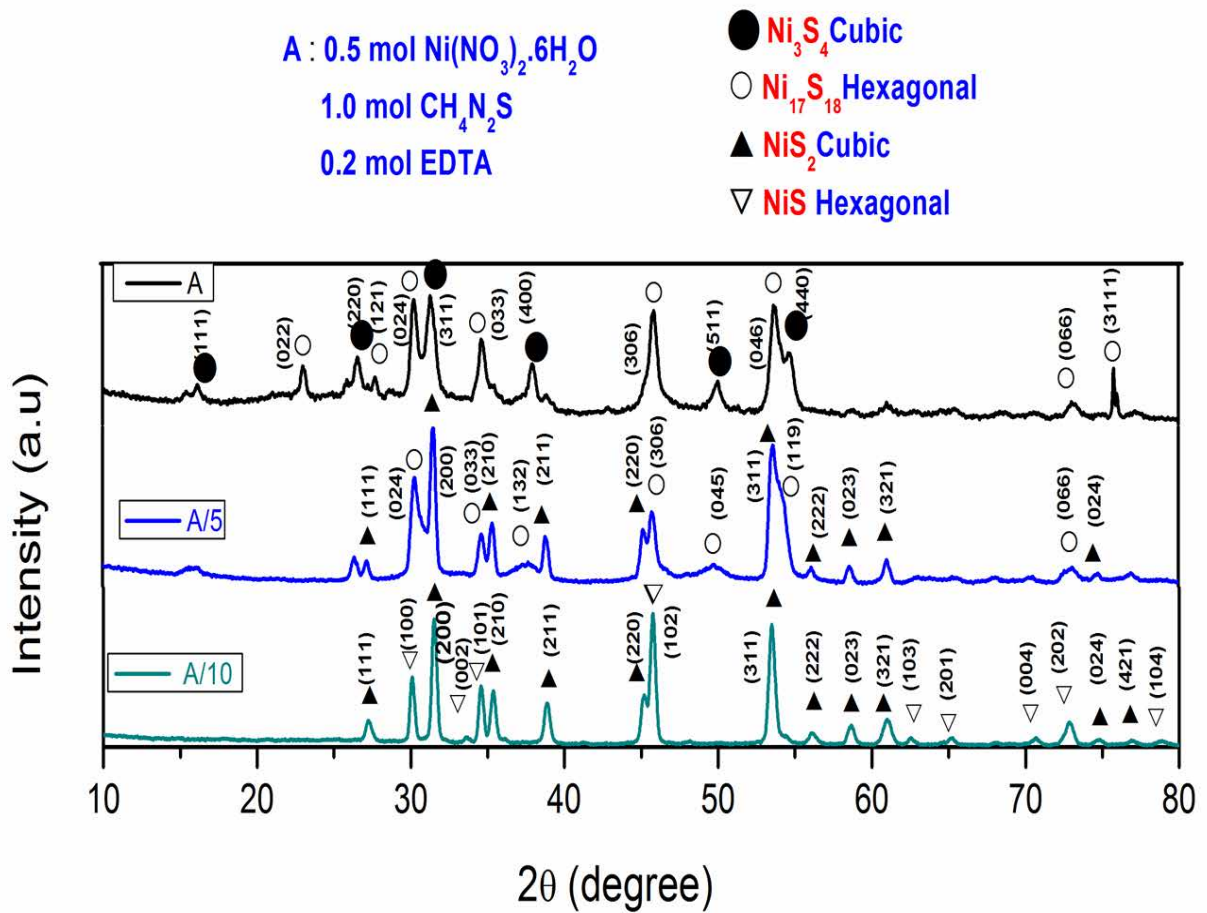


Fig. 2.10 XRD patterns for different stoichiometric precursor material concentrations.

For the A/5 concentration, a large change was observed in the XRD pattern. A phase transformation was observed from NiS to Ni₁₇S₁₈, which can be seen from a shift in the dominant peak positions from 30.06°, 34.55°, and 45.73° to 30.16°, 34.62°, and 45.70°.

respectively (see Fig. 2.10). Along with the $\text{Ni}_{17}\text{S}_{18}$, a NiS_2 phase also appeared and matched the JCPDS card number 01-089-3058 closely. A further increase in concentration (A) resulted in a phase change from NiS_2 to Ni_3S_4 . The new Ni_3S_4 phase matched the JCPDS card number 01-076-1813 closely.

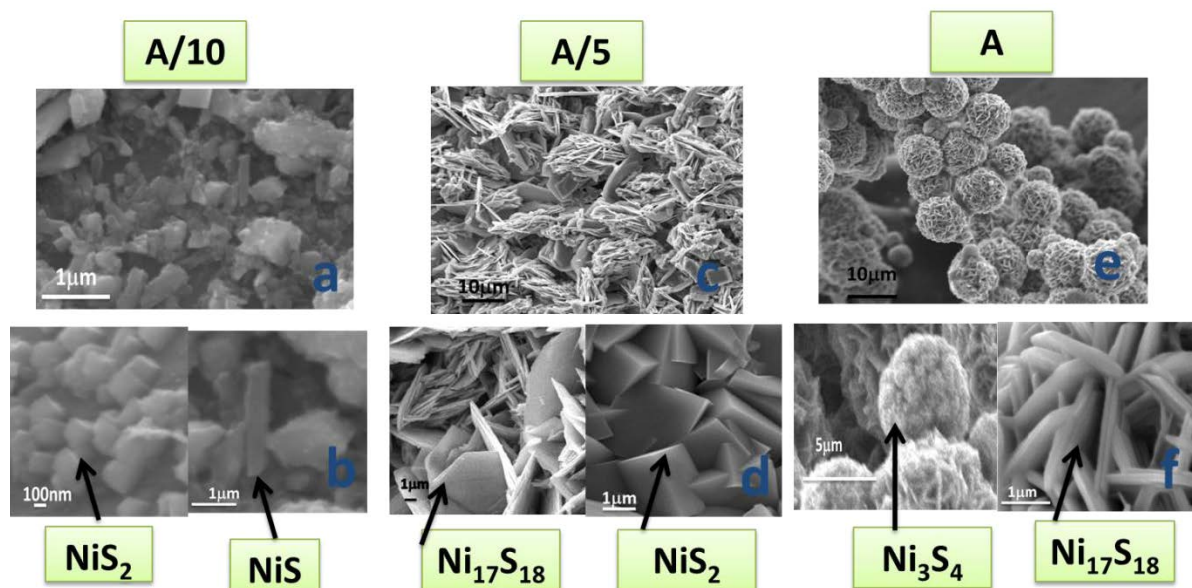


Fig. 2.11 FESEM images for (a,b) A/10, (c,d) A/5, and (e,f) A source material concentrations.

Figures 2.11 (a)–(f) and 2.12 (a)–(f) show the FESEM and TEM images, respectively, of the nickel sulfide samples with different precursor concentrations (a and b) A/10, (c and d) A/5 and (e and f) A. For the A/10 concentration, the product was composed of cubic and rod-like structures, which were nanometers to hundreds of nanometers in size. The TEM images support the observation of mixed morphologies of cubic and rod-like structures as shown in Fig. 2.12 (a). The 2.5 Å interplanar spacing matched the distance between the crystal planes of (210) of the NiS_2 phase as mentioned in Fig. 2.12 (b). The corresponding

Fast-Fourier-Transform (FFT) pattern showed that the synthesized product was crystalline.

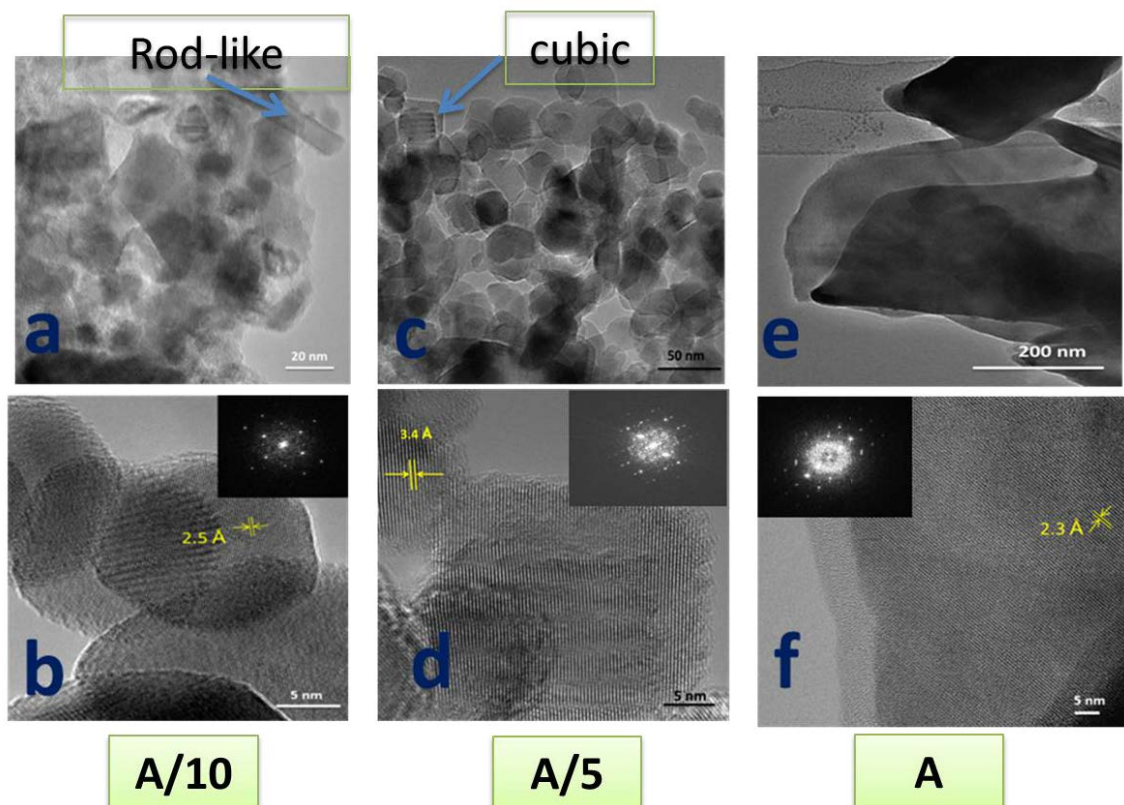


Fig. 2.12 TEM and HRTEM images for (a,b) A/10, (c,d) A/5, and (e,f) A source material concentrations.

When the concentration was increased to A/5, the product was flower-like with a few cubic structures as shown in Fig. 2.11 (c). As can be seen from Fig 2.12 (d), nanosheet-like structures were arranged in flower-like architectures for the sample with A/5 concentrations. Figure 2.12 (c) and (d) are the TEM and HRTEM images, respectively, of the A/5 sample. The TEM images indicate the presence of cubic-shaped nanocrystals and the HRTEM images show that the product is crystalline. The interplanar spacing of 3.4 Å corresponds to the NiS₂ (111) phase. These results are in agreement with the XRD results and show that the product morphology is affected significantly by concentration. The TEM results confirm the mixed

NiS phase. At the A concentration, monodispersed hierarchical morphology was observed as shown in Fig. 2.11 (e) and (f). The monodispersed hierarchical structures were composed of nanosheets and the ball-like structures were composed of cubic nanoparticles. The average diameter of nanosheets was 6–8 μm and that of cube balls diameter was 3–4 μm . Figure 2.12 (e) and (f) show the TEM and HRTEM images of the A sample. The interplanar distance of 2.3 \AA matched the (400) crystalline plane of cubic Ni_3S_4 closely. The clear lattice fringes and FFT pattern confirmed the quality of the prepared materials.

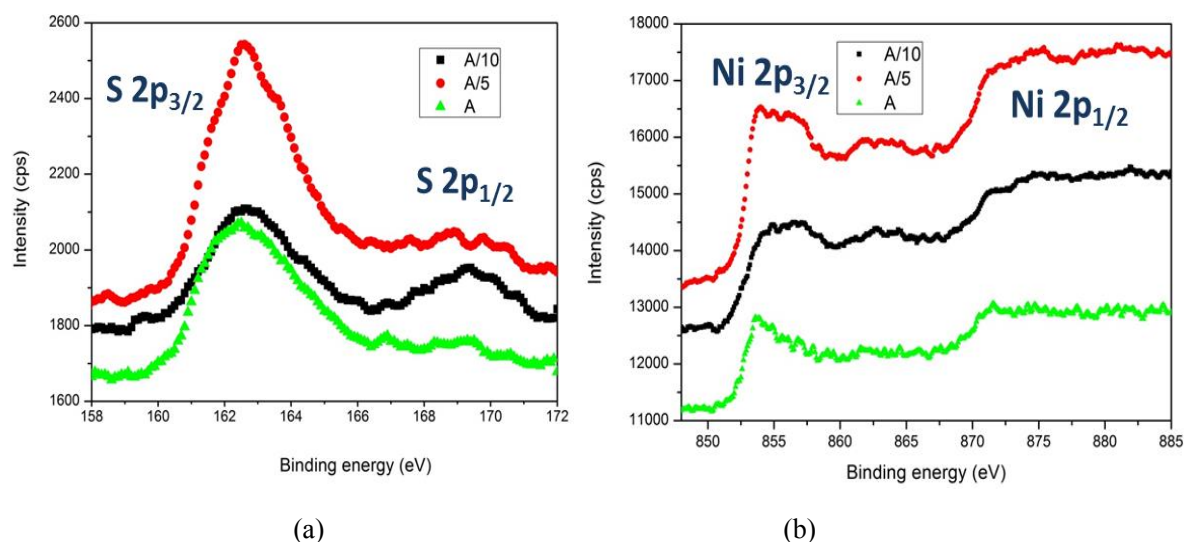


Fig. 2.13 XPS spectra of nickel sulfides after Ar ion etching: (a) S and (b) Ni peaks.

Figure 2.13 (a) and (b) show the XPS spectra of nickel sulfide prepared from different precursor concentrations A/10, A/5, and A. The doublet peaks at 162.5 and 169.2 eV (Fig. 2.13 (a)) correspond to the S 2p_{3/2} and 2p_{1/2} binding energies, and agree closely with literature values²⁸. The doublet peaks of S 2p indicate the presence of mono- and polysulfide for all concentrations tested. Two distinct peaks at 853 and 870 eV correspond to the 2p_{3/2} and 2p_{1/2} states of Ni in nickel sulfide, respectively^{29,30}. The absence of a satellite region of 856

eV at the A concentration supports the fact that there was no nickel sulfate peak (NiSO_4)³¹.

2.3.3 Effect of sulfur source concentrations

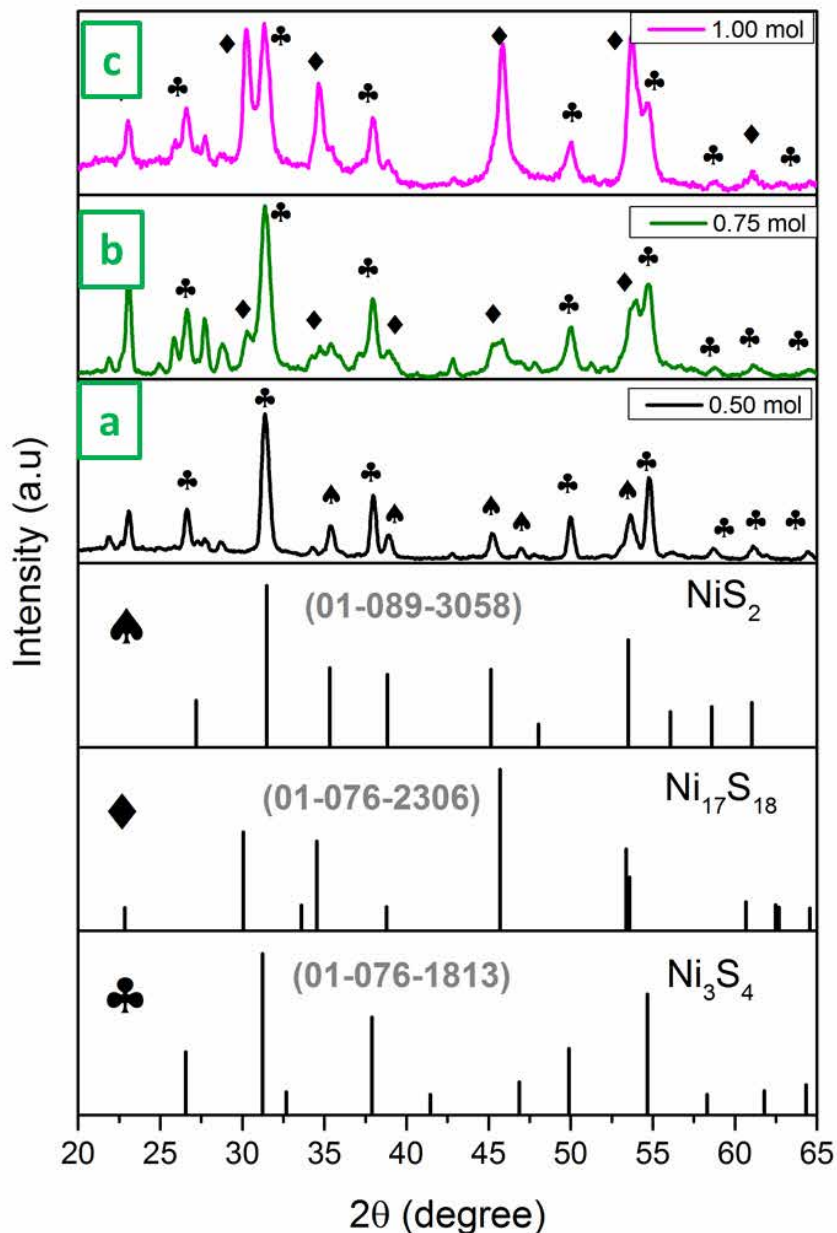


Fig. 2.14 XRD patterns for different sulfur source concentrations a) 0.50 mol b) 0.75 mol and c) 1.00 mol.

To understand the importance of thiourea as a sulfur source, different experiments were carried out by fixing the nickel source concentration as 0.50 mol and capping agent concentration as 0.20 mol. Sulfur source was varied as 0.50, 0.75 and 1.0 mol. Fig. 2.14 and

Fig. 2.15 show the XRD patterns and FESEM images of samples with different sulfur source concentrations.

Table 2.3 Different concentrations of sulfur source experimental conditions.

Experiment	Nickel nitrate (mol)	Thiourea (mol)	EDTA (mol)	Phases observed from XRD analysis
1	0.50	0.50	0.20	NiS ₂ and Ni ₃ S ₄
2	0.50	0.75	0.20	Ni ₁₇ S ₁₈ and Ni ₃ S ₄
3	0.50	1.00	0.20	Ni ₁₇ S ₁₈ and Ni ₃ S ₄

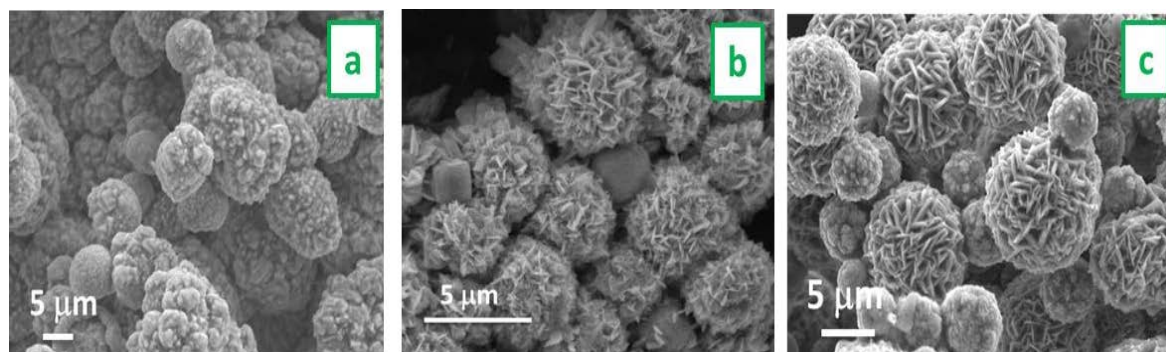


Fig. 2.15 FESEM images a) 0.50 mol b) 0.75 mol and c) 1.00 mol of sulfur source concentrations.

When the concentration was fixed as 1:1 ratio of sulfur to nickel ions, it resulted in the formation of two different phases of nickel sulfide (NiS₂ and Ni₃S₄). When the sulfur concentration was increased to 0.75 mol, reaction between the nickel-EDTA complex and sulfur was increased. This resulted in the appearance of new phase of Ni₁₇S₁₈. Presence of more sulfur ions was favored to react with more number of nickel ions, which resulted the formation of Ni₁₇S₁₈ phase with sheet-like morphology as observed in the FESEM images (Fig. 2.15 (b)). Further increase in the concentration of sulfur with the nickel to sulfur ratio

1:2, stable phases of nickel sulfide ($\text{Ni}_{17}\text{S}_{18}$ and Ni_3S_4) with thick sheets composed hierarchy morphologies were formed.

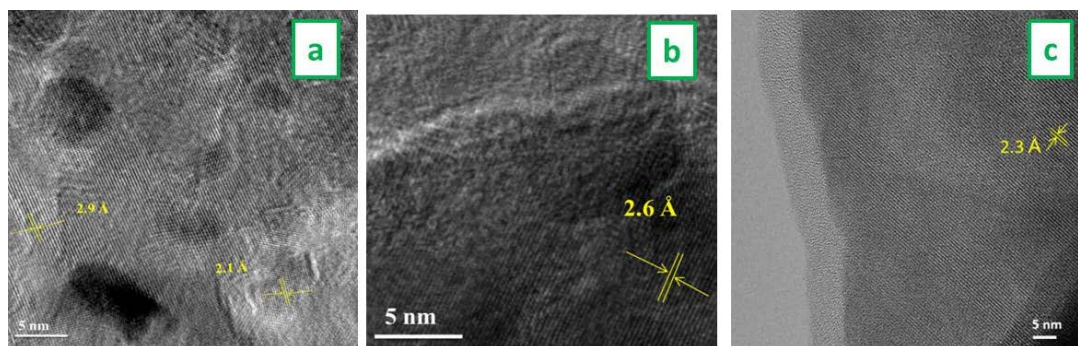


Fig. 2.16 HRTEM images a) 0.50 mol b) 0.75 mol and c) 1.00 mol of sulfur source concentrations.

Fig.2.16 (a) and (b) show the HRTEM images of different sulfur source concentrations. In Fig. 2.16 (a), the interplanar distance of 2.9 Å was well matched with the (311) peak of Ni_3S_4 phase, similarly, interplanar distance of 2.6 Å from Fig.2.16 (b) was well matched with the (244) peak of Ni_3S_4 phase.

2.3.4 Effect of nickel source concentrations

The influence of nickel concentration on the formation of hierarchical structure evolution was studied with the help of different nickel source concentrations experiments and the final phases were shown in table 2.4. Other parameters such as, capping agent, temperature and reaction period and sulfur source were kept constant. The synthesized products XRD patterns are shown in Fig. 2.17 with the corresponding JCPDS reference patterns. When the concentration ratio of nickel to sulfur source 1:2, two different phases were synthesized as Ni_3S_4 and $\text{Ni}_{17}\text{S}_{18}$. The corresponding FESEM images were well discussed

with the previous section (see Fig. 2.15 c and Fig. 2.18 a). The increase in concentration of nickel source as 0.75 mol resulted in the phase change of Ni_3S_4 to NiS_2 observed from the XRD pattern of Fig. 2.17 (b). Morphological changes appeared in the FESEM images of Fig. 2.18 (b). i.e, the sheet composed architectures of $\text{Ni}_{17}\text{S}_{18}$ phase appeared with cube constructed architectures of NiS_2 . The TEM and HRTEM images of 0.75 mol concentration is shown in Fig. 2.19 (a and b). The distance between the atomic planes 5.7 Å was related to the sulfur peak which is present at 22° of 2θ (see Fig. 2.17 b). The small traces of sulfur were synthesized with nickel sulfide phases. The increase of more nickel source with 1.0 mol (2:2 nickel to sulfur ratio), single phases of nickel sulfide (NiS_2) was synthesized as shown in Fig. 2.19 (c). The FESEM image was observed as cube constructed hierarchical architectures in Fig. 2.18 (c). TEM image and HRTEM image shows that the cubic nanoparticles were assembled as microstructures of hierarchical morphology. The lattice distances of 2.5 Å in Fig. 2. 19 (d) was well matched with the (200) plane of NiS_2 in the XRD pattern.

Table 2.4 Different concentrations of sulfur source experimental conditions.

Experiment	Nickel nitrate (mol)	Thiourea (mol)	EDTA (mol)	Phases observed from XRD analysis
1	0.50	1.00	0.20	$\text{Ni}_{17}\text{S}_{18}$ and Ni_3S_4
2	0.75	1.00	0.20	NiS_2 and $\text{Ni}_{17}\text{S}_{18}$
3	1.00	1.00	0.20	NiS_2

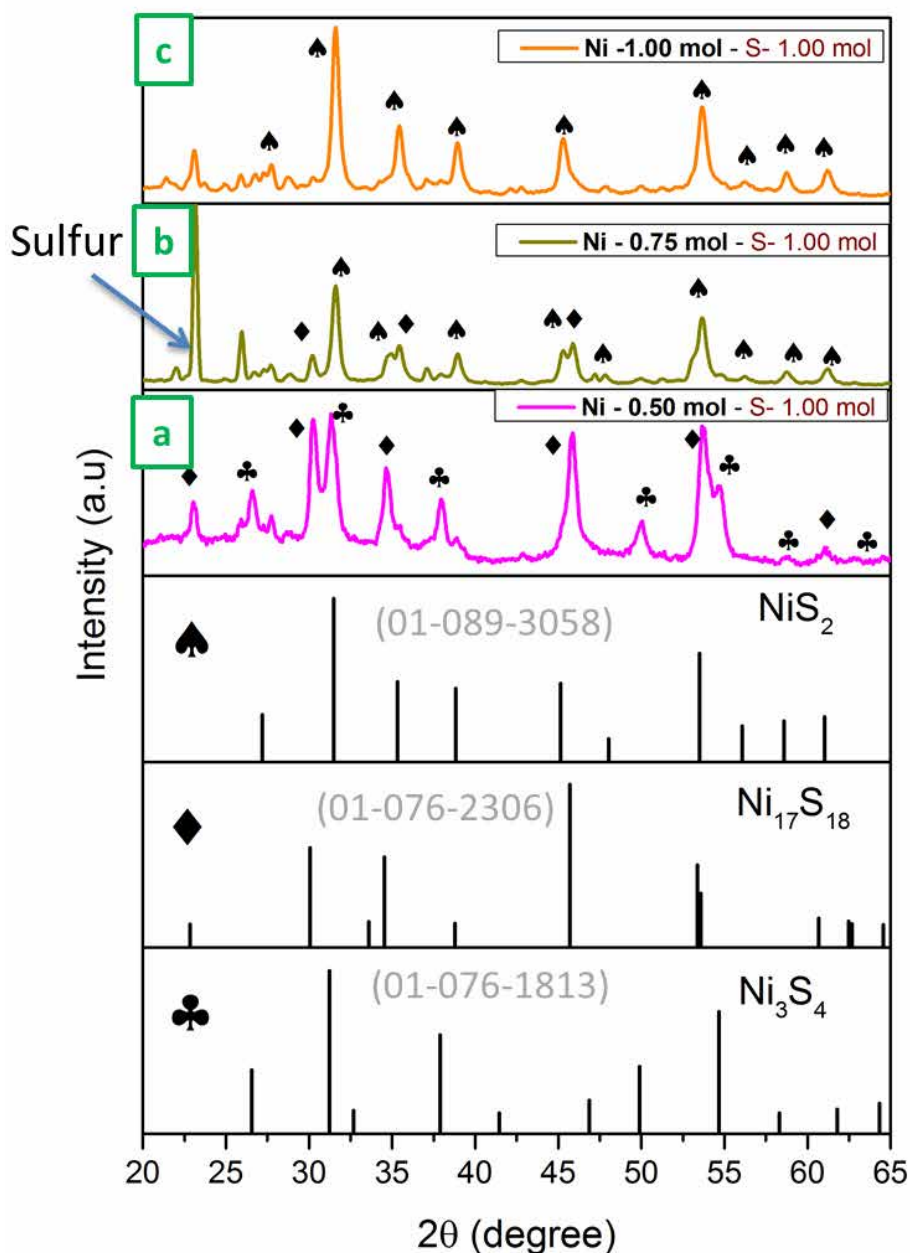


Fig. 2.17 XRD patterns for different nickel source concentrations a) 0.50 mol b) 0.75 mol and c) 1.00 mol.

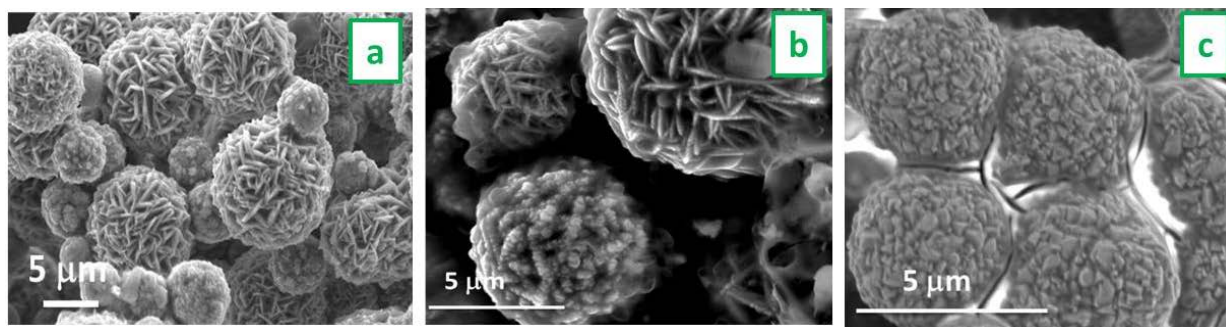


Fig. 2.18 FESEM images of different nickel source concentrations a) 0.50 mol b) 0.75 mol and c) 1.00 mol.

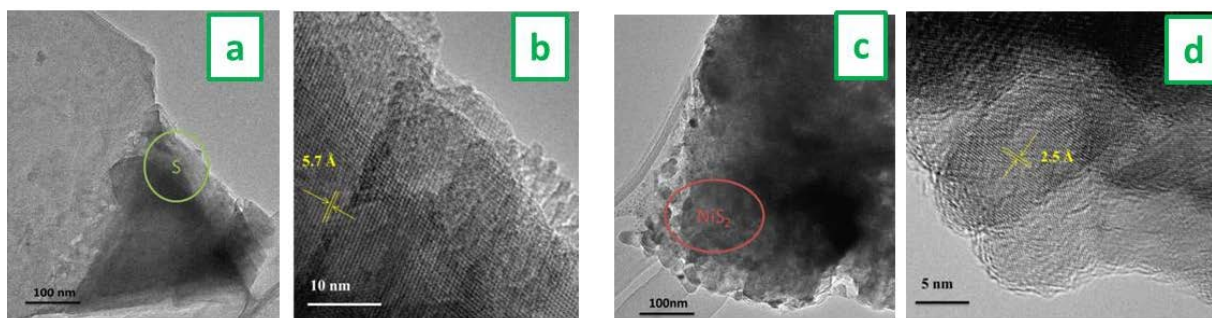


Fig. 2.19 (a, b) TEM and HRTEM images of nickel source concentration of 0.75 mol (c and d) TEM and HRTEM images of nickel source concentration of 1.00 mol.

2.3.5 Catalytic activity of nickel sulfide catalysts for the reduction of 4-nitrophenol

The catalytic property of the synthesized nickel sulfide architectures was evaluated by employing the reduction of 4-nitrophenol into 4-aminophenol^{32,33}. During the reaction, active hydrogen species are firstly transferred to the surface of synthesized products and then the reduction of 4-nitrophenol was taken place by the reaction of adsorbed 4-nitro phenol molecules. The kinetic process was monitored by UV-vis spectroscopy measurements. Fig.2.20 shows the absorbance spectra of 4-nitro phenol and the catalytic reduction with the nickel sulfide products such as A, A/5 and A/10. The absorbance peak at 400 nm was directly associated with the concentration of 4-nitrophenolate ions.

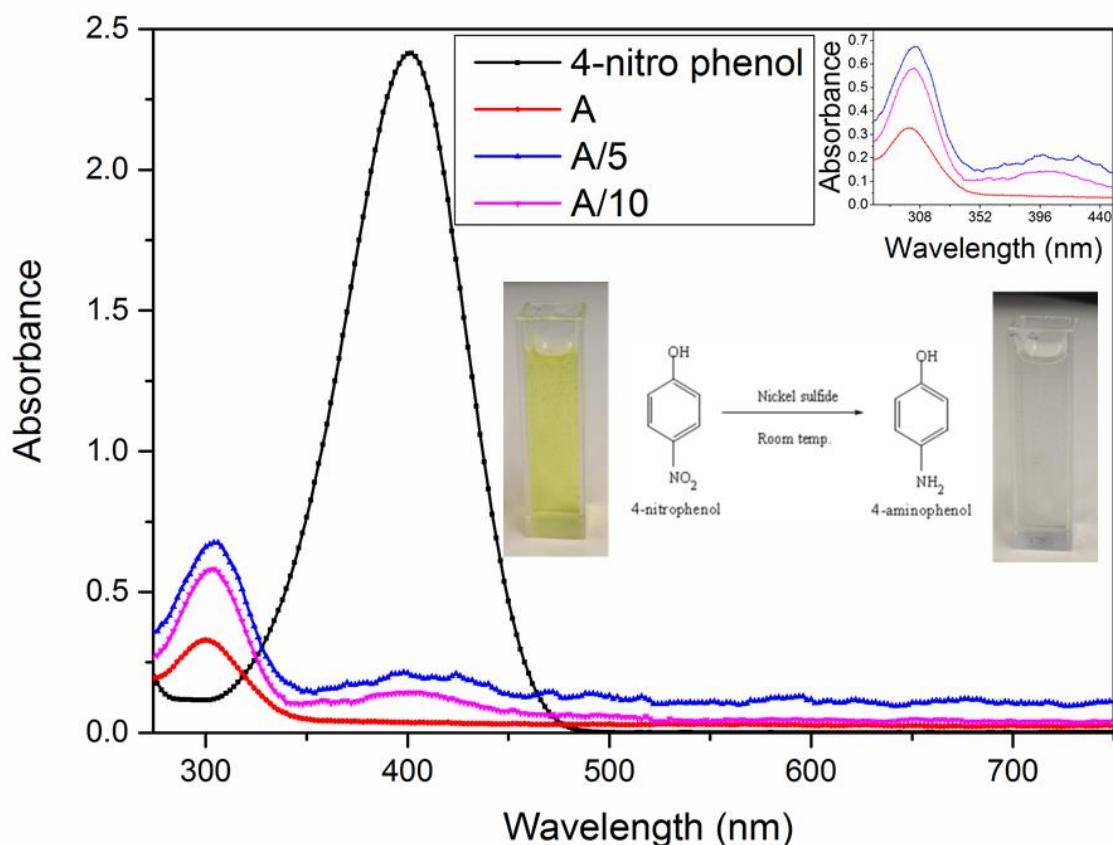


Fig. 2.20 UV-vis spectrum of reduction of 4-NP using nickel sulfide architectures.

Absorbance nature of the catalyst was measured as a function of time. The addition of A/10 and A/5 resulted in a steady decrease in the concentration of 4-nitrophenolate ions in solution as seen in the absorbance spectra. The sample A showed complete disappearance of Ab_{S400nm} compared to the other sample A/10 and A/5 (see Fig.2.20 inset). In addition, the appearance of new peak at 293 nm indicated the formation of 4-aminophenol. All the catalytic reaction was observed with 4-NP for the period of 3 min. The above results clearly demonstrated that the existence of the phases of Ni_3S_4 and $Ni_{17}S_{18}$ greatly enhanced the catalytic property.

2.3.6 Mechanism of hierarchical structures evolution:

Fig. 2.21 (a) and (b) shows the schematics of reaction mechanism and growth process of different nickel sulfide architectures. At the A/10 concentration, the limited availability of nickel and sulfur ions in the precursor solution resulted in simple and near stoichiometric phases of NiS₂ and NiS. Further increase in the concentration of source material in A/5 increased the availability of more molecules for reaction, which leads to the formation of different sulfur-rich phases as shown in Fig. 2.10.

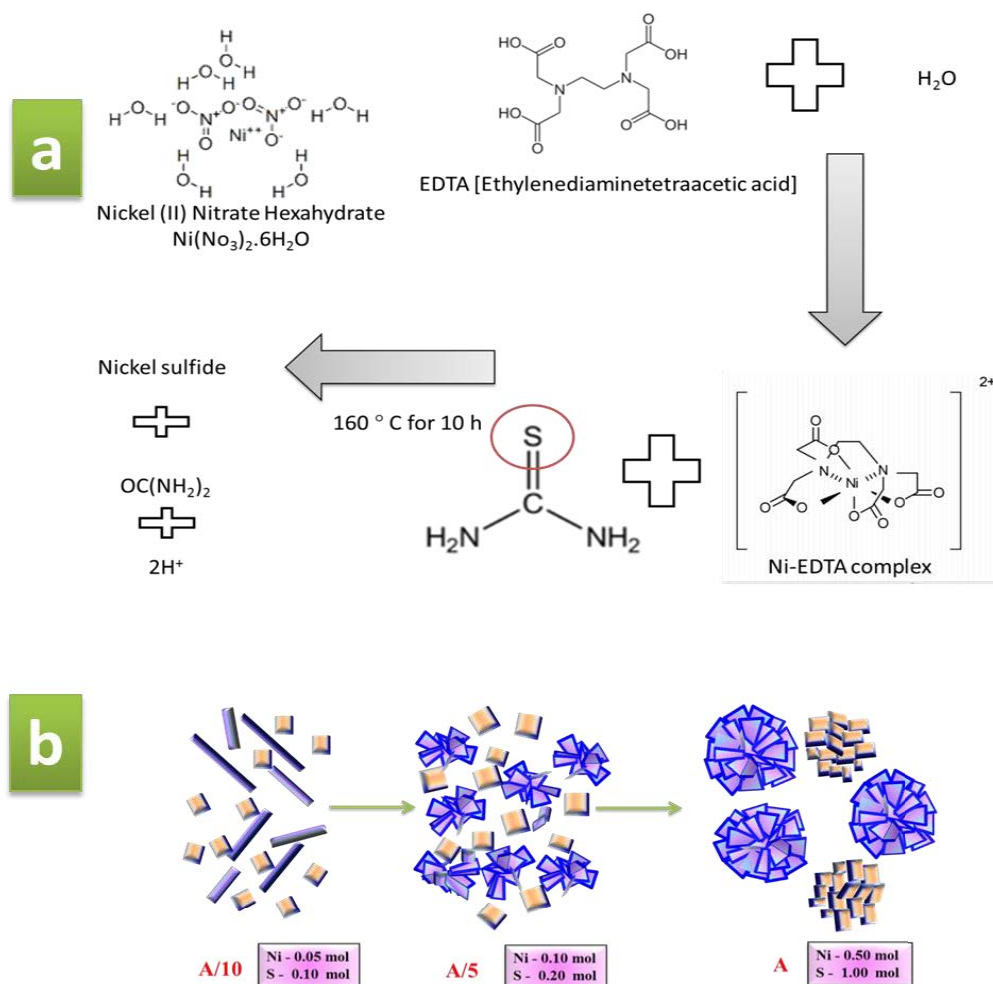


Fig. 2.21 Schematics of (a) reaction mechanism and (b) growth process of different nickel sulfide architectures

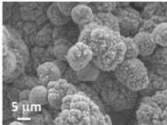
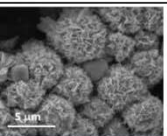
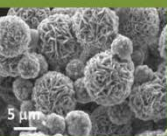
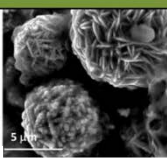
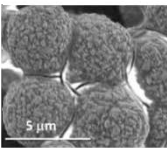
The rod-like morphology was changed to sheet-like morphology due to the addition of source materials. The growth was taken place on the rods and thus the morphology was changed. Further increase of source material (A), the morphology of the sample eventually changed to three dimensional hierarchical structures (Fig. 2.11 (e) and (f)). This is mainly due to the Oswald ripening mechanism³⁴. The high concentration of precursor solution resulted in the formation of different phases of nickel sulfide (Ni_3S_4 and $\text{Ni}_{17}\text{S}_{18}$) confirmed by XRD analysis (Fig. 2.10).

From the catalytic activity of the nickel sulfide catalysts, the reduction ability of sample A was better than the samples A/5 and A/10. Sample A was consisted of two different phases of Ni_3S_4 and $\text{Ni}_{17}\text{S}_{18}$. N. Mahmood et.al, demonstrated the importance of Ni_3S_4 as a catalytic material for the application of lithium ion batteries³⁵. $\text{Ni}_{17}\text{S}_{18}$ was a pure metallic phase with the advantage of having two different catalytic phases in a synthesized product A, therefore the activity was enhanced. The sample A/5 and A/10 consisted of semiconducting phase of NiS_2 along with NiS .

From the different sulfur source concentrations, it is well understood that all different higher concentrations were feasible to form hierarchical architectures. However, amount of sulfur concentration played significant role in the formation of building blocks. When the amount of sulfur concentration was very less or equal ratio of sulfur to nickel ions, reaction between the nickel-EDTA complex and sulfur anion was dominant for the formation

of Ni_3S_4 . A small quantity of NiS_2 was also retained with Ni_3S_4 phases. When the amount of sulfur source was increased to 0.75 mol, thin-sheets composed hierarchical structures ($\text{Ni}_{17}\text{S}_{18}$) were formed with cube constructed balls (Ni_3S_4). The ratio of nickel to sulfur ions of 1:2 resulted in the thick sheets composed balls with cube composed architectures.

Table 2.4 Different phases of hierarchical nickel sulfides.

Experiment	Nickel Nitrate (mol)	Thiourea (mol)	EDTA (mol)	Phases from XRD	Observed Morphologies
1	0.50	0.50	0.20	NiS_2 & Ni_3S_4	
2	0.50	0.75	0.20	Ni_3S_4 & $\text{Ni}_{17}\text{S}_{18}$	
3	0.50	1.00	0.20	Ni_3S_4 & $\text{Ni}_{17}\text{S}_{18}$	
4	0.75	1.00	0.20	NiS_2 & $\text{Ni}_{17}\text{S}_{18}$	
5	1.00	1.00	0.20	NiS_2	

The corresponding results of different nickel concentrations showed the linear change in the synthesized phases as well as morphology. NiS_2 phase was formed when the nickel source concentration varied from 0.50 to 0.75 mol. The increase in more amount of nickel source (1.0 mol) reduced to a single nickel sulphide phase with uniform morphology. These resulted

were well agreed along with different sulphur source concentration experiment. In table. 2.4 different hierarchical structures were summarized with their corresponding source concentrations. The experimental results demonstrate that the precursor concentration plays a significant role in the formation of hierarchical structures and different nickel sulfide phases.

2.4 Conclusion

Monodispersed nickel sulfide hierarchical structures were synthesized by the hydrothermal method. The effect of EDTA capping agent and different concentrations of source materials on the phase, morphology, and stoichiometric ratio were investigated. The addition of an EDTA capping agent resulted in uniform size and morphology. Different precursor material concentrations of A/10, A/5, and A were used to observe the phase changes in the synthesized products. Single phase nickel sulfide (NiS_2) hierarchical structures were synthesized by controlling nickel source. Morphological phase change behavior of all of the synthesized materials was studied using FESEM and TEM analysis. Flower- and ball-like sheet architectures were visible. A significant change in the nickel sulfide phases was observed with respect to source material concentration by XRD analysis. The sulfur-rich Ni_3S_4 and $\text{Ni}_{17}\text{S}_{18}$ phases consisted of two different hierarchical structures which enhanced the catalytic activity.

References

- (1) Li, Y.; Shen, W. *Chem. Soc. Rev.* **2014**, *43*, 1543–1574.
- (2) Wang, C.; Li, Q.; Wang, F. F.; Xia, G.; Li, D.; Li, N.; Spendelow, J.; Wu, G. *ACS Appl. Mater. Interfaces* **2014**, *6*, 1243–1250.
- (3) Milliron, D. J.; Hughes, S. M.; Cui, Y.; Manna, L.; Li, J.; Wang, L.-W.; Alivisatos, a P. *Nature* **2004**, *430*, 190–195.
- (4) Yang, J.; Bao, C.; Zhu, K.; Yu, T.; Li, F.; Liu, J.; Li, Z.; Zou, Z. *Chem. Commun. (Camb)*. **2014**, *50*, 4824–4826.
- (5) Lee, J.-H. *Sensors Actuators B Chem.* **2009**, *140*, 319–336.
- (6) Pang, H.; Wei, C.; Li, X.; Li, G.; Ma, Y.; Li, S.; Chen, J.; Zhang, J. *Sci. Rep.* **2014**, *4*, 3577, 1–8.
- (7) Yang, J.; Bao, C.; Zhu, K.; Yu, T.; Li, F.; Liu, J. **2014**, 1–4.
- (8) Wang, Y.; Zhu, Q.; Tao, L.; Su, X. *J. Mater. Chem.* **2011**, *21*, 9248–9254.
- (9) Hu, J.-S.; Ren, L.-L.; Guo, Y.-G.; Liang, H.-P.; Cao, A.-M.; Wan, L.-J.; Bai, C.-L. *Angew. Chem. Int. Ed. Engl.* **2005**, *44*, 1269–1273.

- (10) Chen, Z.-G.; Zou, J.; Liu, G.; Lu, H. F.; Li, F.; Lu, G. Q.; Cheng, H. M. *Nanotechnology* **2008**, *19*, 055710, 1–5.
- (11) Braga, A.; Giménez, S.; Concina, I.; Vomiero, A.; Mora-Seró, I. *J. Phys. Chem. Lett.* **2011**, *2*, 454–460.
- (12) Lai, C.-H.; Lu, M.-Y.; Chen, L.-J. *J. Mater. Chem.* **2012**, *22*, 19–30.
- (13) Li, T.-L.; Lee, Y.-L.; Teng, H. *J. Mater. Chem.* **2011**, *21*, 5089–5098.
- (14) Stein, A.; Bailey, S. M. *Redox Biol.* **2013**, *1*, 32–39.
- (15) Liu, T.; Zhao, Y.; Gao, L.; Ni, J. *Sci. Rep.* **2015**, *5*, 9307, 1–5.
- (16) Zhang, B.; Ye, X.; Dai, W.; Hou, W.; Xie, Y. *Chem. - A Eur. J.* **2006**, *12*, 2337–2342.
- (17) Shi, Y.; Wang, Y.; Wong, J. I.; Tan, A. Y. S.; Hsu, C.-L.; Li, L.-J.; Lu, Y.-C.; Yang, H. *Y. Sci. Rep.* **2013**, *3*, 2169, 1–8.
- (18) Zhang, Z.; Wang, Q.; Zhao, C.; Min, S.; Qian, X. *ACS Appl. Mater. Interfaces* **2015**, *7*, 4861–4868.
- (19) Mao, L.; Wang, Y.; Zhong, Y.; Ning, J.; Hu, Y. *J. Mater. Chem. A* **2013**, *1*, 8101–8104.

- (20) Zhou, J.; Tian, G.; Chen, Y.; Shi, Y.; Tian, C.; Pan, K.; Fu, H. *Sci. Rep.* **2014**, *4*, 4027, 1–9.
- (21) Meng, Z.; Peng, Y.; Yu, W.; Qian, Y. *Mater. Chem. Phys.* **2002**, *74*, 230–233.
- (22) Jiang, X.; Xie, Y.; Lu, J.; Zhu, L.; He, W.; Qian, Y. *Adv. Mater.* **2001**, *13*, 1278–1281.
- (23) Salavati-niasari, M.; Davar, F.; Emadi, H. **2010**, *7*, 647–655.
- (24) Liu, X. *Mater. Sci. Eng. B* **2005**, *119*, 19–24.
- (25) Reddy, D. A.; Murali, G.; Vijayalakshmi, R. P.; Reddy, B. K. *Appl. Phys. A* **2011**, *105*, 119–124.
- (26) Mondal, S.; Verma, S. *Zeitschrift für Anorg. und Allg. Chemie* **2014**, *640*, 1095–1101.
- (27) Gnanam, S.; Rajendran, V. *J. Phys. Sci.* **2013**, *17*, 185–190.
- (28) Krishnakumar, S.; Sarma, D. *Phys. Rev. B* **2003**, *68*, 155110, 1–7.
- (29) Chi, W. S.; Han, J. W.; Yang, S.; Roh, D. K.; Lee, H.; Kim, J. H. *Chem. Commun. (Camb)*. **2012**, *48*, 9501–9503.
- (30) Nesbitt, H. W.; Legrand, D.; Bancroft, G. M. *Phys. Chem. Miner.* **2000**, *27*, 357–366.
- (31) Egrand, D. A. L. L.; Esbitt, H. W. A. N.; Ancroft, G. M. I. B. **1998**, *83*, 1256–1265.

- (32) Zhang, J.; Chen, G.; Chaker, M.; Rosei, F.; Ma, D. *Appl. Catal. B Environ.* **2013**, *132-133*, 107–115.
- (33) Yu, T.; Zeng, J.; Lim, B.; Xia, Y. *Adv. Mater.* **2010**, *22*, 5188–5192.
- (34) Haibo Li, Lanlan Chai, Xiaoqing Wang, Xueying Wu, Guangcheng Xi, yankuan Liu, and Y. Q. *J. Cryst. Growth Des.* **2007**, *7*, 1918–1922.
- (35) Mahmood, N.; Zhang, C.; Hou, Y. *Small* **2013**, *9*, 1321–1328.

Chapter 3

Single-step synthesis and catalytic activity of structure-controlled nickel sulfide nanoparticles

3.1 Background

Size effect brings about large effects on the properties of nanoparticles over the bulk materials. Engineering nanoparticles or any intentionally produced nanoparticles less than 100 nm in size with the same chemical composition result in higher orders. There are many studies on the properties of nanoparticles such as, optical¹, magnetic², electrical³, electronic⁴ properties and applications such as catalysis⁵ and biological imaging⁶. Among the various nanocrystals, size-confined metal sulfides have been attracting attention because of its quantum confinement effects⁷. Jin Joo et.al, have investigated the synthesis of various semiconducting nanocrystals (PbS, ZnS, CdS and MnS) by temperature dependent thermolysis method⁸. Synthesized chalcogenide nanoparticle must be environmental friendly in energy applications⁹⁻¹².

Synthesis of nickel sulfide nanoparticles has more complexity due to its availability of number of phases. Nickel sulfide has more complex phases such as NiS (α -NiS and β -NiS), Ni₃S₂, NiS₂, Ni₃S₄, Ni₉S₈, and Ni₇S₆¹³. A wide range of morphology and shapes were investigated by different methods in the recent years¹⁴⁻¹⁹. Previous chapter, I have

synthesized phase controlled hierarchical structures of nickel sulfide²⁰. The synthesis of nickel sulfide phases such as Ni_3S_4 requires a two-step reduction process²¹ to control the phase and morphology. For the better understanding and control of single phase nickel sulfide along with structural and size effects, I have developed a single-step injection process using oleylamine as a solvent.

Temperature-controlled injection reactions have several advantages in the synthesis of nanoparticles, such as low cost and better productivity²². Shape control of sulfur-based nanocrystals by injecting a molecular precursor into high-boiling-point solvents was reported by Lee et al²³. Recently, many groups have focused on using different amines for the size- and structure-controlled synthesis of individual metal sulfide phases^{12,24–26}. The use of oleylamine–metal complexes has been well studied by Joo et al.; they had reported the synthesis of various size-controlled metal sulfides such as PbS, ZnS, CdS, and MnS, with particle sizes of 6–13 nm²⁷. Sulfur–oleylamine interactions lead to the formation of H_2S , which reacts with a metal precursor to form metal sulfide nanoparticles²⁵.

In this chapter, I describe the single-step, structure-controlled synthesis of nickel sulfide nanoparticles with different phases, using a precursor hot-injection (temperature assisted) method with oleylamine as the solvent. The catalytic properties of the different phases of nickel sulfide were investigated.

3.2 Synthesis procedure of phase controlled nickel sulfide

3.2.1 Materials

$\text{Ni}(\text{NO}_3)_2 \cdot 6\text{H}_2\text{O}$ (purity 98 %), elemental sulfur, ethanol (99.5%), 4-nitrophenol, NaBH_4 , and acetone (purity 99.9%) were purchased from Wako Pure Chemical Industries, Ltd., Japan. Oleylamine (70%) was purchased from Sigma Aldrich. The reagents were used without further purification.

3.2.2 Experimental procedure

A typical procedure for nickel sulfide particle synthesis was as follows. Fig. 3.1 shows the schematic view of experimental procedure. $\text{Ni}(\text{NO}_3)_2 \cdot 6\text{H}_2\text{O}$ (1 mmol) was mixed with oleylamine (10 mL) in a 100 mL three-necked flask (A). The solution was heated at 100 °C for 1 h to remove moisture and O_2 in the oleylamine. Elemental sulfur (1 mmol) and oleylamine (10 mL) were placed in a separate 100 mL three-necked flask (B) and heated at 70 °C for 30 min to form a sulfur–amine mixture. The transparent yellow sulfur–oleylamine solution (B) was loaded into a glass syringe and injected into the nickel–oleylamine solution mixture (A). This mixture of the sources in a concentration ratio of 1:1 gave the NiS phase. The temperature was raised to 240 °C and the mixture was continually stirred for 1 h under a N_2 atmosphere to initiate the reaction. After cooling, the particles were collected by

centrifugation, washed with ethanol, and dried under vacuum for 1 h. The particles were dispersed in an organic solvent and stored in a tightly closed container.

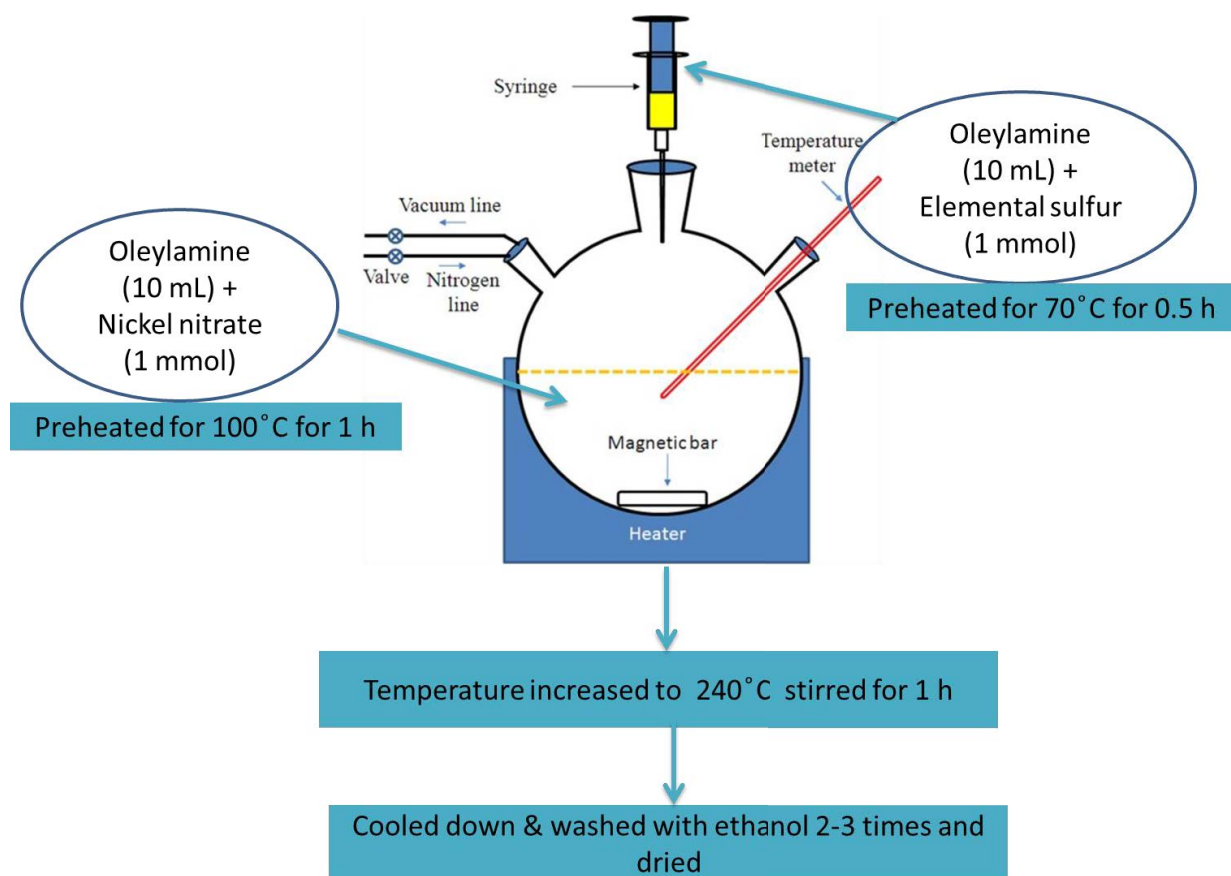


Fig. 3.1 Schematic view of the experimental procedure

Table 3.1 Different concentration ratios of nickel and sulfur sources and the corresponding phases of synthesized materials

Name	Nickel source (g)	Sulfur source (g)	Concentration ratio	Phase
I – 1	0.290	0.032	1:1	NiS
I – 2	0.290	0.064	1:2	NiS ₂
I – 3	0.435	0.064	3:4	Ni ₃ S ₄
I – 4	0.435	0.032	3:2	Ni ₇ S ₆

When the temperature was raised to 210 °C, the sulfur–amine mixture released H₂S, which reacted with the metal–oleylamine complex to form a nickel sulfide product²². These procedures were repeated using Ni(NO₃)₂·6H₂O:elemental sulfur concentration ratios of 1:2, 3:4, and 3:2 to synthesize nickel sulfide nanoparticles with different phases. The oleylamine acted as both a solvent and a capping agent. Table 3.1 shows details of the phases present in the synthesized products with respect to concentration.

3.2.3 Catalytic Study

The catalytic activities of the synthesized nickel sulfide nanoparticles were investigated as follows. Aqueous solutions of 4-nitrophenol (10 mg in 50 mL of distilled water) and NaBH_4 (750 mg in 200 mL of distilled water) were freshly prepared. 4-Nitrophenol and NaBH_4 in a concentration ratio of 1:10 were mixed with nickel sulfide nanoparticles (4.0 mg). The mixture was placed in a quartz cuvette and the reaction was monitored using UV-vis spectroscopy. This step was repeated several times to study the stability of the nanoparticles.

3.2.4 Characterizations

The crystalline phases of the final precipitates were identified by powder X-ray diffraction (XRD) performed at a scan rate of 0.04 s^{-1} in the 2θ range 10° to 80° (RINT-2200 diffractometer, Rigaku, Japan, $\text{CuK}\alpha$ radiation, $\lambda = 1.54178 \text{ \AA}$). The particle sizes and morphologies of the final precipitates were determined using transmission electron microscopy (TEM) and high-resolution TEM (HRTEM; JEOL JEM 2100F) at an accelerating voltage of 200 kV. Binding energies were investigated using X-ray photoelectron spectroscopy (XPS; Shimadzu ESCA 3100). Fourier-transform infrared spectroscopy (FTIR) was performed using a JEOL JIR-WINSPEC 50 spectrometer.

3.3 RESULTS AND DISCUSSION

3.3.1 NiS Phase

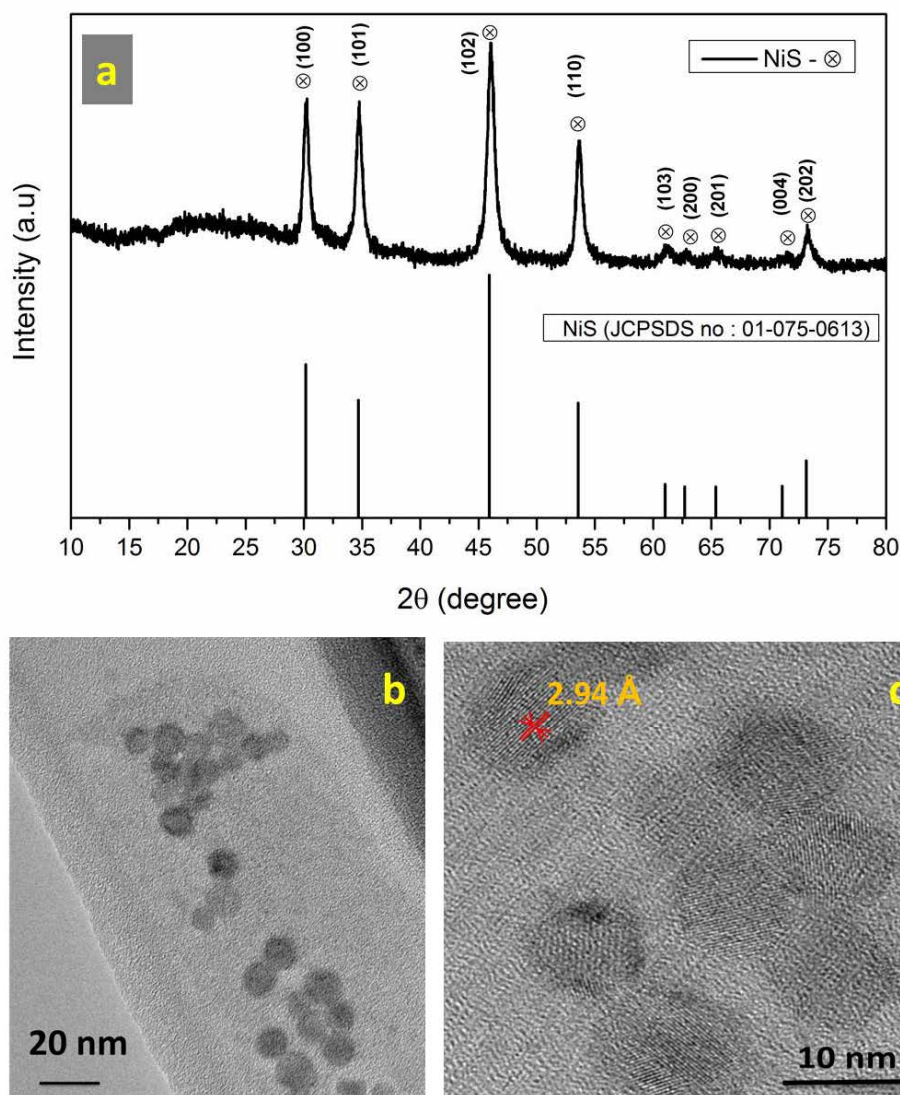


Fig. 3.2 (a) XRD pattern, and (b) TEM and (c) HRTEM images of NiS phase.

A typical XRD pattern of the nickel sulfide particles prepared using the temperature-dependent injection method is shown in Fig. 3.2(a). The pattern shows that the sample is crystalline. The pattern in Fig. 3.2(a) corresponds to the α -NiS phase. The use of a

1:1 concentration ratio of nickel to sulfur in the presence of oleylamine resulted in formation of a nickel monosulfide phase. JCPDS reference 01-075-0613, i.e., α -NiS, matched the synthesized sample well. Fig.2 (b) and (c) show TEM and HRTEM images of the NiS nanoparticles. The TEM image shows that the sizes of the spherical nanoparticles ranged from 8 to 10 nm. The high-magnification image shows that the distance between the atomic layers was 2.94 Å, which matches the d -spacing of the (100) plane of the NiS phase (Fig. 3.2a). A single phase with good crystallinity was obtained in a single step at 210 °C. Oleylamine helped to make the particle size distribution uniform.

3.3.2 NiS₂ Phase

The XRD pattern shown in Figure 3.3(a) matched JCPDS reference 00-011-0099, i.e., the NiS₂ phase. A source material concentration ratio of 1:2 resulted in formation of nickel disulfide nanoparticles. Fig. 3.3(b) and (c) show the sample morphology. The TEM image shows that the cubic particles were well distributed, and of size 6–8 nm. The distance between the atomic layers of the cubic nanoparticles was 2.77 Å (Fig. 3.3c), which matches that of the (200) plane of the NiS₂ phase.

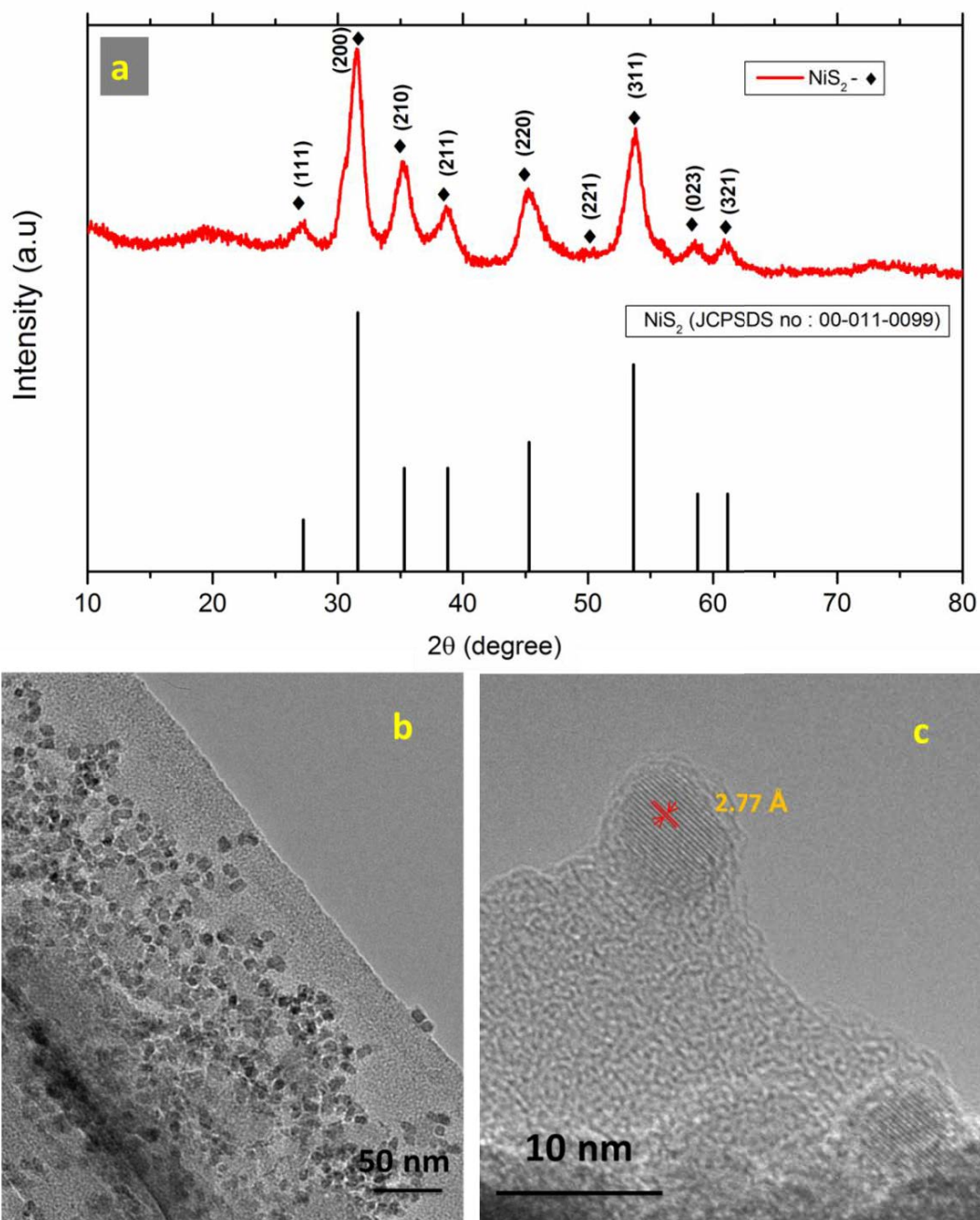


Fig. 3.3 (a) XRD pattern, and (b) TEM and (c) HRTEM images of NiS_2 phase.

3.3.3 Ni_3S_4 Phase

A concentration ratio of 3:4 (nickel source 1.5 mmol, 0.435 g; sulfur source 2 mmol, 0.064 g) gave the sulfur-rich phase Ni_3S_4 . The XRD pattern, shown in Fig. 3.4(a) matched

JCPDS reference 00-047-1739 well. The TEM and HRTEM images in Fig. 3.4(b) and (c) show that the particles had a bulging spherical morphology. The d -spacing observed from the HRTEM image, 2.78 Å, was close to that of the (311) plane (see Fig. 3.4a). The d -spacing value of 2.33 Å corresponded to the (220) plane of the Ni_3S_4 phase.

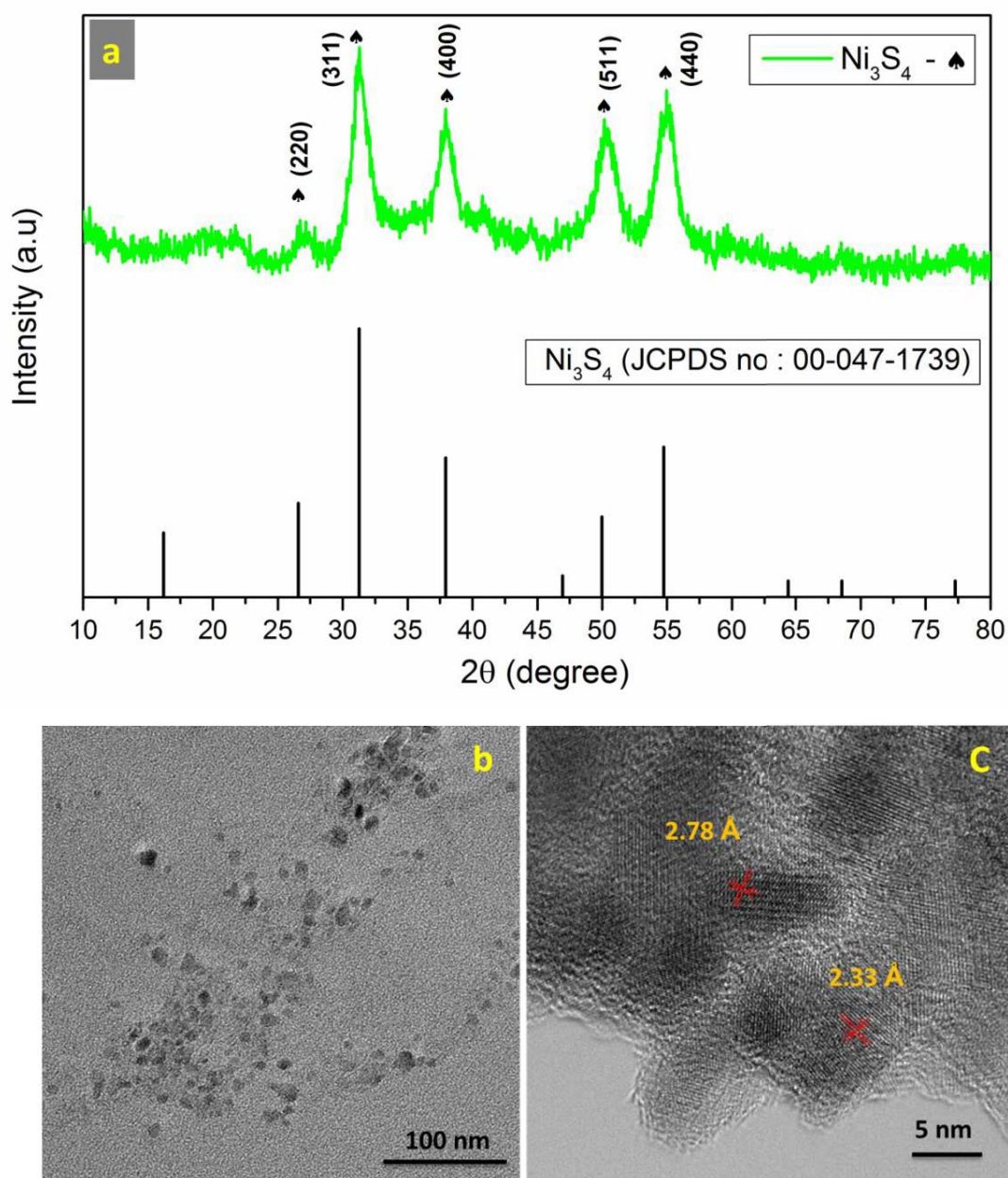


Fig. 3.4 (a) XRD pattern, and (b) TEM and (c) HRTEM images of Ni_3S_4 phase.

3.3.4 Ni₇S₆ Phase

The XRD pattern of the material synthesized using a source concentration ratio of 3:2 matched that of the nickel-rich phase Ni₇S₆ (Fig. 3.5 (a); JCPDS reference 00-014-0364). Fig. 3.5(b) and (c) show the TEM and HRTEM images of Ni₇S₆. The TEM image shows that the well-distributed particles consisted of spherical and elongated spherical particles of size 8–20 nm. The broad particle size distribution is caused by the high nickel concentration in the source. The HRTEM image shows that the distances between the atomic layers in spherical and elongated spherical nanoparticles were different. The spherical nanoparticle *d*-spacing, 2.85 Å, corresponds to the (121) plane and the elongated spherical particle *d*-spacing, 3.12 Å, corresponds to the (042) plane.

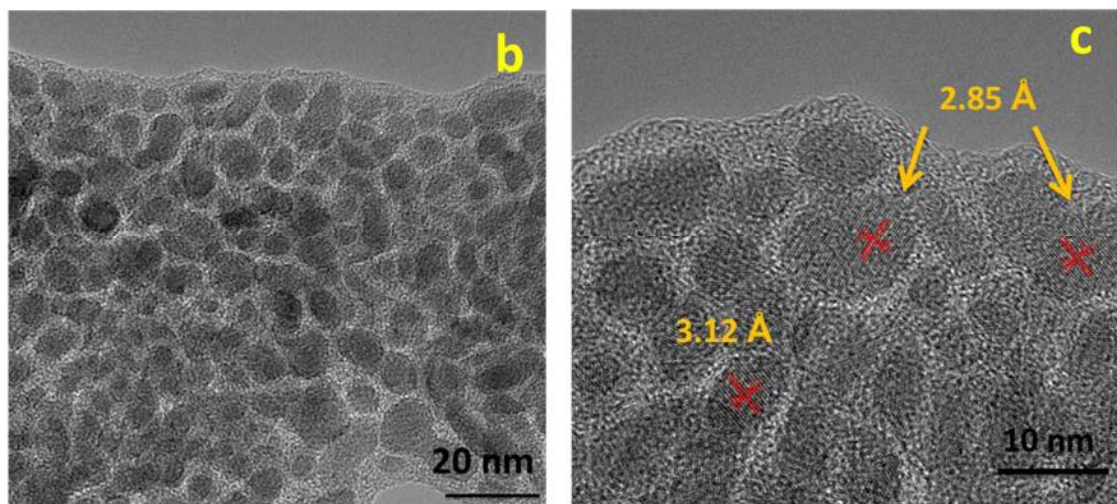
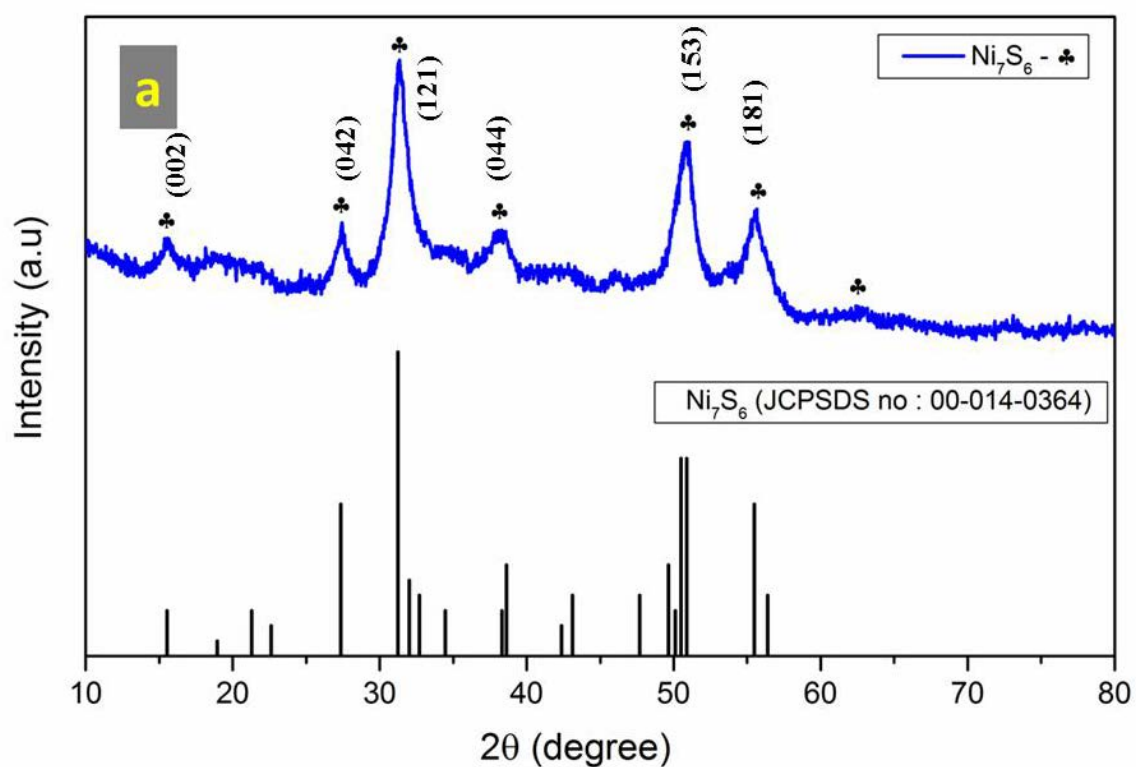


Fig. 3.5 (a) XRD pattern, and (b) TEM and (c) HRTEM images of Ni_7S_6 phase.

3.3.5 FTIR Analysis

Fig. 3.6 shows the FTIR spectra of the synthesized nickel sulfide nanoparticles with different phases. The peaks from the C–H stretching modes are observed at 2921 and

2852 cm^{-1} ,^{28–30}, the broad peak at 3400 cm^{-1} corresponds to the N–H stretching³¹ of free amines, and the peak at 1653 cm^{-1} is related to N–H rocking vibrations. The absence of the peaks at 1389 and 3400 cm^{-1} in the spectrum of the Ni_7S_6 sample indicates lower reactivity's of the C–N and N–H bonds in organic ligands³¹.

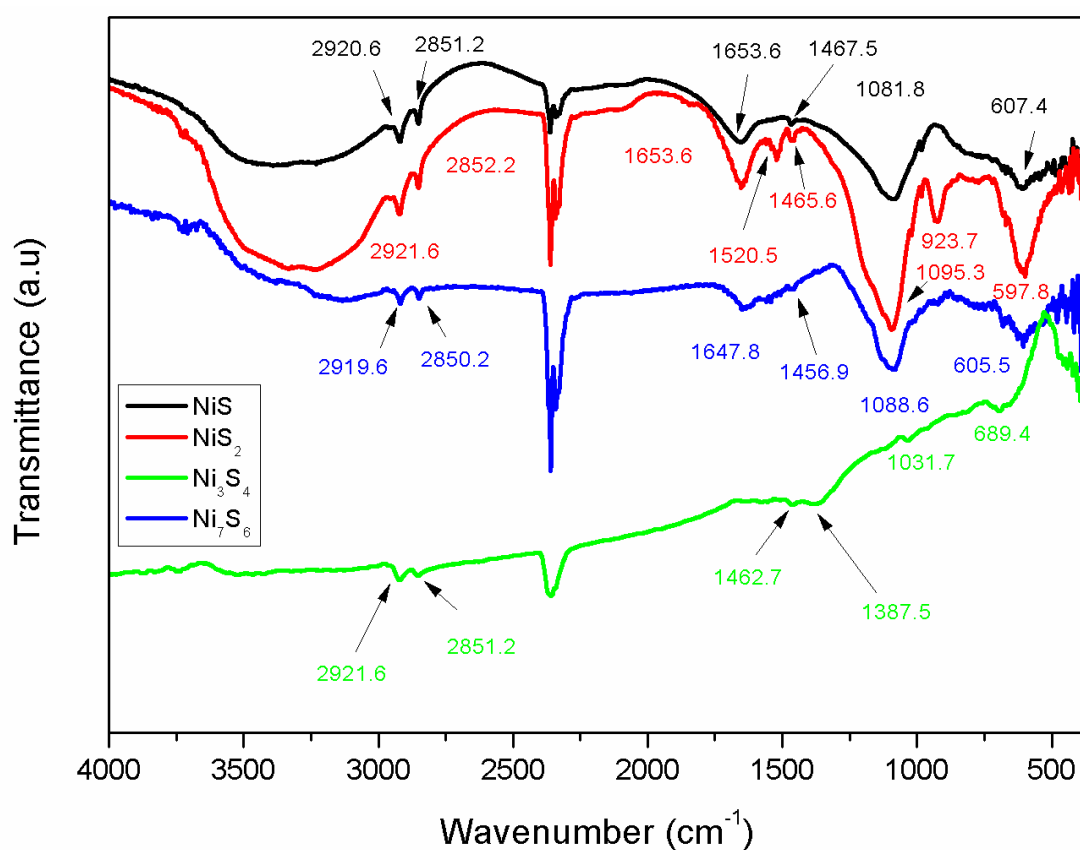


Fig. 3.6 FTIR patterns of different nickel sulfide phases.

3.3.6 XPS Analysis

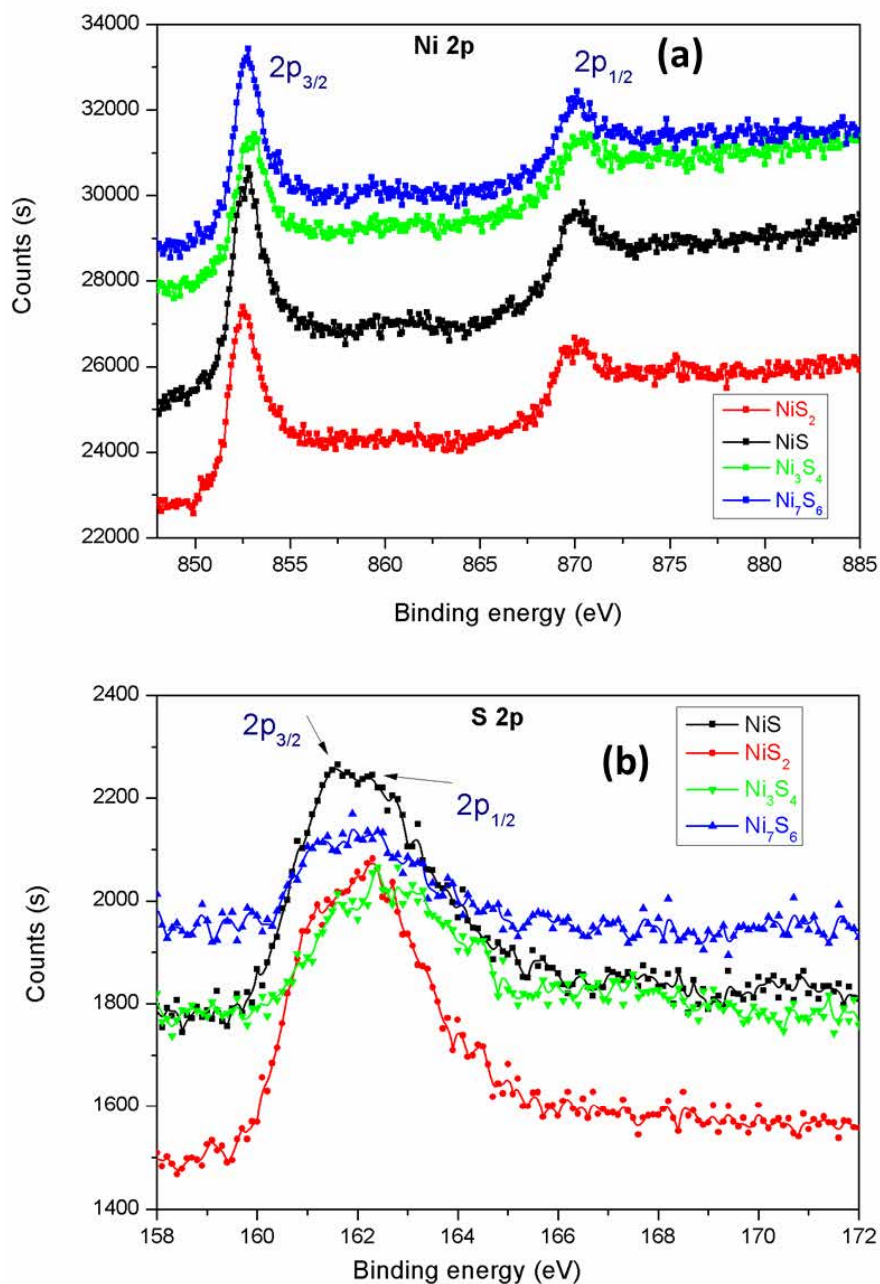


Fig. 3.7 (a) Ni 2p and (b) S 2p XP spectra of different nickel sulfide phases.

The X-ray photoelectron spectra (XPS) of the different phases of the synthesized nanoparticles are shown in Fig. 3.7. Table 3.2 shows the binding energies of the synthesized

phases. The binding energy of 852.8 eV (Ni 2p_{3/2}) for the NiS and Ni₇S₆ samples matched the reported values³². The binding energies for NiS₂ and Ni₃S₄, i.e., 852.5 and 853.1 eV, respectively, were close to the reported values of 852.85 and 854.3 eV. All the Ni 2p_{1/2} binding energies matched the reported values^{25,33,34}. The difference between the binding energies of Ni 2p_{1/2} and Ni 2p_{3/2} is approximately equal to the standard value for nickel doublet peaks (17.4)³⁵, but this difference is 18.4 eV in the case of NiO bonds. This confirms that the materials are protected from oxidation by oleylamine capping of the particles. Doublet peaks of S 2p_{3/2} and S 2p_{1/2} for NiS₂, i.e., 161.2 and 162.8 eV, matched the reported NiS₂ data³³. These values are similar to those for the nickel-rich phase Ni₇S₆. The other phases such as NiS and Ni₃S₄ had sulfur doublet peaks consistent with the reported values³².

Table 3.2 XPS binding energy values

Phase	Ni 2p_{3/2} (eV)	Ni 2p_{1/2} (eV)	Ni 2p_{3/2} - Ni 2p_{1/2} (eV)	S 2p_{3/2} (eV)	S 2p_{1/2} (eV)
NiS	852.8	870.4	17.6	161.4	162.8
NiS ₂	852.5	870	17.5	161.2	162.8
Ni ₃ S ₄	853.1	870.4	17.3	161.6	162.8
Ni ₇ S ₆	852.8	870.1	17.3	161.2	162.8

The different materials obtained using different molar concentrations of the source materials (Table 3.1) show that the availability of the nickel source for reaction with the sulfur–amine mixture is very important in synthesizing single-phase nickel sulfides. The local nickel concentration increased during the reaction to form the more stable Ni_3S_4 phase. In this case, all the sulfur source molecules reacted with the metal precursor. The complex phases in the nickel sulfide phase diagram, such as Ni_3S_4 and Ni_7S_6 , were obtained without sulfur impurities. The results for the NiS and NiS_2 phases clearly show that any stable phase of nickel sulfide can be synthesized by single-step temperature-controlled synthesis with the help of oleylamine.

3.4 Catalytic Activities of Nickel Sulfide Catalysts

I investigated the reduction of 4-nitrophenol to 4-aminophenol to understand the catalytic activities of the synthesized nickel sulfide phases^{36,37}. No reduction reaction was observed without the presence of nickel sulfide catalysts. Fig. 3.8 shows photographs of 4-nitrophenol reduction and the chemical equation. Fig. 3.9 shows the UV-vis absorbance spectra with respect to time. During the reaction, hydrogen species were first transferred to the surface of the synthesized products and then 4-nitrophenol was reduced to 4-aminophenol³⁸. In Fig. 3.9, the absorption peak at 400 nm represents the 4-nitrophenolate ion and the peak at 293 nm is related to 4-aminophenol.

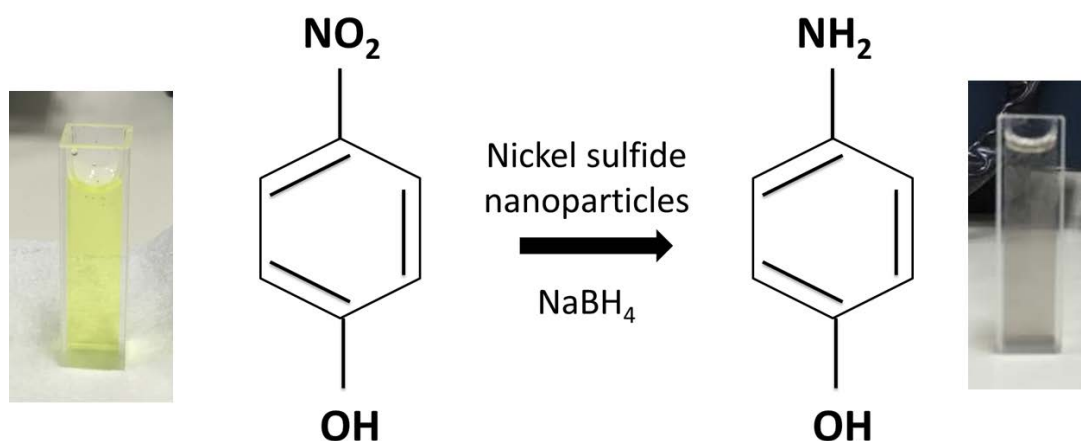


Fig. 3.8 Catalytic reduction of 4-nitrophenol to 4-aminophenol.

When NiS nanoparticles were added to the solution, reduction to 4-aminophenol was complete in about 300 s (Fig. 3.9a). The catalytic activities of the sulfur-rich phases were lower than that of the NiS phase. The reduction times using NiS₂ and Ni₃S₄ were both 400 s (Fig. 3.8b and c). For the Ni₇S₆ phase, reduction was complete in 500 s. The NiS phase had much higher catalytic activity.

Fig. 3.10 shows the reduction rates with different nickel sulfide phases. The reaction rate increased linearly with respect to time. The reduction rate constant (K_{obs}) was calculated using the absorption values for the 4-nitrophenol reduction reaction^{38,39}.

$$K_{\text{obs}} = \frac{\ln \left[\frac{A_{\infty} - A_0}{A_{\infty} - A_t} \right]}{t}$$

Where A_0 , A_t , and A_∞ are the initial absorbance, absorbance at time t , and absorbance at infinite time, respectively. The calculated K_{obs} values for NiS, NiS₂, Ni₃S₄, and Ni₇S₆ are

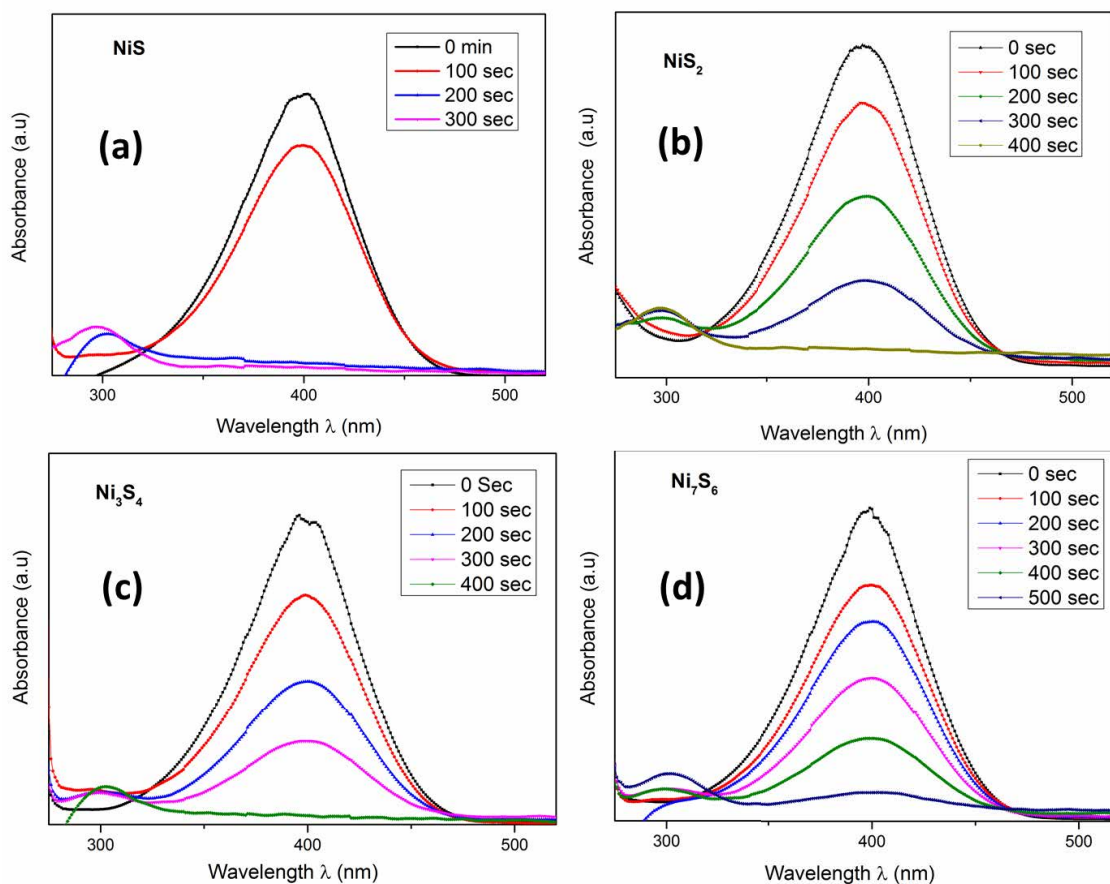


Fig. 3.9 UV-vis spectra of 4-nitrophenol reduction with (a) NiS, (b) NiS₂, (c) Ni₇S₆, and (d) Ni₃S₄ phases.

8.949×10^{-3} , 3.030×10^{-3} , 3.728×10^{-3} , and $2.737 \times 10^{-3} \text{ s}^{-1}$, respectively. Among the four synthesized nickel sulfide phases, NiS gave the highest rate of degradation of 4-nitrophenol because of its higher metallic nature¹⁵. To study the structural change after its catalytic reduction, nanoparticles of NiS phase were collected by centrifugation and investigated the structure by XRD analysis. Fig.10 shows the XRD pattern of NiS phase after its catalytic

activity. The corresponding JCPDS reference 00-001-1286 was well matched with the NiS phase. No phase change was observed even after its catalytic reduction but the crystal system was changed from hexagonal to rhombohedral of NiS phase. The repeated catalytic activity of NiS phase was well matched with the initial experiment of Fig.3. 11 and its reduction time of 4-nitrophenol to 4-aminophenol is 300 sec.

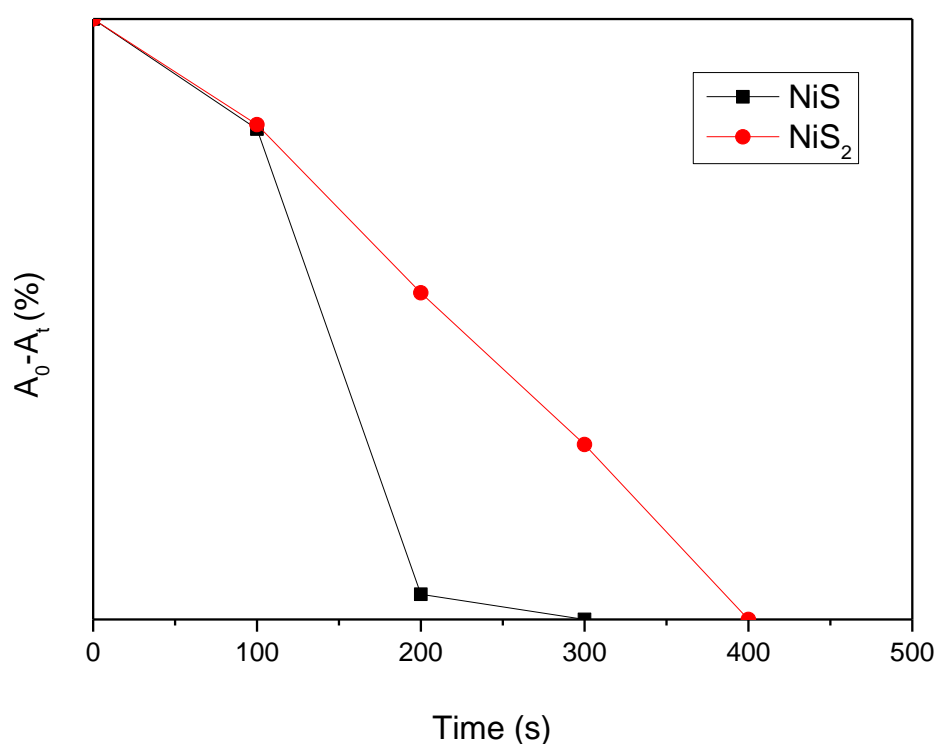


Fig. 3.10 Effects of different nickel sulfide phases on reduction of 4-nitrophenol.

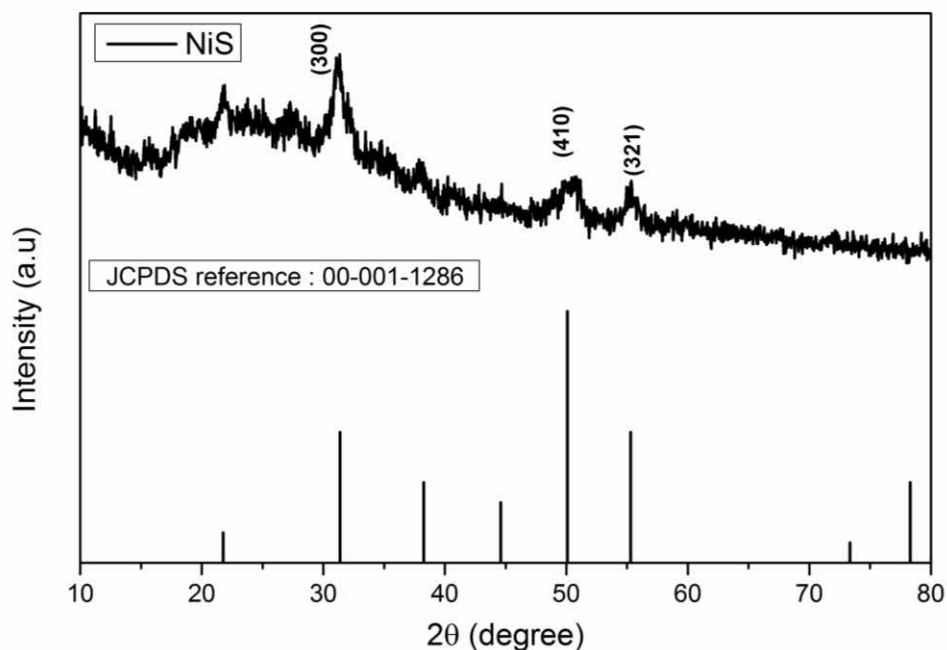


Fig. 3.11 XRD pattern for NiS phase after its catalytic activity

3.5 CONCLUSION

I have successfully synthesized nickel sulfide nanoparticles with different phases via a simple temperature-controlled injection method in oleylamine solvent. The products were uniform-sized nanocrystals. The injection method enabled the sulfur ions to react slowly with the well-dispersed nickel ions in the presence of oleylamine, to form nickel sulfide nanoparticles. This enabled formation of the desired phase instead of mixed phases. The complications in the synthesis of Ni_3S_4 were overcome by adjusting the source concentrations. XRD and TEM analyses confirmed the presence of single-phase nanoparticles of sizes less than 15 nm for all the synthesized products. The presence of sulfur and nickel and the peak shifts with respect to phase formation were observed using XPS. The catalytic activities of

the synthesized nickel sulfide nanoparticles were investigated; the NiS phase had the best activity and the phase was stable even after its catalytic reduction experiment.

REFERENCES

- (1) Scholes, G. D. *Adv. Funct. Mater.* **2008**, *18*, 1157–1172.
- (2) Chen, J.; Sorensen, C.; Klabunde, K.; Hadjipanayis, G.; Devlin, E.; Kostikas, a. *Phys. Rev. B* **1996**, *54*, 9288–9296.
- (3) Cornelius, T. W.; Toimil-Molares, M. E.; Neumann, R.; Karim, S. *J. Appl. Phys.* **2006**, *100*, 114307. 1–5.
- (4) Yoffe, a. D. *Adv. Phys.* **1993**, *42*, 173–262.
- (5) Zhou, W. P.; Lewera, A.; Larsen, R.; Masel, R. I.; Bagus, P. S.; Wieckowski, A. *J. Phys. Chem. B* **2006**, *110*, 13393–13398.
- (6) Daniel, M. C.; Astruc, D. *Chem. Rev.* **2004**, *104*, 293–346.
- (7) Bawendi, M. Steigerwald. M, B. L. *Annu. Rev. Phys. Chem.* **1990**, *41*, 477–496.
- (8) Choi, S. H.; An, K.; Kim, E. G.; Yu, J. H.; Kim, J. H.; Hyeon, T. *Adv. Funct. Mater.* **2009**, *19*, 1645–1649.

- (9) Peng, X.; Manna, L.; Yang, W.; Wickham, J.; Scher, E.; Kadavanich, a; Alivisatos, A. *Nature* **2000**, *404*, 59–61.
- (10) Barrelet, C. J.; Wu, Y.; Bell, D. C.; Lieber, C. M. *J. Am. Chem. Soc.* **2003**, *125*, 11498–11499.
- (11) Hasegawa, Y.; Afzaal, M.; O'Brien, P.; Wada, Y.; Yanagida, S. *Chem. Commun. (Camb)*. **2005**, *1*, 242–243.
- (12) Liu, Q.; Díaz, A.; Prosvirin, A.; Luo, Z.; Batteas, J. D. *Nanoscale* **2014**, *6*, 8935–8942.
- (13) Kullerud, G.; Yund, R. a. *J. Petrol.* **1962**, *3*, 126–175.
- (14) Jiang, X.; Xie, Y.; Lu, J.; Zhu, L.; He, W.; Qian, Y. *Adv. Mater.* **2001**, *13*, 1278–1281.
- (15) Sparks, J.; Komoto, T. *Phys. Lett.* **1967**, *25*, 5–6.
- (16) Sparks, J.; Komoto, T. *Rev. Mod. Phys.* **1968**, *40*, 752–754.
- (17) A. S. Barker, J. and J. P. R. *Phys. Rev. B* **1974**, *10*, 987–994.
- (18) Wang, L.; Zhu, Y.; Li, H.; Li, Q.; Qian, Y. *J. Solid State Chem.* **2010**, *183*, 223–227.

- (19) Chen, S.; Zeng, K.; Li, H.; Li, F. *J. Solid State Chem.* **2011**, *184*, 1989–1996.
- (20) R.Karthikeyan, M. Navaneethan, J. Archana, D. Thangaraju, M. Arivanandhan, Y. H. *Dalton Trans.* **2014**, *43*, 17445–17452.
- (21) Ghezelbash, A.; Korgel, B. a. *Langmuir* **2005**, *21*, 9451–9456.
- (22) Wu, B.; Zheng, N.; Fu, G. *Chem. Commun. (Camb)*. **2011**, *47*, 1039–1041.
- (23) Lee, S. M.; Jun, Y. W.; Cho, S. N.; Cheon, J. *J. Am. Chem. Soc.* **2002**, *124*, 11244–11245.
- (24) Lut, A.; Malik, M. A.; Brien, P. O.; Tuna, F. **2012**, 2253–2259.
- (25) Thomson, J. W.; Nagashima, K.; Macdonald, P. M.; Ozin, G. a. **2011**, 3–5.
- (26) Dyal, A.; Loos, K.; Noto, M.; Chang, S. W.; Spagnoli, C.; Shafi, K. V. P. M.; Ulman, A.; Cowman, M.; Gross, R. a. *J. Am. Chem. Soc.* **2003**, *125*, 1684–1685.
- (27) Kriegel, I.; Rodríguez-Fernández, J.; Wisnet, A.; Zhang, H.; Waurisch, C.; Eychmüller, A.; Dubavik, A.; Govorov, A. O.; Feldmann, J. *ACS Nano* **2013**, *7*, 4367–4377.
- (28) Polavarapu, L.; Xu, Q.-H. *Nanotechnology* **2009**, *20*, 185606, 1–7.

- (29) He, J.; Kanjanaboos, P.; Frazer, N. L.; Weis, A.; Lin, X. M.; Jaeger, H. M. *Small* **2010**, *6*, 1449–1456.
- (30) Khare, A.; Wills, A. W.; Ammerman, L. M.; Norris, D. J.; Aydil, E. S. *Chem. Commun.* **2011**, *47*, 11721–11723.
- (31) Zhang, L.; Wang, L.; Jiang, Z.; Xie, Z. *Nanoscale Res. Lett.* **2012**, *7*, 312, 1–6.
- (32) Salavati-Niasari, M.; Davar, F.; Mazaheri, M. *Mater. Res. Bull.* **2009**, *44*, 2246–2251.
- (33) Yang, S.-L.; Yao, H.-B.; Gao, M.-R.; Yu, S.-H. *CrystEngComm* **2009**, *11*, 1383–1390.
- (34) Sangaletti, L.; Thio, T.; Bennett, J. W. **1997**, *55*, 9514–9519.
- (35) Wagner, C. D.; Riggs, W. M.; Davis, L. E.; Moulder, J. F. *Handbook of X-ray Photoelectron Spectroscopy*; 1979.
- (36) Yu, T.; Zeng, J.; Lim, B.; Xia, Y. *Adv. Mater.* **2010**, *22*, 5188–5192.
- (37) Lin, F. H.; Doong, R. A. *J. Phys. Chem. C* **2011**, *115*, 6591–6598.

- (38) Gu, S.; Wunder, S.; Lu, Y.; Ballauff, M.; Fenger, R.; Rademann, K.; Jaquet, B.; Zacccone, A. *J. Phys. Chem. C* **2014**, *118*, 18618–18625.
- (39) Murugan, E.; Jebaranjitham, J. N. *J. Mol. Catal. A Chem.* **2012**, *365*, 128–135.

Chapter 4

Synthesis of reduced graphene oxide functionalized nickel sulfide nanoparticles and its catalytic activity

4.1 Background

More than 90% of the commercially producing chemical products use catalysts at some stages, to contribute the human society. However concerns have been raised on the cost, stability, biocompatibility and availability of the catalysts. On the other hand, recent advancement in the field of colloidal nanocrystals made it possible to synthesize various types of metal sulfides such as nickel, cobalt, iron, zinc, copper and various other sulfides, with controlled size-dependent characteristics. But the uses of these nanoparticles for the protection of environment are most important factors to be considered. Removal of environment pollutions has been a major issue in recent years to avoid the inhibition into water and soil resources. 4-nitrophenol¹ is a common pollutant in wastewater. Many different processes have been developed such as adsorption², microbial degradation^{3,4}, catalytic reduction⁵, photocatalytic degradation^{6,7}, electrochemical treatment⁸ and etc. to remove or reduce 4-nitrophenol. Catalytically reduced 4-nitrophenol into 4-aminophenol has number of uses in the production of drugs, photographic developer, corrosion inhibitor and anti-corrosion lubricants⁹.

Graphene or graphene based materials are considered as very promising material

because of their excellent physical, chemical and mechanical properties¹⁰. Specifically, graphene based materials have been utilized as counter electrodes¹¹, electrochemical sensor¹² and supercapacitor electrodes¹³. In the field of catalysis, different graphene based materials such as gold nanoparticles incorporated graphene material¹⁴⁻¹⁶, platinum incorporated graphene sheets^{17,18}, palladium with graphene¹⁹ and etc. have shown very good catalytic activity. Liu et.al analyzed the 4-nitrophenol reduction with the help of magnetically recoverable Pt/Ni bimetallic nanoparticles doping on graphene supports¹⁷. Zhu et.al, synthesized ternary hybrid nanostructures with Pt/SnO₂/graphene and the reduction along with the platinum and metal oxide hybrid were carried out in one-pot chemical synthesis method¹⁸.

Metal-free catalysts are encouraged because of the environmental friendly need. Kong et.al studied N-doped graphene as a metal-free catalyst for the reduction of 4-nitrophenol and proposed the pseudo-zero order kinetics²⁰. However, on the understanding of its kinetics, research is limited. For the Industrial demand such as low cost and high availability, the following materials are encouraged. i.e., metal, metal oxides, metal sulfide based graphene composites.

Towards the finding of new catalyst with better catalytic activity and reduction rate, I have investigated phase controlled nickel sulfide nanoparticles. Several researchers attempted to synthesize nickel sulfide/ graphene oxide hybrid nanostructures for the application of solar

cells²¹, lithium-ion batteries^{22–24}, supercapacitors^{25–30} and etc. But due to the difficulties in control of phase along with graphene reduction, the research is limited. To utilize the vast property of graphene with the binary phase controlled nickel sulfide, I have developed two different synthesis processes. One is to synthesis of reduced graphene oxide/phase controlled nickel sulfide nanoparticles using single solvent, and second is to use multi-solvent through hot injection method. The catalytic properties of the synthesized materials were studied with 4-nitrophenol reduction experiments.

4.2 Experimental procedures

4.2.1 Materials

Graphite powder (particle size-150 μm) was prepared from the graphite rod (purity 99.99%). Sulfuric acid H_2SO_4 (purity 99%), phosphoric acid (purity 99%), potassium permanganate KMnO_4 (purity 99.9%), hydrogen peroxide (H_2O_2), hydrochloric acid HCl (purity 37% assay), nickel nitrate hexahydrate $\text{Ni}(\text{NO}_3)_2 \cdot 6\text{H}_2\text{O}$ (purity 98%), elemental sulfur, ethanol (99.95%), 4-nitrophenol, NaBH_4 , and acetone (purity 99.9%) were purchased from Wako Pure Chemical Industries, Ltd., Japan. Oleylamine (purity 70%), octadecine (purity 99%), oleic acid (purity 99 %) were purchased from Sigma Aldrich. The reagents were used without further purification.

4.2.2 Synthesis of graphene oxide by improved Hummer's method

Graphene oxide was synthesized from the graphite flakes of 150 microns by improved Hummers method³¹. Fig. 4.1 shows the schematic view of the experimental procedure of improved Hummer's method. A mixture of concentrated $\text{H}_2\text{SO}_4/\text{H}_3\text{PO}_4$ (135 mL) was added to the graphite flakes (1.0 g) under stirring for 30 min. KMnO_4 (6 g) was added to the above mixture at the temperature $0\text{ }^\circ\text{C}$.

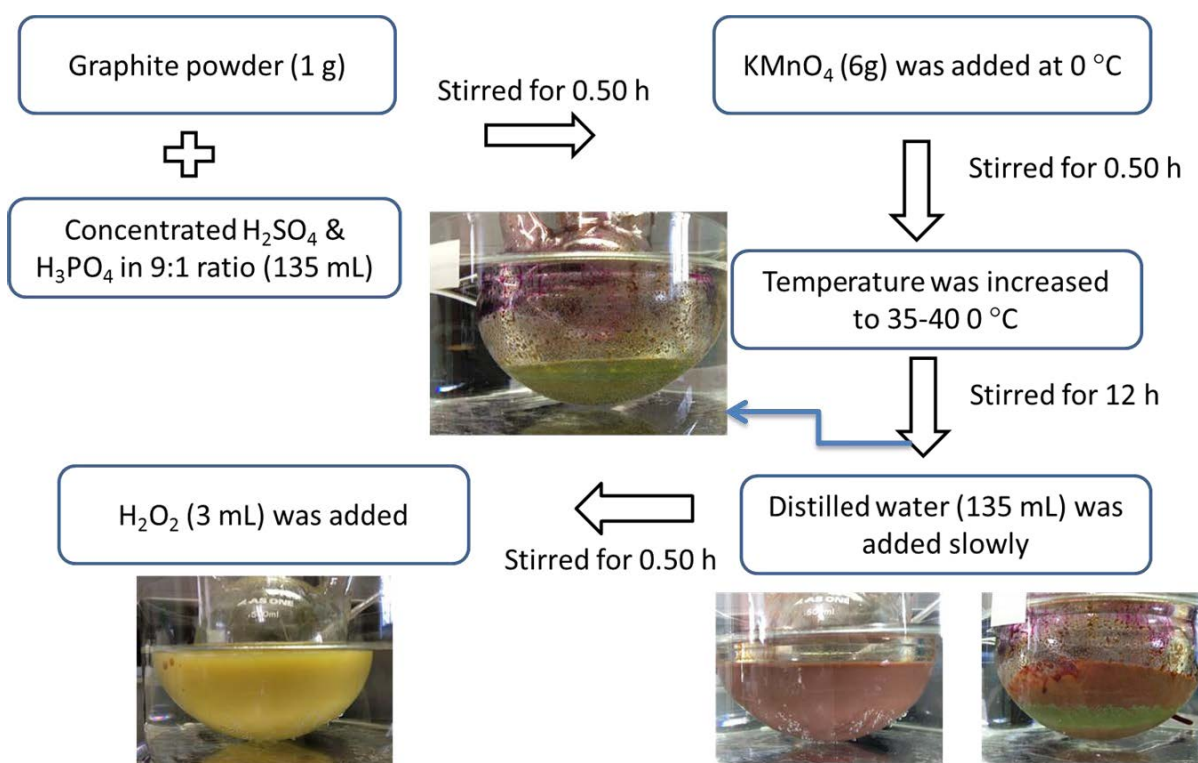


Fig. 4.1 Schematic experimental procedure of improved Hummer's method

The mixture was raised to the temperature $40\text{--}45\text{ }^\circ\text{C}$ and maintained for about 15 h. It was cooled down to room temperature and poured into 120 mL of distilled water. With the

addition of distilled water, oxidation reaction was initiated into the mixture. To terminate the oxidation reaction, H_2O_2 (3 mL) was added into the mixture. The mixture was filtered and the filtrate was washed with the succession of 100 mL of water and 100 mL of 1 mol HCl (37 %) for several times. The resultant product was vacuum-dried for 12 h at room temperature to obtain the final graphene oxide powder.

4.2.3 Synthesis of reduced graphene oxide/nickel sulfide by hot injection method

4.2.3.1 Single-solvent:

Graphene oxide powders were dispersed by oleylamine (10 mL) as a single-solvent and ultrasonicated for 1 h. In a separate conical flask, elemental sulfur (1 mmol) was taken with oleylamine (5 mL) and preheated at 70 °C for 30 min to form a sulfur–amine mixture. For the reaction ratio of 1:1 (nickel to sulfur ratio), $\text{Ni}(\text{NO}_3)_2 \cdot 6\text{H}_2\text{O}$ (1 mmol) was taken with dispersed graphene of single-solvent oleylamine (10 mL) in a 100 mL three-necked flask (A). The solution was heated at 100 °C for 1 h to remove moisture and O_2 in the oleylamine. The transparent yellow sulfur–oleylamine solution (B) was loaded into a glass syringe and injected into the nickel–oleylamine solution mixture (A). The temperature was raised to 220 °C and the mixture was continually stirred for 1 h under a N_2 atmosphere to initiate the reaction. After cooling, the particles were collected by centrifugation, washed with ethanol, and dried under vacuum for 1 h. The particles were dispersed in an organic solvent and stored

in a tightly closed container. The similar different concentration ratios of experiments 1:2, 3:4 and 3:2 were carried out with the above procedure.

4.2.3.2 Multi-solvent:

The multi-solvent experiments were carried out for the dispersion of graphene oxide powder. Instead of oleylamine as a single-solvent, graphene oxide powders were dispersed by oleylamine (10 mL), oleic acid (10 mL), Octadecine (7.5 mL) mixture and ultrosonicated for 1 h. In a separate conical flask, elemental sulfur (1 mmol) was taken with octadecine (5 mL) and preheated at 70 °C for 30 min to form a sulfur–octadecine mixture. The other procedures were followed to the single-solvent experiment to get the final products of 1:1 (nickel to sulfur ratio) graphene/nickel sulfide product. The other concentration ratios of 1:2, 3:4 and 3:2 experiments were carried with the similar procedure.

4.2.4 Catalytic Study

The catalytic activities of the synthesized nickel sulfide/graphene nanoparticles were investigated as follows. Aqueous solutions of 4-nitrophenol (10 mg in 50 mL of distilled water) and NaBH₄ (325 mg in 200 mL of distilled water) were freshly prepared. 4-Nitrophenol and NaBH₄ in a concentration ratio of 2:3 were mixed with nickel sulfide nanoparticles (5.0 mg). The mixture was placed in a quartz cuvette and the reaction was

monitored using UV-vis spectroscopy. This step was repeated several times to study the stability of the nanoparticles.

4.2.5 Characterization techniques

The samples were characterized by powder X-ray diffraction (XRD) performed at a scan rate of 0.04 s^{-1} in the 2θ range 10° to 80° (RINT-2200 diffractometer, Rigaku, Japan, $\text{CuK}\alpha$ radiation, $\lambda = 1.54178\text{ \AA}$). The particle sizes and morphologies of the final precipitates were determined using transmission electron microscopy (TEM) and high-resolution TEM (HRTEM; JEOL JEM 2100F) at an accelerating voltage of 200 kV.

4.3 Results and discussion

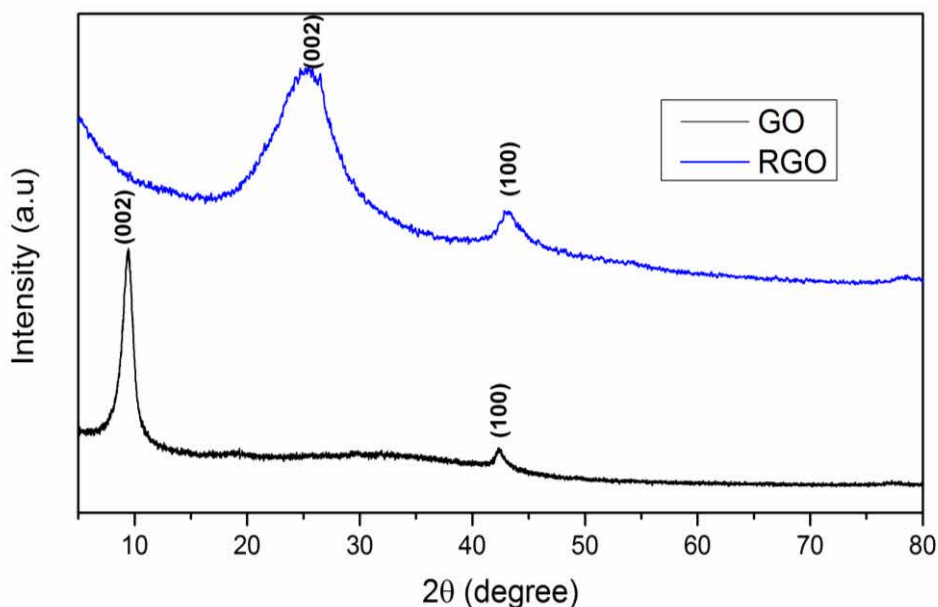


Fig. 4.2 XRD patterns of graphene oxide (GO) and reduced graphene oxide (RGO)

Before the synthesis of nickel sulfide in graphene oxide dispersion, the as-synthesized graphene oxide (GO) was characterized by XRD analysis. To confirm the reduction process with oleylamine, a separate experiment was carried out. The synthesized graphene oxide powders were taken in oleylamine solvent at 210° C. The synthesized products were vacuum dried to get the reduced graphene oxide (rGO) powder. Fig. 4.2 shows the XRD patterns of GO and rGO samples. The interlayer distances of GO and rGO were calculated from the XRD patterns. From 2 θ peak of GO at 9.48°, the interlayer distance was calculated as 9.32 Å. It indicates that the graphite powder was fully oxidized into GO through chemical oxidation by Improved hummer's method. In contrast to the GO powder, the rGO yielded a broad peak at 24.70°, suggesting that the rGO was fully reduced. The interlayer distance of rGO was 3.60 Å, which was nearly close to the literature value of graphite powder (3.34 Å)^{32,33}. Fig. 4.3 shows the TEM images of (a) reduced graphene oxide sheet and (b) nickel sulfide/rGO hybrid nanostructure.

Table 4.1 shows details of the phases present in the synthesized products with respect to concentration. The samples GN-1 to GN-4 were synthesized with the single solvent oleylamine. The concentration ratios were determined from the previous chapter of structure controlled nickel sulfide nanoparticles. Where four different phases NiS, NiS₂, Ni₃S₄ and Ni₇S₆ were synthesized with respect to the concentration ratios 1:1, 1:2, 3:4, 3:2. To study the

phases formation on graphene support, the experiments were carried out in single-solvent (oleylamine) and multi- solvent (oleylamine, octadecine, oleic acid).

Table 4.1 Different concentration ratios of nickel and sulfur sources and the phases of synthesized materials with reduced graphene oxide

Name	Nickel source (g)	Sulfur source (g)	Concentration ratio	Phases
GN – 1	0.290	0.032	1:1	NiS and Ni ₉ S ₈
GN – 2	0.290	0.064	1:2	NiS ₂ and NiS
GN – 3	0.435	0.064	3:4	NiS
GN – 4	0.435	0.032	3:2	Ni ₃ S ₄
G – 1	0.290	0.032	1:1	Ni ₃ S ₂
G – 2	0.290	0.064	1:2	Ni ₃ S ₄
G – 3	0.435	0.064	3:4	NiS
G – 4	0.435	0.032	3:2	Ni ₃ S ₂

4.3.1. Concentration ratio of 1:1

Fig.4.4 shows XRD pattern of single solvent synthesized rGO functionalized nickel sulfide nanoparticles. In this method, oleylamine was utilized to reduce the graphene oxide to become reduced graphene oxide nanosheets. The nickel sulfide nanoparticles were well attached on the sheets, and the TEM image of Fig. 4.5 (a, b) shows uniform dispersion throughout the nanosheets. The XRD pattern was well matched with the JCPDS references of two different phases NiS and Ni₉S₈. The corresponding phase change was observed from the TEM images. The particles had different morphologies such as rod-like and spherical shape. From the HRTEM image (Fig. 4.4 c); the distance between the atomic layers of spherical nanoparticles was 2.8 Å, matched well with (100) plane of NiS phase. The measured distance between the atomic layers of 2.9 Å of rod-like nanoparticle was related to (222) plane of Ni₉S₈ phase. The sizes of the spherical nanoparticles ranged from 10 to 15 nm, and rod-like particles length varied from 15 to 20 nm. For the synthesis with the single solvent of oleylamine the products were sulfur deficient. This led to the formation of two different phases of NiS and Ni₉S₈.

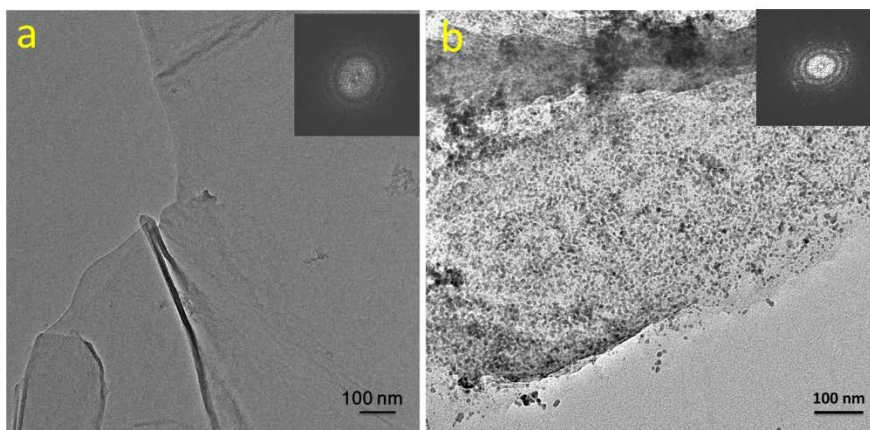


Fig. 4.3 TEM images of (a) reduced graphene oxide (rGO) and nickel sulfide/rGO hybrid (Ni₃S₂ phase)

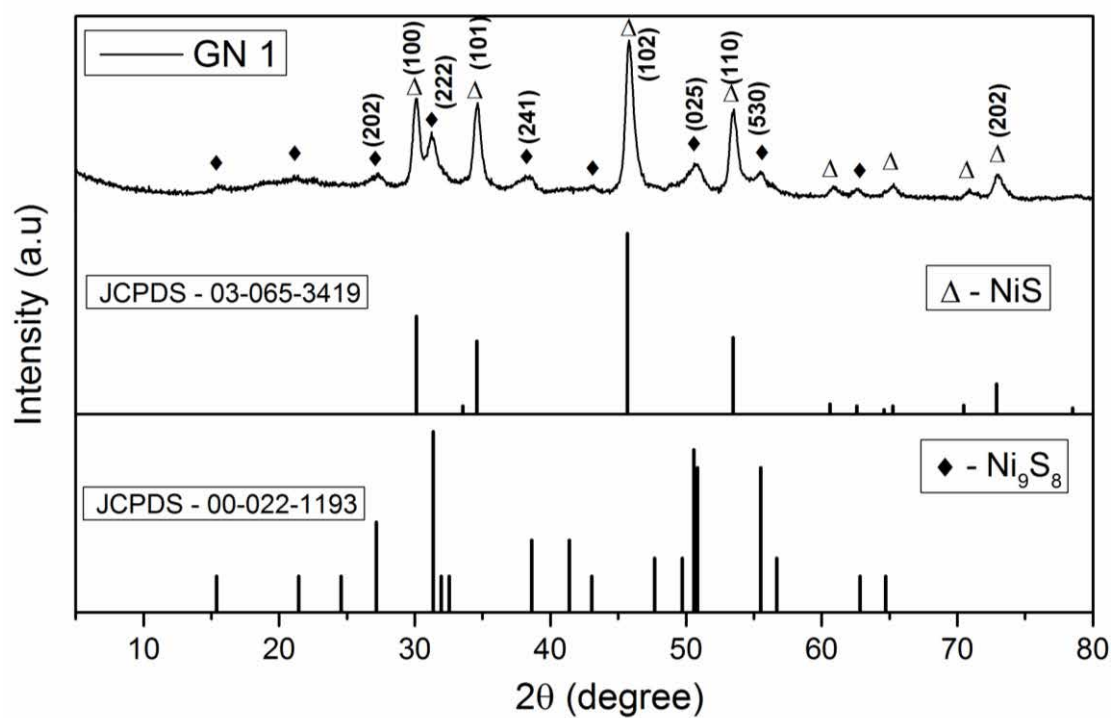


Fig. 4.4 XRD pattern of NiS and Ni₉S₈ phase (GN-1).

To improve the phase controlled nickel sulfide on graphene support, mixers of three solvents were used. The XRD pattern of the synthesized nickel sulfide on graphene is shown in Fig. 4.5. The synthesized product for the concentration ratio of 1:1 consisted of single phase nickel sulfide (Ni_3S_2) with rGO. The peak broadness at 20° was related to the presence of rGO nanosheets. It is well matched with the reference pattern of 00-044-1418. Fig. 4.6 (a, b) shows the TEM images of synthesized product over the rGO supports. The shape of the particles was elongated spherical and size ranged from 8 to 10 nm. From the HRTEM image of Fig. 4.6 (c), the distance between the atomic layers of 2.7 \AA was well matched with the (110) plane of Ni_3S_2 phase.

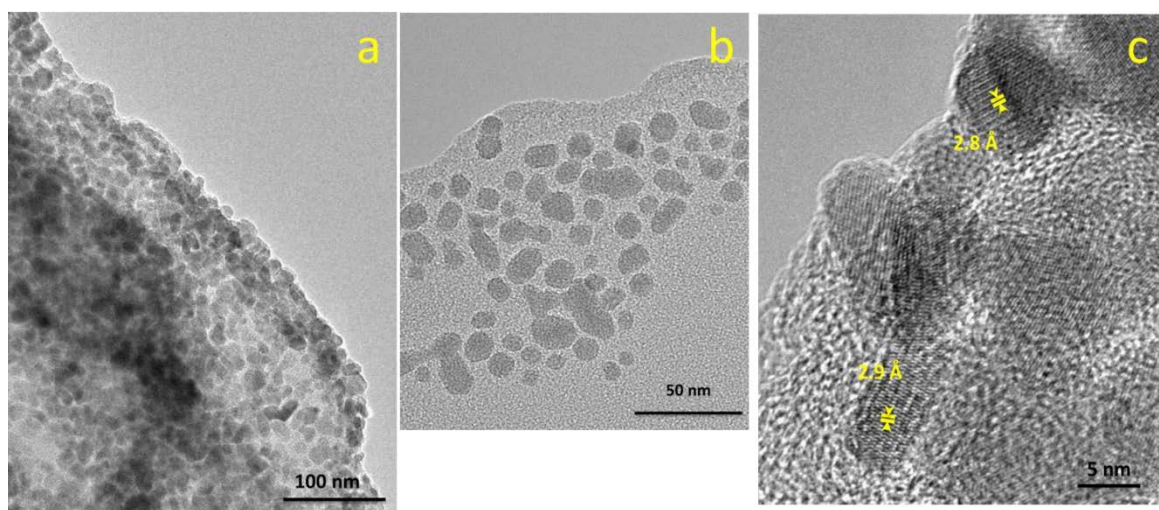


Fig. 4.5 (a, b) TEM and (c) HRTEM images of NiS and Ni_3S_2 phase (G-1).

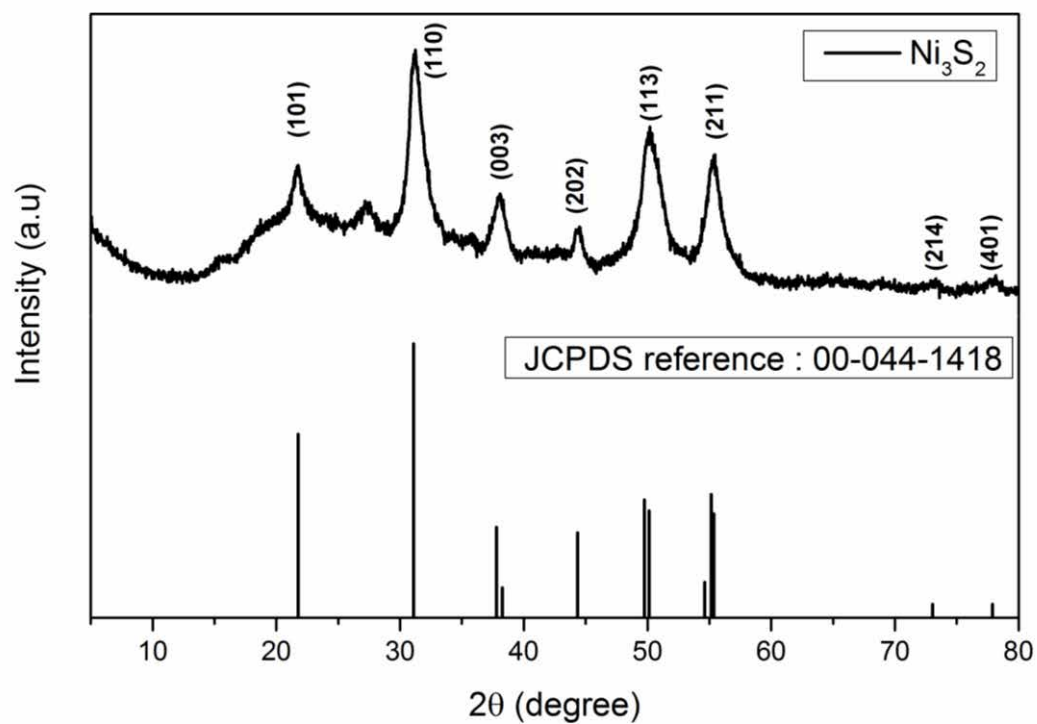


Fig. 4.5 XRD pattern of Ni_3S_2 phase (G-1).

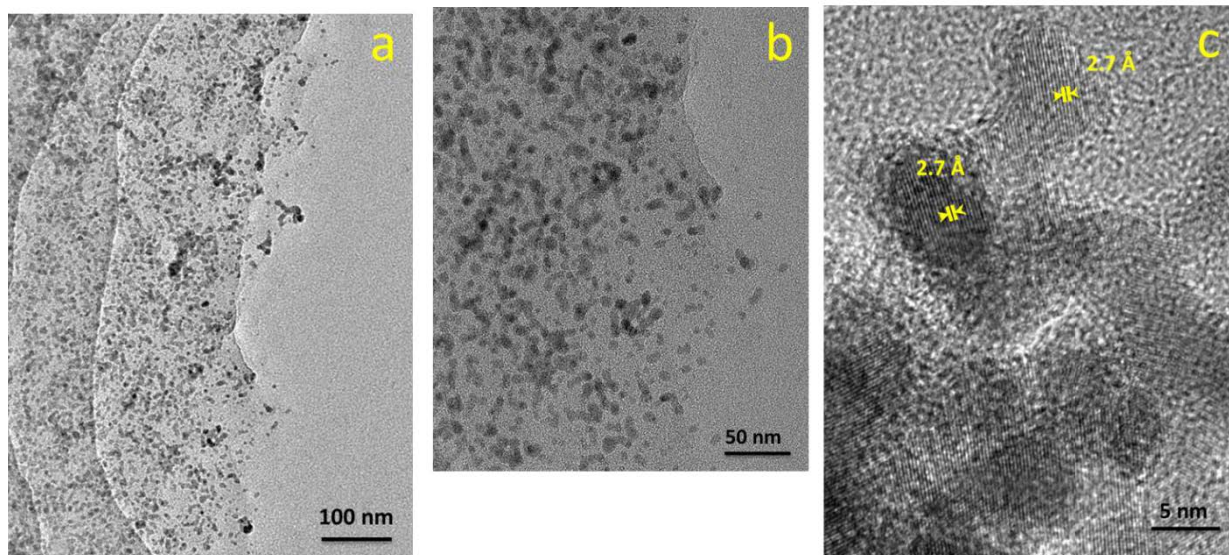


Fig. 4.6 (a, b) TEM and (c) HRTEM images of Ni_3S_2 phase (G-1).

4.3.2. Concentration ratio of 1:2

For the concentration of 1:2 in single solvent, the synthesized product consisted of two phases of nickel sulfide such as NiS_2 and NiS . The reference patterns were well matched with the observed pattern as shown in Fig. 4.7. These phases were also observed in the TEM and HRTEM images in Fig. 4.8. The nanoparticles were well dispersed on rGO supports and two different morphologies were observed from the TEM and HRTEM images. The cubic nanoparticles atomic layers distances of 2.6 \AA was well matched with (210) plane of NiS_2 phase. The rod-like particles of 2.0 \AA was related to (102) plane of NiS phase. These planes corresponded to the dominant peak positions in XRD pattern.

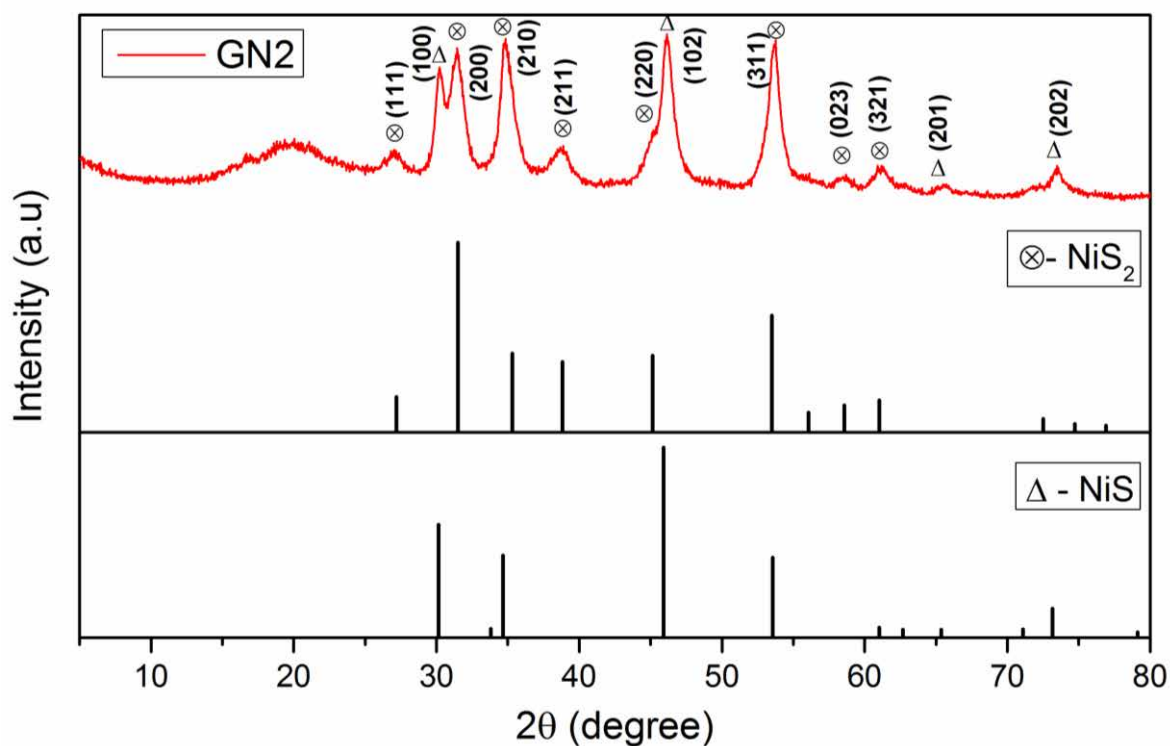


Fig. 4.7 XRD pattern of NiS_2 and NiS phase (GN-2).

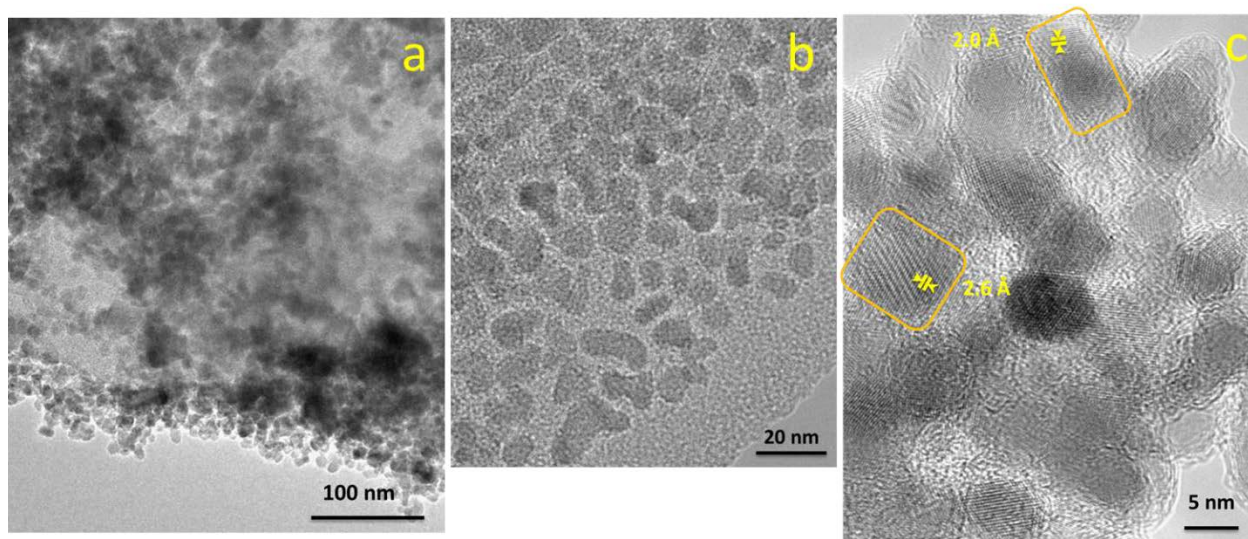


Fig. 4.8 (a, b) TEM and (c) HRTEM images of NiS₂ and NiS phase (G-2)

When the same concentration experiment was performed under multi-solvent condition, the synthesized product resulted in Ni₃S₄ phase as seen in XRD pattern of Fig. 4.9. The morphologies of the well dispersed particles were spherical and elongated spherical. The sizes of the nanoparticles were in the range of 6 to 8 nm. From the HRTEM images of Fig. 4.10 (c), lattice distances 2.5 Å and 2.9 Å were well matched with (400) and (311) planes of the dominant peak positions in the XRD pattern (Ni₃S₄ phase). The phase control of single phase nickel sulfide/rGO was possible by the multi-solvent synthesis process.

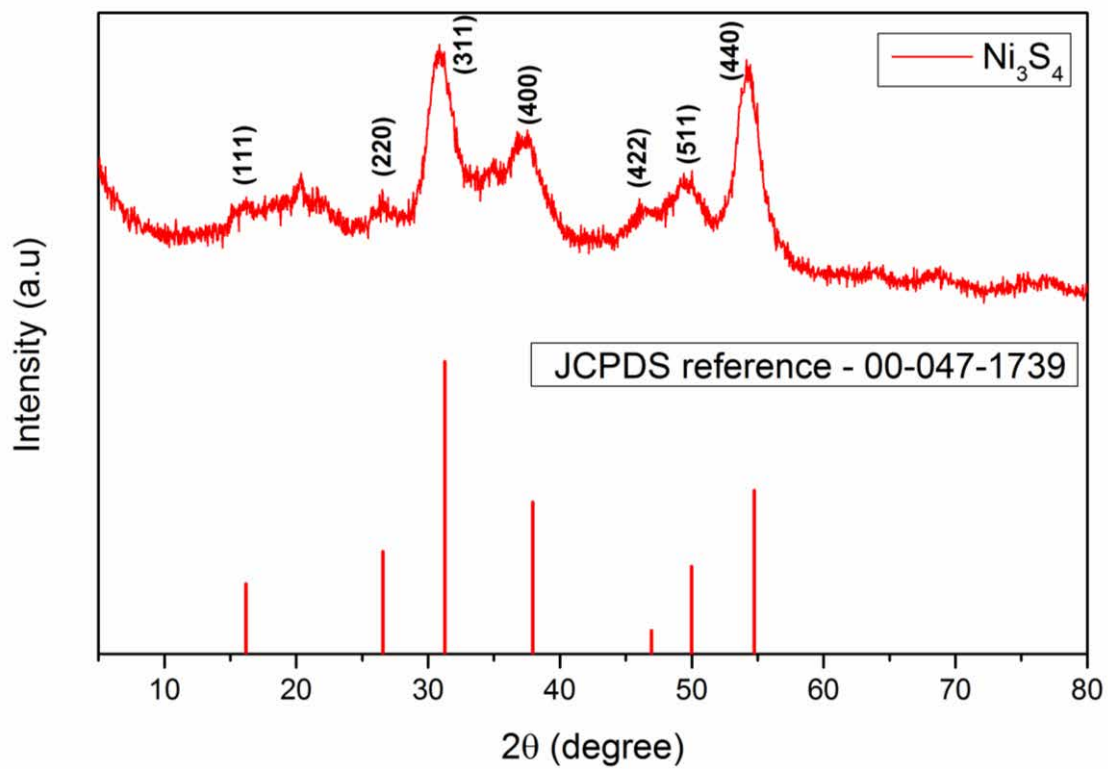


Fig. 4.9 XRD pattern of Ni_3S_4 phase (G-2).

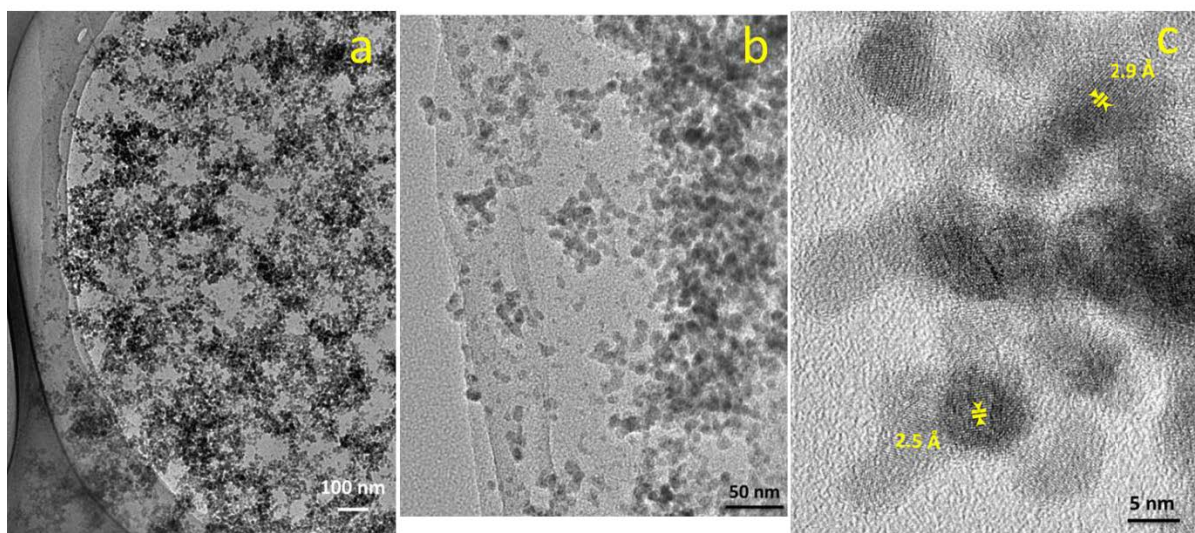


Fig. 4.10 (a, b) TEM and (c) HRTEM images of Ni_3S_4 phase (G-2)

4.3.3. Concentration ratio of 3:4

In the presence of oleylamine single solvent, 3:4 concentrations resulted in single phase nickel monosulfide (NiS). The XRD pattern was well matched with the JCPDS reference of 01-075-0613 as shown in Fig. 4.11. Fig. 4.12 (a, b) shows the well dispersed nanoparticles of nickel sulfide on rGO sheets. The sizes of the nanoparticles were from 10 to 12 nm. From the HRTEM image (Fig.4.12 c) atomic layers distance 2.6 Å was well matched with (101) plane of NiS phase. From this experiment, it was found that the excess of sulfur content was required to synthesize the uniform single phase of nickel sulfide on graphene supports.

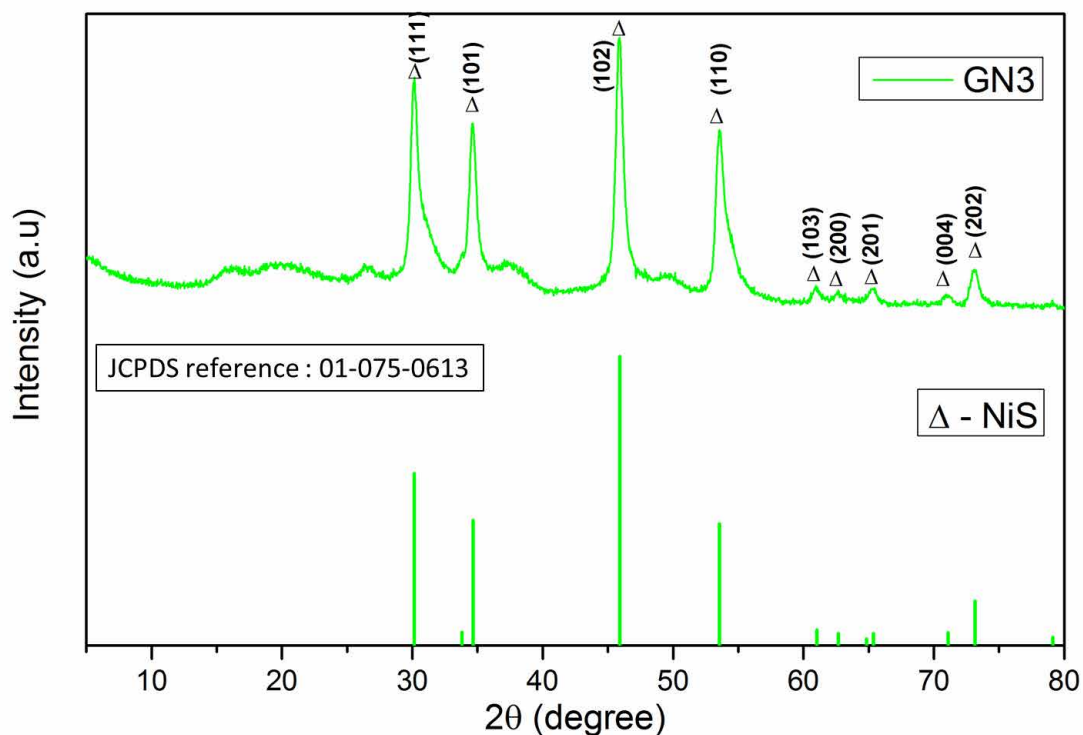


Fig. 4.11 XRD pattern of NiS phase (GN-3).

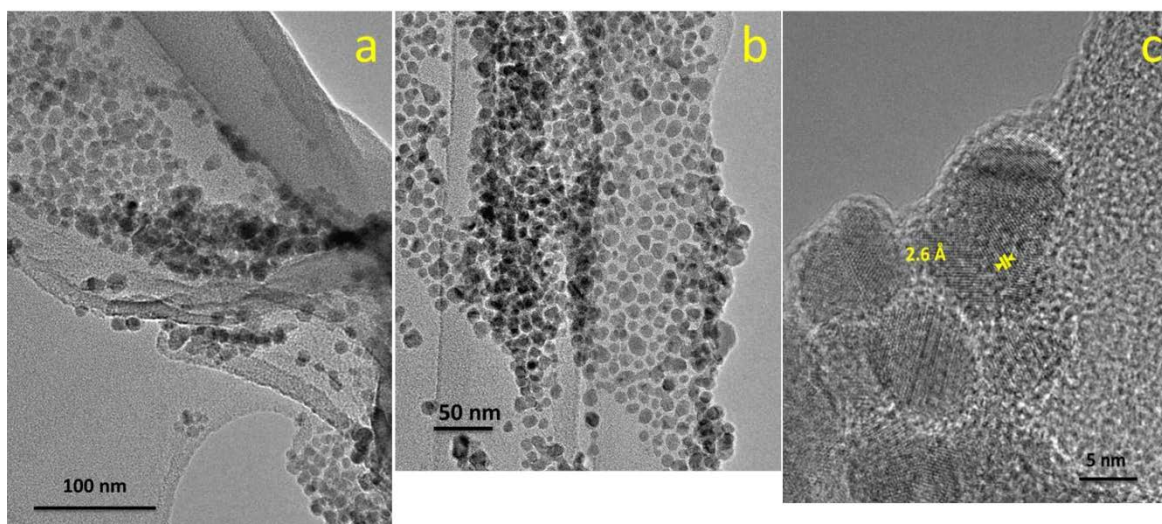


Fig. 4.12 (a, b) TEM and (c) HRTEM images of NiS phase (GN-3)

Similarly, for the concentration ratios of 3:4 in the presence of multi-solvent, nickel monosulfide (NiS) phase was retained. The XRD pattern was well matched with the JCPDS reference of 01-075-0613 as shown in Fig. 4.13. From the TEM images of Fig. 4.14 (a, b), nickel sulfide nanoparticles were well dispersed throughout the graphene support. The shapes of the nanoparticles were spherical morphologies and the sizes were ranging from 8 to 10 nm. From the HRTEM image in Fig. 4.14 (c), lattice distance 1.9 Å and 2.5 Å were well related to the planes of (102) and (101) of NiS phase, respectively. In the presence of multi-solvent, to synthesize the graphene functionalized nickel sulfide nanoparticle with the phase of NiS, excess of sulfur concentration source was required.

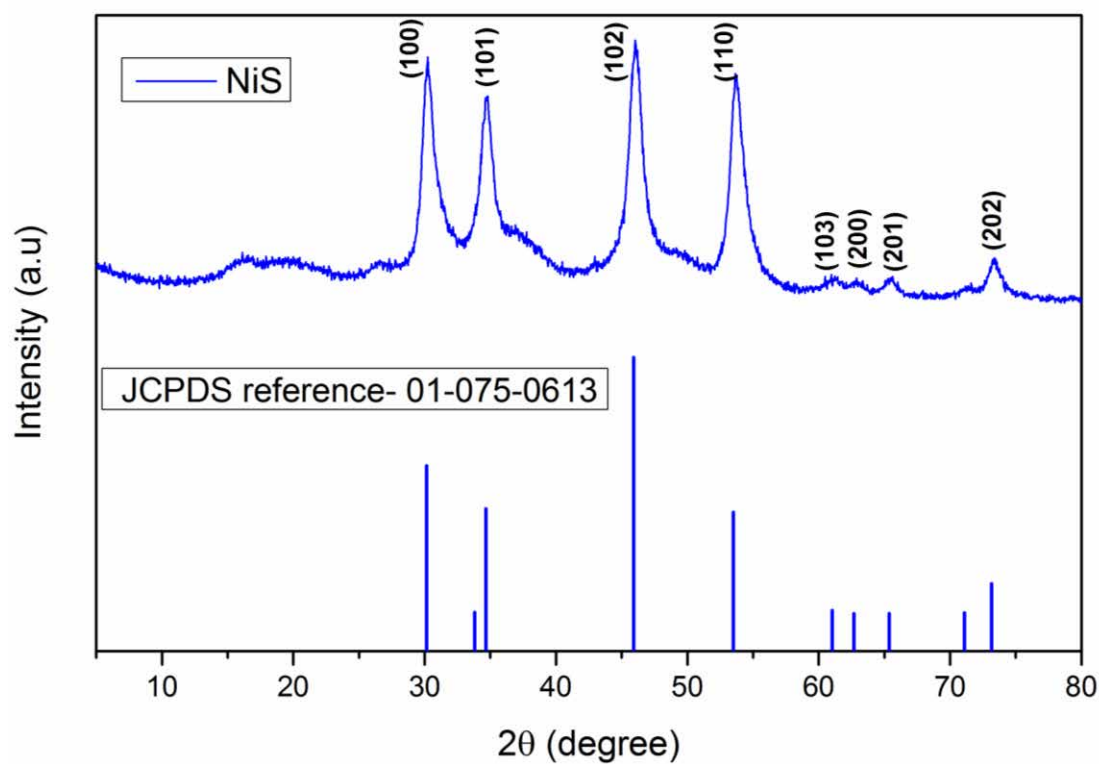


Fig. 4.13 XRD pattern of NiS phase (G-3).

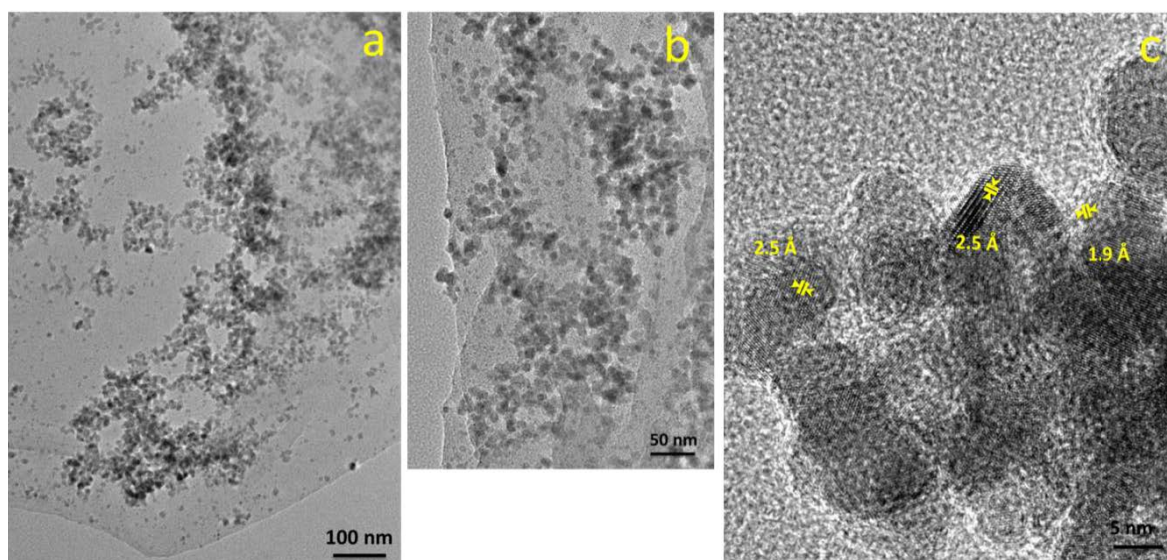


Fig. 4.14 (a, b) TEM and (c) HRTEM images of NiS phase (G-3)

4.3.4. Concentration ratio of 3:2

Fig 4.15 shows the XRD patterns of synthesized product with the concentration ratio of 3:2 under single solvent. The presence of broad peak at 20° was related to reduced graphene oxide (rGO). The peaks of synthesized nickel sulfide nanoparticles were well matched with the JCPDS reference of 00-047-1739 for Ni_3S_4 phase. The TEM images of Fig. 4.16 (a, b) show that the synthesized nanoparticles were well dispersed on the sheets of rGO. The HRTEM image of Fig. 4.16 (c) shows the particles with spherical shape morphologies and the sizes 6 to 10 nm. The lattice distance 2.7 \AA matched with the dominant plane of (311) from the XRD pattern (see Fig. 4.14). In the presence of single solvent, excess amount of nickel concentration was not reacted completely with all the sulfur source atoms and resulted in sulfur deficient Ni_3S_4 phase.

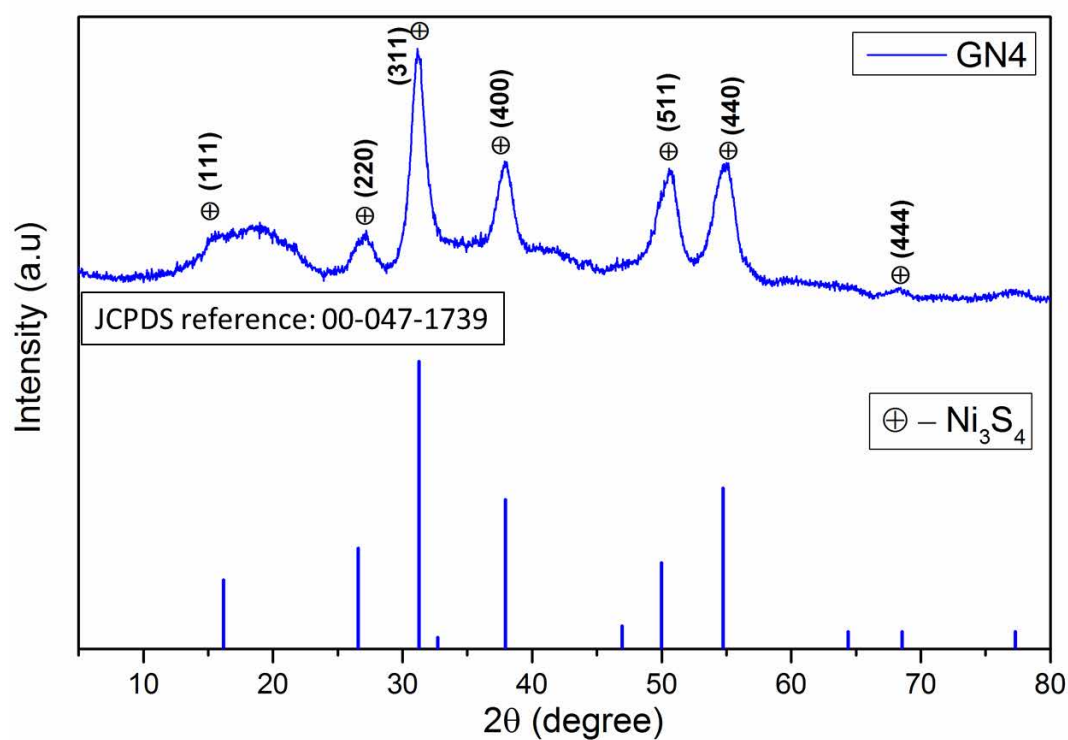


Fig. 4.15 XRD pattern of Ni_3S_4 phase (GN-4).

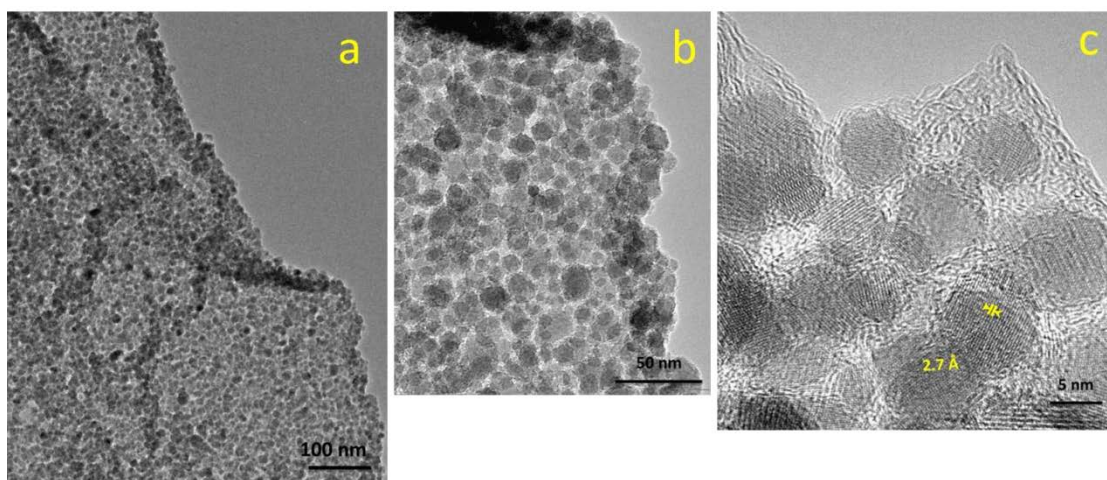


Fig. 4.16 (a, b) TEM and (c) HRTEM images of Ni_3S_4 phase (GN-4).

In the presence of multi-solvent with the same concentration ratio 3:2, the expected nickel sulfide phase of Ni_3S_2 was synthesized. The XRD patterns in Fig. 4.17 was well

matched with the JCPDS reference of 01-073-0698. The peak broadness at 20° was related to the presence of reduced graphene oxide.

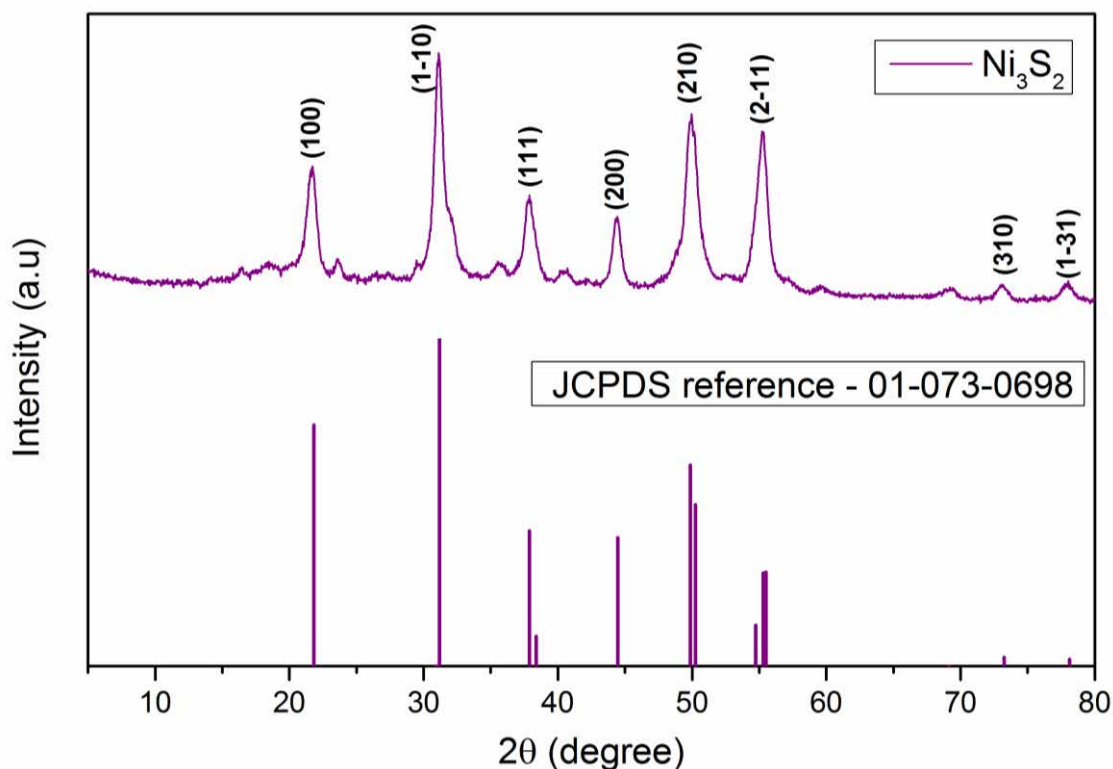


Fig. 4.17 XRD pattern of Ni_3S_2 phase (G-4).

The oleylamine single solvent was used as reducing agent for graphene oxide nanoparticles, which less reacted with sulfur ions. The interaction between the oleylamine and graphene oxide was better than nickel and sulfur ion, which lead to the formation of uncontrolled nickel sulfide phases on reduced graphene oxide. To overcome this problem, multi-solvent experiment was preferred to form nickel sulfide on rGO supports. All the solvents were belongs to the family of octadecine with high boiling surfactant nature. In

addition to the phase control, the particle sizes were uniform in the multi-solvent experiment.

In all the experiments on rGO sheets, the excess sulfur concentration was required to achieve the phase controlled nickel sulfide/rGO structures.

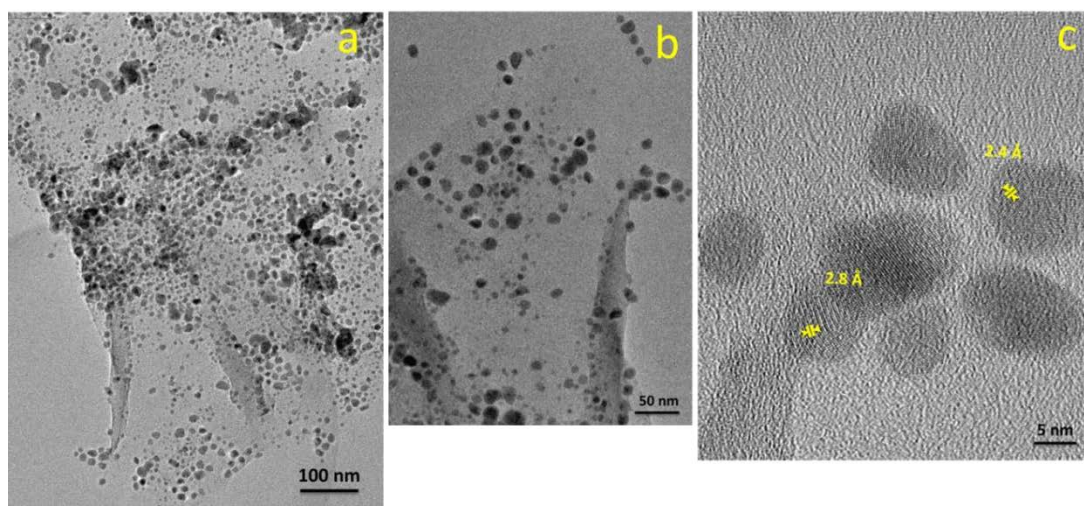


Fig. 4.18 (a, b) TEM and (c) HRTEM images of Ni₃S₂ phase (G-4).

4.3.5 Growth Process

Fig. 4.19 shows the schematics of growth process of rGO/nickel sulfide hybrid nanostructures prepared by different solvent methods. During the in-situ growth, the influence of multi-solvents were clearly resulted with the formation of phase controlled nickel sulfide nanoparticles on reduced graphene oxide (rGO) sheets over the single-solvent methods. The parameters such as temperature and concentration of the source materials were kept constant for both single-solvent and multi-solvent experiments is shown in Fig. 4.19.

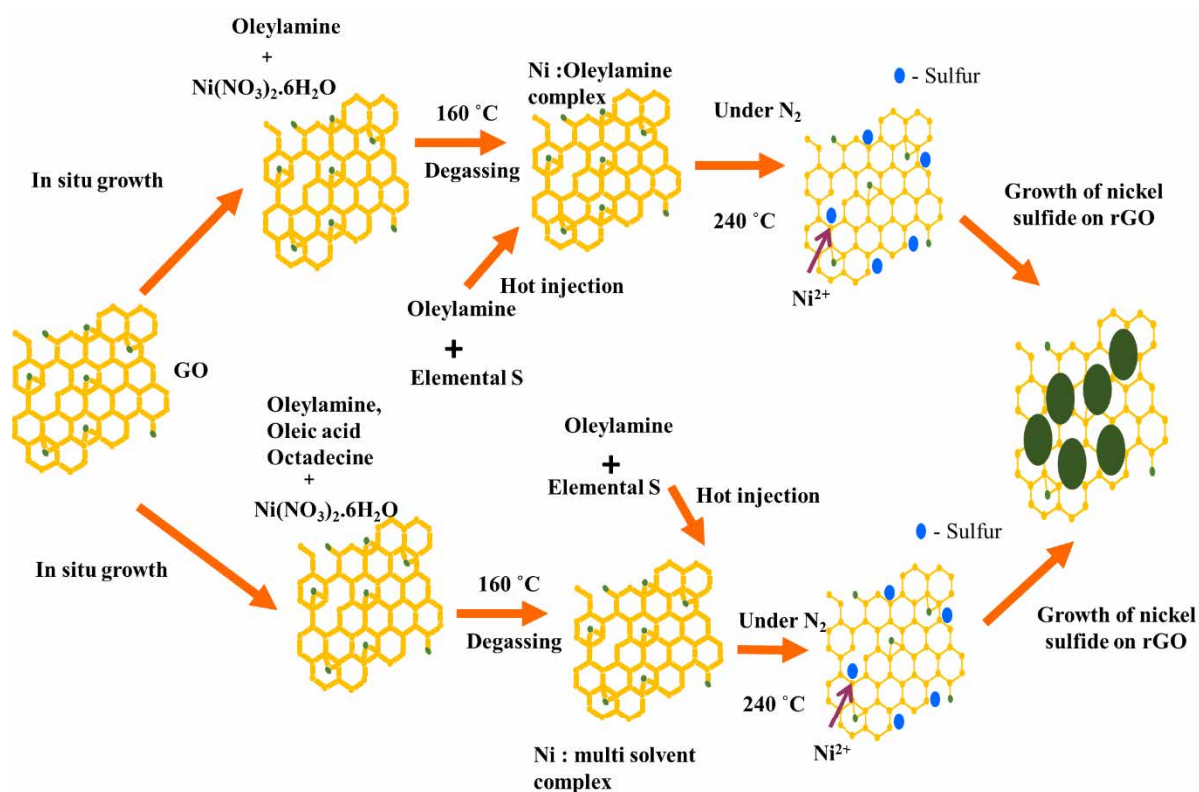


Fig. 4.19 Schematics of growth processes of rGO/nickel sulfide hybrid structures by different solvent methods

4.4 Catalytic Activities for the reduction of 4-nitrophenol

The investigation of 4-nitrophenol to 4-aminophenol reduction was carried out for the reduced graphene oxide/nickel sulfide nanoparticles prepared with mixed solvent method to understand the catalytic activities of the synthesized products¹⁶. Fig. 4.20 shows photographs of 4-nitrophenol reduction and the chemical equation. Fig. 4.21 shows the UV-visible absorbance spectra with respect to time. Because of the addition of reduced graphene oxide, the reaction rate increased in rapidly. Therefore monitoring with UV visible

spectroscopy became very difficult. The concentration of NaBH_4 was intentionally reduced to 335 mg in 200 mL water to compare the results in the previous chapter. The activity of rGO/nickel sulfide and pure nickel sulfide (NiS phase) nanoparticles were compared.

The addition of nickel sulfide was preferred on reduced graphene oxide because of its two dimensional high surface area property. In addition, the mechanical stability, excellent conductivity and thermal stability will improve the catalytic activity. Fig. 4.21 shows the schematic of nickel sulfide on reduced graphene oxide sheets. The reduction process of graphene oxide and the formation of nickel sulfide/reduced graphene oxide hybrids were synthesized in a single-step formation process.

Fig.4.23 shows the UV-visible spectroscopy measurements for the reduction of 4-nitrophenol to 4-aminophenol. The reduction measurements of rGO/NiS, rGO/Ni₃S₂ and rGO/Ni₃S₄ were carried out and compared with pure NiS phase. The reduction of absorption peak at 400 nm was measured for about 30 min. The corresponding appearance of 4-nitrophenolate ion was observed from the peak position of 400 nm. The peak position of 293 nm was related to 4-aminophenol. For the same concentration of NaBH_4 in 4-nitrophenol solution, rGO samples were tested. Fig.4.23 (a) shows that the complete reduction of 4-nitrophenolate ions required about 300 s for the sample rGO/NiS phase of nickel sulfide.

Similarly, for the nickel-rich phase of rGO/Ni₃S₂, reaction completed less than 500 sec and sulfur-rich phase of rGO/Ni₃S₄ were finished within 260 s.

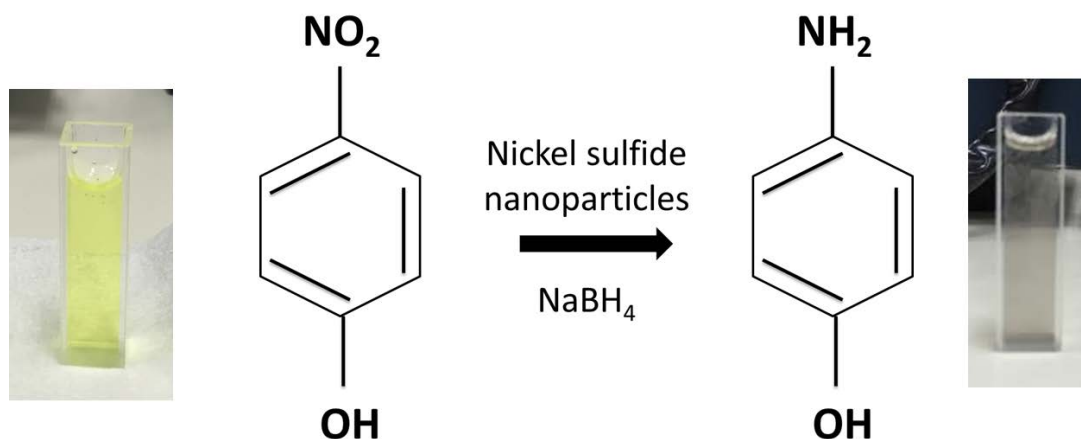


Fig. 4. 20 Catalytic reduction of 4-nitrophenol to 4-aminophenol.

Fig. 4.24 shows the reduction rate percentage with respect to time for different materials. The reaction rate linearly increased with respect to time. The reduction rate constant (k_{obs}) was calculated using the absorption values for the 4-nitrophenol reduction reaction.

$$K_{\text{obs}} = \frac{\ln \left[\frac{A_{\infty} - A_0}{A_{\infty} - A_t} \right]}{t}$$

Where A_0 , A_t , and A_{∞} are the initial absorbance, absorbance at time t , and absorbance at infinite time, respectively. The calculated K_{obs} values for pure NiS, rGO/NiS, rGO/Ni₃S₄, and rGO/Ni₃S₂ are 1.127×10^{-3} , 16.332×10^{-3} , 14.456×10^{-3} , and $9.975 \times 10^{-3} \text{ s}^{-1}$, respectively.

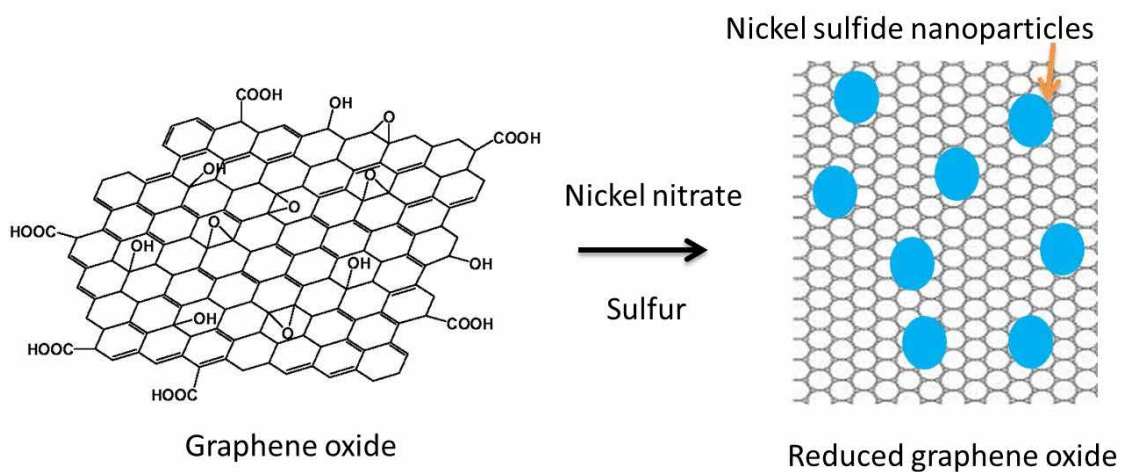


Fig. 4. 21 Schematic of nickel sulfide nanoparticles on reduced graphene oxide

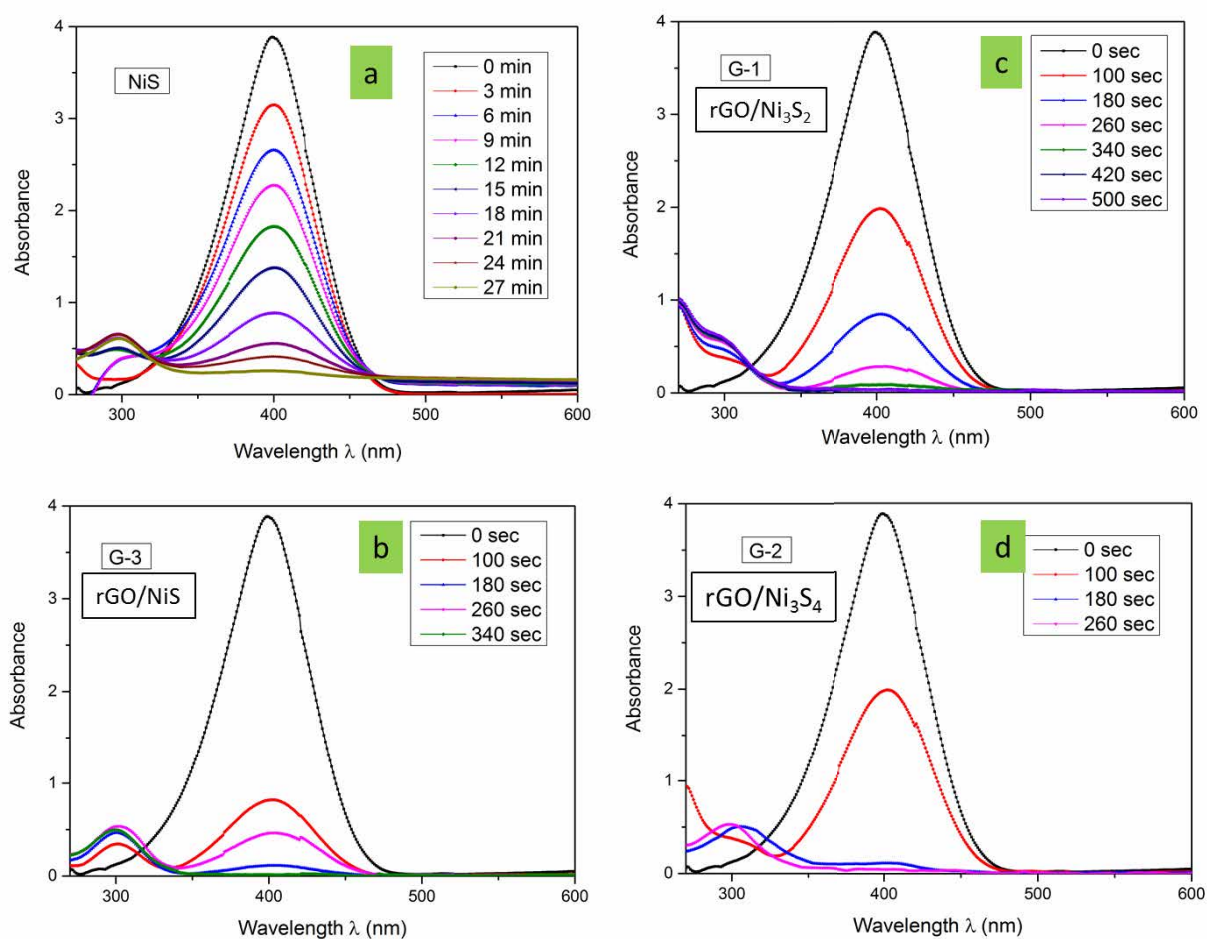


Fig. 4.22 UV-vis spectra of 4-nitrophenol reduction with (a) NiS, (b) rGO/NiS, (c) rGO/Ni₃S₂, and (d) rGO/Ni₃S₄ phases.

The function of reduced graphene oxide in the catalytic activity is schematically given in Fig. 4.23. Reduced graphene oxide (rGO) has a good water solubility, which is inducing an efficient contact between nickel sulfide and 4-nitrophenol. It has an abundant absorption sites due to π - π stacking between 4-Np and rGO, resulting in a high concentration of 4-Np near nickel sulfide nanoparticles. The hybrid rGO/nickel sulfide has a smaller particle sizes than unsupported nickel sulfide nanoparticles providing more nickel sulfide active sites because of its higher surface area.

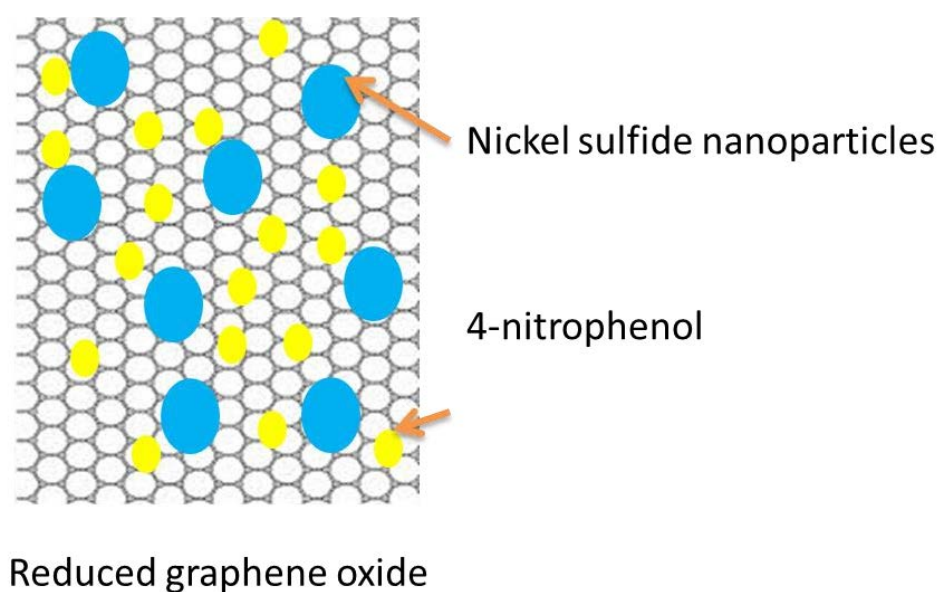


Fig. 4. 23 Schematic of 4-nitrophenol adsorption of rGO/nickel sulfide hybrid structures

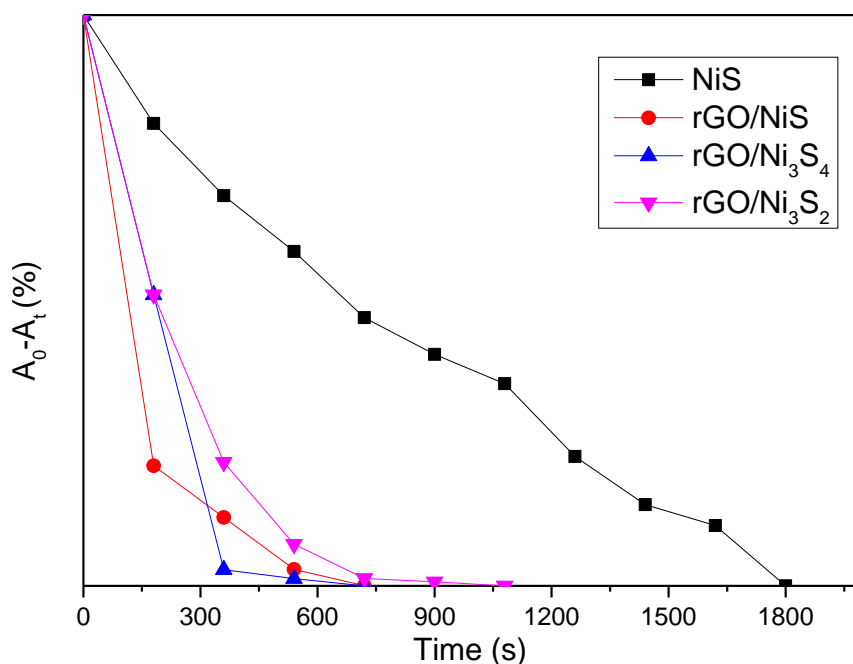


Fig. 4.24 Effect of 4-nitrophenol reduction with different materials

4.5 Conclusion

I have successfully synthesized rGO/nickel sulfide nanoparticles with different phases via a simple temperature-controlled injection method in mixed solvent. The products were uniform-sized nanocrystals. Multi-solvent experiment was preferred to form structure controlled nickel sulfide on rGO supports. The injection method enabled the sulfur ions to react slowly with the well-dispersed nickel ions in the presence of multi-solvent, to form nickel sulfide nanoparticles on rGO. This enabled formation of the desired phase instead of mixed phases. The complications in the synthesis of rGO functionalized nickel sulfide nanoparticles were overcome by adjusting the solvent and source concentrations. XRD and

TEM analyses confirmed the presence of single-phase nanoparticles of sizes less than 20 nm for all the synthesized products. The catalytic activities of the synthesized rGO/nickel sulfide nanoparticles were investigated and it was found that the rGO/NiS phase had the best activity.

References

- (1) U.S. Public Health Service. *Agency Toxic Subst. Dis. Regist.* **1992**, 1–104.
- (2) Marais, E.; Nyokong, T. *J. Hazard. Mater.* **2008**, *152*, 293–301.
- (3) Hayakawa, K.; Yoshimura, T.; Esumi, K. *Langmuir* **2003**, *19*, 5517–5521.
- (4) Wunder, S.; Polzer, F.; Lu, Y.; Mei, Y.; Ballauff, M. *J. Phys. Chem. C* **2010**, *114*, 8814–8820.
- (5) Pradhan, N.; Pal, A.; Pal, T. *Colloids Surfaces A Physicochem. Eng. Asp.* **2002**, *196*, 247–257.
- (6) Mele, G.; Del Sole, R.; Vasapollo, G.; García-López, E.; Palmisano, L.; Schiavello, M. *J. Catal.* **2003**, *217*, 334–342.
- (7) Di Paola, a.; Marci, G.; Palmisano, L.; Schiavello, M.; Uosaki, K.; Ikeda, S.; Ohtani, B. *J. Phys. Chem. B* **2002**, *106*, 637–645.

- (8) Canizares, P.; Sez, C.; Lobato, J.; *Al. Ind. Eng. Chem. Res.* **2004**, *43*, 1944–1951.
- (9) Rode, C. V.; Vaidya, M. J.; Chaudhari, R. V. *Org. Process Res. Dev.* **1999**, *3*, 465–470.
- (10) Sun, Y.; Wu, Q.; Shi, G. *Energy Environ. Sci.* **2011**, *4*, 1113–1132.
- (11) Zhao, W.; Lin, T.; Sun, S.; Bi, H.; Chen, P.; Wan, D.; Huang, F. *J. Mater. Chem. A* **2013**, 194–198.
- (12) Li, J.; Kuang, D.; Feng, Y.; Zhang, F.; Xu, Z.; Liu, M. *J. Hazard. Mater.* **2012**, *201-202*, 250–259.
- (13) Nie, G.; Lu, X.; Lei, J.; Yang, L.; Wang, C. *Electrochim. Acta* **2015**, *154*, 24–30.
- (14) Choi, Y.; Bae, H. S.; Seo, E.; Jang, S.; Park, K. H.; Kim, B.-S. *J. Mater. Chem.* **2011**, *21*, 15431–15436.
- (15) Li, J.; Liu, C.; Liu, Y. *J. Mater. Chem.* **2012**, *22*, 8426–8430.
- (16) Zhang, Y.; Liu, S.; Lu, W.; Wang, L.; Tian, J.; Sun, X. *Catal. Sci. Technol.* **2011**, *1*, 1142–1144.
- (17) Liu, R.; Zhao, Q.; Li, Y.; Zhang, G.; Zhang, F.; Fan, X. *J. Nanomater.* **2013**, *2013*, 1–7.

- (18) Zhu, C.; Wang, P.; Wang, L.; Han, L.; Dong, S. *Nanoscale* **2011**, 3, 4376–4382.
- (19) Sun, T.; Zhang, Z.; Xiao, J.; Chen, C.; Xiao, F.; Wang, S.; Liu, Y. *Sci. Rep.* **2013**, 3, 2527, 1–6.
- (20) X. Kong, Z. Sun, M.Chen, C. C. and Q. C. *Energy Environ. Sci.* **2013**, 6, 3260–3266.
- (21) Gong, F.; Zhou, G.; Wang, Z. *Chinese Sci. Bull. (Chinese Version)* **2013**, 58, 294.
- (22) Mahmood, N.; Zhang, C.; Hou, Y. *Small* **2013**, 9, 1321–1328.
- (23) Pan, Q.; Xie, J.; Liu, S.; Cao, G.; Zhu, T.; Zhao, X. *RSC Adv.* **2013**, 3, 3899–3906.
- (24) Mi, L.; Ding, Q.; Chen, W.; Zheng, Z.; Hou, H.; Liu, C.; Shen, C. *RSC Adv.* **2012**, 2, 6817–6823.
- (25) Sun, C.; Yang, J.; Zhang, Y.; Chen, P.; Huang, W.; Dong, X. **2014**, 1–6.
- (26) Xing, Z.; Chu, Q.; Ren, X.; Tian, J.; Asiri, A. M.; Alamry, K. a.; Al-Youbi, A. O.; Sun, X. *Electrochem. commun.* **2013**, 32, 9–13.
- (27) Liu, X.; Qi, X.; Zhang, Z.; Ren, L.; Liu, Y.; Meng, L.; Huang, K.; Zhong, J. *Ceram. Int.* **2014**, 40, 8189–8193.
- (28) Zhang, H.; Guo, D.; Zhu, J.; Li, Q.; Chen, L.; Wang, T. *Electrochim. Acta* **2015**.

- (29) Wang, A.; Wang, H.; Zhang, S.; Mao, C.; Song, J.; Niu, H.; Jin, B.; Tian, Y. *Appl. Surf. Sci.* **2013**, 282, 704–708.
- (30) Zhang, H.; Yu, X.; Guo, D.; Qu, B.; Zhang, M.; Li, Q.; Wang, T. *ACS Appl. Mater. Interfaces* **2013**, 5, 7335–7340.
- (31) Marcano, D. C.; Kosynkin, D. V.; Berlin, J. M.; Sinitskii, A.; Sun, Z.; Slesarev, A.; Alemany, L. B.; Lu, W.; Tour, J. M. *ACS Nano* **2010**, 4, 4806–4814.
- (32) Cui, P.; Lee, J.; Hwang, E.; Lee, H. *Chem. Commun.* **2011**, 47, 12370–12372.
- (33) Guo, H.-L.; Wang, X.-F.; Qian, Q.-Y.; Wang, F.-B.; Xia, X.-H. *ACS Nano* **2009**, 3, 2653–2659.

Chapter 5

Summary and Future work

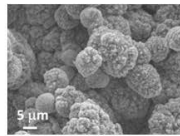
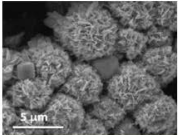
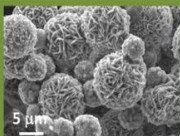
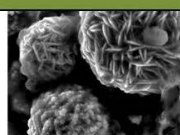
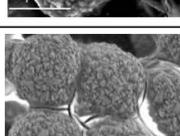
5.1 Summary

The phase dependent catalytic activity of nickel sulfide and hybrid rGO/nickel sulfides were investigated for the first time. Hydrothermal growth and temperature assisted hot injection synthesis method were carried out for the preparation of nickel sulfide nano and microstructures. The growth conditions were optimized to obtain the desired phase and morphologies of nickel sulfide. Various capping ligands such as, ethylenediaminetetraacetic acid (EDTA), oleylamine, oleic acid, octadecine were used as a surface passivating ligands and solvents to achieve the monodispersity in size and morphology. Functional properties of the synthesized nickel sulfide nanostructures were characterized by variety of instrumentation techniques such as powder X-ray diffractometer (XRD), field emission scanning electron microscopy (FE-SEM), transmission electron microscopy (TEM), Fourier transform infra-red (FTIR) measurements and X-ray photoelectron spectroscopy (XPS) analysis. In addition to that the synthesized nickel sulfide nanostructures were utilized to reduce the 4-nitrophenol for the catalytic applications and the reduction characteristics were performed by UV visible absorption analysis.

The molar concentrations of EDTA on the formation and functional properties of nickel sulfide hierarchical architectures by hydrothermal method were studied. The sulfur

source and nickel source concentration were fixed as 0.5 and 1.0 molar. The obtained results were compared with the uncapped nickel sulfide. It was found that the addition of EDTA concentration influences the growth of uniform phase controlled hierarchical structures and it restricted the addition of sulfur source to react with Ni-EDTA complex.

Table.5. Summary of hydrothermal method results

Experiment	Nickel Nitrate (mol)	Thiourea (mol)	EDTA (mol)	Phases from XRD	Observed Morphologies
1	0.50	0.50	0.20	NiS ₂ & Ni ₃ S ₄	
2	0.50	0.75	0.20	Ni ₃ S ₄ & Ni ₁₇ S ₁₈	
3	0.50	1.00	0.20	Ni ₃ S ₄ & Ni ₁₇ S ₁₈	
4	0.75	1.00	0.20	NiS ₂ & Ni ₁₇ S ₁₈	
5	1.00	1.00	0.20	NiS ₂	

On the other hand, molar concentrations of thiourea (sulfur source), nickel nitrate (nickel source) and whole precursor concentrations were varied by keeping its growth temperature and period as constant. The XRD and TEM analysis confirmed the changes in its phase with respect to the source concentrations. The obtained results of nickel sulfide

nanoparticles phase and morphological results were summarized in table.5. Highly monodispersed sheet composed $\text{Ni}_{17}\text{S}_{18}$ and ball-like Ni_3S_4 phases of hierarchical architectures were synthesized. The catalytic activity of synthesized nanoparticles were investigated by the reduction experiments of 4-nitrophenol to 4-aminophenol. It is found that $\text{Ni}_{17}\text{S}_{18}$ and Ni_3S_4 phases exhibited better catalytic performance than the other phases.

Facile synthesis of phase controlled nickel sulfide nanoparticles with the sizes less than 20 nm were fabricated via temperature assisted hot injection method. This method enabled the sulfur ions to react slowly with nickel ions in the presence of oleylamine, to form desired nickel sulfide phases with respect to its initial concentration. The complications for the synthesis of specific phases were overcome by adjusting the source concentrations. The presence of nickel and sulfur and the peak shifts with respect to the phase formation were observed using X-ray photoelectron spectroscopy. The functional properties of nickel sulfide nanoparticles were investigated for the reduction of 4-nitrophenol applications. The better catalytic activity and the reaction rate of $8.949 \times 10^{-3} \text{ s}^{-1}$ was achieved for the NiS phase. The stability of the NiS phase was investigated and there was no phase change observed even after its catalytic reduction and the repeated reaction rate was well matched with the initial experiments.

Reduced graphene oxide (rGO) functionalized nickel sulfide nanoparticles were synthesized through a one-step hot injection method. Investigations of solvents and phase

control of nickel sulfide nanoparticles on rGO supports were studied. Multi-solvent (oleylamine, octadecine, oleic acid) method was preferred over single solvent (oleylamine) method, because of its better control on size and structure. Phase controlled rGO/NiS; rGO/Ni₃S₂ and rGO/Ni₃S₄ hybrid nanostructures were synthesized with uniform dispersion of nanoparticles. TEM analysis confirmed presence of single-phase nanoparticles of sizes less than 20 nm for all the synthesized products. The schematics of the in-situ growth processes were discussed between phase controlled nickel sulfide and reduced graphene oxide sheets. The higher surface area of rGO/nickel sulfide was utilized for the catalytic reaction because of its higher adsorption sites (π - π stacking between rGO and 4-nitrophenol), which increases the high concentration of 4-nitrophenol near the nickel sulfide sites. The catalytic activities of the synthesized nanostructures were investigated and it was found that rGO/NiS phase had the best activity with the highest reaction rate of $16.332 \times 10^{-3} \text{ s}^{-1}$.

5.2 Future works

In the present work, the influences of materials source concentrations on the formation of phase controlled nickel sulfide nanostructures have been investigated. The catalytic applications of 4-nitrophenol reduction were carried out and the performances were evaluated.

In future, it is aimed to utilize the synthesized catalytic materials of nickel sulfide for

the fabrication of photo cathodes in dye sensitized solar cells applications. During the fabrication and device characteristics the following factors such as, thickness, stability and efficiencies of the photocathodes will be evaluated with respect to its phases of nickel sulfide nanostructures. The characterizations such as FESEM and atomic force microscopy (AFM) will be utilized for the control on roughness factors of photocathodes. The synthesized rGO/nickel sulfide hybrid structures will also be aimed to replace the commercial platinum photocathode in dye sensitized solar cells.

Another focus is to investigate the effect of addition of cobalt in the formation of ternary nanostructures by controlling their phase and morphology by hydrothermal and temperature assisted hot injection method. The functional properties of ternary nanostructures will be analyzed with the characterizations such as, FESEM, XRD, TEM and XPS analysis. The effect of catalytic reduction of bimetallic chalcogenides will be investigated with 4-nitrophenol reduction experiments. The synthesized materials will be utilized as a photocathode for dye sensitized solar cells applications.

List of publications

(A) Journal publications

- (1) **R. Karthikeyan**, M. Navaneethan, J. Archana, D. Thangaraju, M. Arivanandhan, Y. Hayakawa, (2014) “Shape controlled synthesis of hierarchical nickel sulfide by hydrothermal method”, Dalton Transactions, 43: 17445-17452. [IF-4.197]
- (2) **R. Karthikeyan**, D. Thangaraju, N. Prakas, Y. Hayakawa, (2015) “Single-step synthesis and catalytic activity of structure-controlled nickel sulfide nanoparticles”, Crystal Engineering. Communications, 17: 5431-5439. [IF-4.034]

(B) Other publications (Journals)

- (1) D. Thangaraju, **R. Karthikeyan**, N. Prakash, S. Moorthy Babu, Y. Hayakawa, (2015) “Growth and optical properties of Cu₂ZnSnS₄ decorated reduced graphene oxide nanocomposites”, Dalton Transactions, 44: 15031- 15041. [IF-4.197]
- (2) N. Prakash, **R. Karthikeyan**, D. Thangaraju, M. Navaneethan, M. Arivanandhan, T. Koyama, Y. Hayakawa, (2015), “Effect of erbium on the photocatalytic activity of TiO₂/Ag nanocomposites under visible light irradiation”, ChemPhysChem, (Accepted). [IF-3.419]
- (3) G. Rajakumar, A. Rahuman, J. Chidambaram, T. Santhoshkumar, M. Sampath, C. Kamaraj, A. Bagavan, A/ Zahir, A. Vishnu Kirthi, G. Elango, A. Pooja, **R. Karthikeyan**, S. Manikandan, S. Jose, (2014) “Solanum trilobatum

ectract-mediated synthesis of titanium dioxide nanoparticles to control pediculus humans capitis, Hyalomma antolicum and Anopheles subpictus” Journal of Parasitology Research”, 113, 469-479. [IF-2.327]

- (4) **R. Karthikeyan**, M. Navaneethan, J. Archana, M. Arivanandhan, Y. Hayakawa, (2013) “Low cost synthesized carbon materials as a photo cathode for dye sensitized solar cells”, IEICE. Tech. Rep, 113, 40, 469-479.

(C) Conference proceedings

- (1) **R. Karthikeyan**, M. Navaneethan, J. Archana, M. Arivanandhan, T. Koyama, Y. Hayakawa, (2013) “Preparation of alternate counter electrodes by novel method for the replacement of platinum in DSSCs”, Proceedings of the 15th Takayanagi Kenjiro Memorial Symposium, (November 12th -13th, 2013, Shizuoka University, Japan).

(D) Conferences

- (1) **R. Karthikeyan**, M. Navaneethan, J. Archana, M. Arivanandhan, Y. Hayakawa, “Facile synthesis of activated carbon from organic waste for DSSC”, The International Conference on Nanoscience and Nanotechnology ICONN-2013, Poster presentation (SRM university, Chennai, India, March 18th – 20th, 2013).

- (5) **R. Karthikeyan**, M. Navaneethan, D. Thangaraju, M. Arivanandhan, Y. Hayakawa, “Phase control of nickel sulfide hierarchical structures”, The International Conference NANOCON-2014, Poster presentation (Brno, Czech Republic, EU. November 5th – 7th, 2014).
- (6) **R. Karthikeyan**, M. Navaneethan, J. Archana, M. Arivanandhan, T. Koyama, Y. Hayakawa, “Low cost synthesized carbon materials as a photocathode for dye sensitized solar cells”, The Institute of Electronics, Information and Communication Engineers Conference, pp.51-54 (Shizuoka University, Hamamatsu May 16th – 17th, 2013).
- (7) **R. Karthikeyan**, M. Navaneethan, J. Archana, M. Arivanandhan, T. Koyama, Y. Hayakawa, “Synthesis of carbon from organic waste for using as a photocathode in dye sensitized solar cells“, The 73rd Autumn Meeting of the Japan Society of Applied Physics and Related Societies, (Doshisha University, September 16th – 20th, 2013).
- (8) **R. Karthikeyan**, M. Navaneethan, J. Archana, M. Arivanandhan, T. Koyama, Y. Hayakawa, “Formation of nickel sulfide hierarchical structures by hydrothermal

method”, The 61st Spring Meeting of the Japan Society of Applied Physics and Related Societies, (Aoyama Gakuin University, March 17th – 20th, 2014).

- (9) **R. Karthikeyan**, M. Navaneethan, D. Thangaraju, M. Arivanandhan, Y. Hayakawa, “Facile synthesis of nickel sulfide hierarchical structures and its phase changes”, The 75th Autumn Meeting of the Japan Society of Applied Physics and Related Societies, (Hokkaido University, Sapporo campus, September 17th – 20th, 2014).

- (10) N. Prakash, **R. Karthikeyan**, M. Navaneethan, M. Arivanandhan, T. Koyama, Y. Hayakawa, “Synthesis of Ag deposited TiO₂ nanostructures and their photocatalytic degradation of dye”, The 75th Autumn Meeting of the Japan Society of Applied Physics and Related Societies, (Hokkaido University, Sapporo campus, September 17th – 20th, 2014).

- (11) **R. Karthikeyan**, M. Navaneethan, D. Thangaraju, N. Prakash, M. Arivanandhan, Y. Hayakawa, “Effect of source concentration on the formation of hierarchical nickel sulfide”, SSSV workshop, (Shizuoka University, Hamamatsu campus, January 8th 2015).

- (12) N. Prakash, **R. Karthikeyan**, D. Thangaraju, M. Navaneethan, M. Arivanandhan, T. Koyama, Y. Hayakawa, “Preparations of Ag-Er-TiO₂ nanocomposites and their photocatalytic activity”, The 62nd Japan Society of Applied Physics Spring Meeting, (Tokai University, Shonan campus, March 11th – 14th, 2015).
- (13) D. Thangaraju, M. Michel, **R. Karthikeyan**, N. Prakash, T. Koyama, Y. Hayakawa, “Capillary flow reactor synthesis of upconversion colloidal nanoparticles”, The 62nd Japan Society of Applied Physics Spring Meeting, (Tokai University, Shonan campus, March 11th – 14th, 2015).
- (14) N. Prakash, **R. Karthikeyan**, D. Thangaraju, M. Navaneethan, M. Arivanandhan, T. Koyama, Y. Hayakawa, “Synthesis of Silver/Titania nanocomposites and their photocatalytic degradation of dye”, SSSV workshop, (Shizuoka University, Hamamatsu campus, January 8th 2015).
- (15) D. Thangaraju, P. Gredin, M. Mortier, T. Aubert, C. Neaime, S. Cordier, F. Grasset, **R. Karthikeyan**, M. Arivananthan, Y. Hayakawa “Energy transferred emission of NaGdF₄:Yb:Tm@NaGdF₄/Cs₂Mo₆Br₁₄”, The 16th Takayanagi Kenjiro Memorial Symposium, (November 12th -13th, 2013, Shizuoka University, Japan) (2013.11).